MASS TRANSFER FROM A CYLINDER TO AN AIR STREAM IN AXISYMMETRICAL FLOW (AN EXPERIMENTAL STUDY)

Thesis by

Shiou-Shan Chen

In Partial Fulfillment of the Requirements

For the Degree of

Doctor of Philosophy

California Institute of Technology

Pasadena, California

1966

(Submitted July 6, 1965)

ACKNOWLEDGMENTS

The author wishes to express his sincere gratitude to Professor B. H. Sage, without his inspiring guidance and constant encouragement this work would not have been completed at this time.

Appreciation is also due to H. T. Couch, W. M. Dewitt, G. Griffith, H. H. Reamer and H. E. Smith for their help in the construction and operation of the experimental equipment.

Financial support in the form of Scholarships and Graduate Assistantships from the California Institute of Technology, and a Woodrow Wilson Summer Fellowship is gratefully acknowledged.

ABSTRACT

Mass transfer from wetted surfaces on one-inch cylinders with unwetted approach sections was studied experimentally by means of the evaporation of n-octane and n-heptane into an air stream in axisymmetrical flow, for Reynolds numbers from 5,000 to 310,000. A transition from the laminar to the turbulent boundary layer was observed to occur at Reynolds numbers from 10,000 to 15,000. The results were expressed in terms of the Sherwood number as a function of the Reynolds number, the Schmidt number, and the ratio of the unwetted approach length to the total length. Empirical formulas were obtained for both laminar and turbulent regimes. The rates of mass transfer obtained were higher than theoretical and experimental results obtained by previous investigators for mass and heat transfer from flat plates.

TABLE OF CONTENTS

TABLE OF CONTENTS (Continued)

LIST OF FIGURES

LIST OF FIGURES (Continued)

LIST OF TABLES

INTRODUCTION

Mass transfer between a solid surface and a fluid is one of the most important subjects in chemical engineering. It occurs in many chemical engineering operations, such as drying, absorption, adsorption, extraction, heterogeneous chemical reactions (in particular, surface catalytic reactions) etc. An understanding of mass transfer is therefore essential to the design and operation of process equipment. It is also important in the field of aeronautical engineering in the study of problems such as ice formation on aircraft and the maintenance of tolerable temperatures on the surface of high-speed aircraft by the use of transpiration cooling.

In most cases of industrial importance, the fluid flows relative to the solid surface and creates convective mass transfer in addition to the molecular diffusion. It is therefore important to study the relationship between fluid flow and mass transfer or, more specifically, the dependence of mass transfer on fluid flow. Industrial mass transfer processes usually involve complex equipment, and the basic principles of mass transfer are often complicated by the geometry and flow patterns. In order to understand the basic mechanism of mass transfer, it is desirable to study situations where boundary conditions are simple and well defined. The most frequently studied cases are flow past a flat plate[1, 2, 3]*, sphere[1, 4, 5], cylinder perpendicular[1, 6, 7] or

---

*Numbers in parentheses indicate references listed on pages 64 to 68.

parallel[8, 9] to the flow direction and, of course, flow in pipes[10, 11] and flow between parallel plates[11, 12].

Axisymmetrical boundary layers occur in flows past axially symmetrical bodies. The axisymmetrical case differs from the two-dimensional case by including the effect of curvature in a plane transverse to the flow direction. The influence of this curvature on the values of local skin friction and thermal transfer has been studied theoretically by Seban and Bond[8] by considering the problem of forced convection from a heated cylinder into the surrounding axisymmetrical, incompressible, laminar boundary layer produced by a uniform stream. No satisfactory theoretical treatment is yet available for the corresponding turbulent boundary layer case, and experimental work on this problem is lacking.

The purpose of the present investigation was to study experimentally the rate of mass transfer from a one-inch-diameter porous cylinder to an air stream. The air stream flowed parallel to the axis of the cylinder (axisymmetrical flow) and formed a boundary layer along the surface of the cylinder. The boundary layer was either laminar or turbulent depending on the flow conditions. The porous section was preceded by an unwetted length. There was no mass transfer between the unwetted surface and the air stream, and thus the mass flux of the diffusing component on the unwetted surface was zero. This unwetted length is called the "approach length"[13].

Liquid was injected at a predetermined rate to the porous

section and raised by capillary force to form a thin film on the porous surface. The Reynolds number was varied from 5,000 to 310,000 by changing the air velocity as well as the length of the approach section.

Two liquids, n-heptane and n-octane, were used as the diffusing components. The difference in the vapor pressures of these two compounds served to study the effect of the surface concentration of the diffusing component on the rate of mass transfer.

Both isothermal evaporation and non-isothermal evaporation were tested and the results were compared. The isothermal evaporation was achieved by supplying energy from a heater located inside the porous section.

In summary, the following problems were considered in the present investigation:

1. Dependence of the rate of mass transfer on the Reynolds number.
2. Influence of the approach length on the rate of mass transfer.
3. Influence of the transverse curvature on the rate of mass transfer.
4. Effect of the surface concentration of the diffusing component on the rate of mass transfer.
5. Isothermal versus nonisothermal mass transfer.

THEORETICAL CONSIDERATIONS AND LITERATURE REVIEW

Theoretical analyses relevant to this work are systematically discussed in this chapter. For the convenience of comparing this work with measurements made by other investigators, previous experimental results directly related to this work are reviewed. Analogies and differences among momentum, heat, and mass transfer will be discussed as the situation arises.

Differential Equations

For the case of two-dimensional, incompressible, steady flow with negligible viscous dissipation, the boundary layer equations can be written as follows

continuity:

$$\frac{\partial(\rho u)}{\partial x} + \frac{\partial(\rho v)}{\partial y} = 0 \qquad (1)^*$$

momentum:

$$u\frac{\partial u}{\partial x} + v\frac{\partial u}{\partial y} = \frac{1}{\rho}\frac{\partial \tau_{xy}}{\partial y} - \frac{1}{\rho}\frac{\partial P}{\partial x} \qquad (2)$$

energy:

$$u\frac{\partial T}{\partial x} + v\frac{\partial T}{\partial y} = -\frac{1}{\rho c_p}\frac{\partial \dot{q}_y}{\partial y} \qquad (3)$$

---

*Table of nomenclature is given on page 61.

diffusion:

$$u \frac{\partial(\rho_k/\rho)}{\partial x} + v \frac{\partial(\rho_k/\rho)}{\partial y} = - \frac{1}{\rho} \frac{\partial \dot{m}_{ky}}{\partial y} \tag{4}$$

For the corresponding axisymmetrical case, the boundary layer equations assume the following form

$$\frac{\partial(r\rho u)}{\partial x} + \frac{\partial(r\rho v)}{\partial r} = 0 \tag{5}$$

$$u \frac{\partial u}{\partial x} + v \frac{\partial u}{\partial r} = \frac{1}{\rho r} \frac{\partial(r\tau_{xr})}{\partial r} - \frac{1}{\rho} \frac{\partial P}{\partial x} \tag{6}$$

$$u \frac{\partial T}{\partial x} + v \frac{\partial T}{\partial r} = - \frac{1}{\rho c_p r} \frac{\partial(r\dot{q}_r)}{\partial r} \tag{7}$$

$$u \frac{\partial(\rho_k/\rho)}{\partial x} + v \frac{\partial(\rho_k/\rho)}{\partial r} = - \frac{1}{\rho r} \frac{\partial(r\dot{m}_{kr})}{\partial r}$$

As is well known, no general solutions for the above equations are available. It has been possible to obtain exact solutions only for some simple problems such as laminar flow past a flat plate at zero incidence[1, 2]. Approximate methods have been developed to solve more complicated situations. We shall first discuss important results for the two-dimensional case, which has been much better explored and usually gives a good first approximation to the axisymmetrical case. The

influence of the transverse curvature on the transport processes will then be discussed to illustrate the difference between the two-dimensional and axisymmetrical cases.

Laminar Boundary Layer

The momentum boundary layer equation was transformed into an ordinary differential equation and solved exactly for the case of flow along a flat plate at zero incidence by Blasius[1,14]. The local friction factor was found to be a function of the Reynolds number as follows:

$$f = \frac{0.664}{\sqrt{Re_x}} \tag{9}$$

The corresponding heat transfer problem for a flat plate with a constant wall temperature was first solved by Pohlhausen[3,15]. The rate of heat transfer was expressed in the form of the Nusselt number as a function of the Reynolds number and the Prandtl number. The result can be approximated by the following formula with good accuracy

$$Nu_x = 0.332\, Pr^{1/3} Re_x^{1/2} \tag{10}$$

In the presence of an approach length the above equation is not applicable because the thermal boundary layer does not

start at the same position as the momentum boundary layer, as shown in Figure 1. This problem was solved by Meyman [16] and Eckert[17] by substituting a third-power polynomial into the heat flux equation[1]. This approximate method leads to the following result

$$Nu_x = 0.332\, Pr^{1/3} Re_x^{1/2} \frac{1}{\sqrt[3]{1-(x_o/\ell)^{3/4}}} \qquad (11)$$

The function $[1-(x_o/\ell)^{3/4}]^{-1/3}$ represents the influence of the inert approach length on the local Nusselt number and is called the "approach-length function." The change of the surface temperature in the form of a step function is of practical importance. A solution to this problem opens the way to the prediction of the heat transfer rates from surfaces of arbitrary temperature distribution by means of the principle of superposition, as one recalls that the energy boundary layer equation is linear. Methods for solving the problem of arbitrary temperature distributions along the surface of a flat plate have been given by Lighthill[18], and Tribus and Klein[19].

It is seen that when the plate is heated over its entire length, i.e. $x_o = 0$, Equation 11 reduces to the result of Pohlhausen, Equation 10.

Integrating Equation 10 from $x = 0$ to $x = \ell$, one obtains the following expression for the mean Nusselt number

$$Nu_{\ell} = 0.664\ Pr^{1/3} Re_{\ell}^{1/2} \tag{12}$$

Equations 10 and 12 can also be derived from the Reynolds analogy and the Blasius solution for momentum transfer for the special case of $Pr = 1$[1].

For mass transfer with small solid-fluid interfacial velocities, an equation analogous to Equation 11 can be derived

$$Sh_x = 0.332 Sc^{1/3} Re_x^{1/2} \frac{1}{\sqrt[3]{1 - (x_o/\ell)^{3/4}}} \tag{12}$$

If the entire length is maintained at a constant concentration, Equation 12 becomes

$$Sh_x = 0.332\ Sc^{1/3} Re_x^{1/2} \tag{13}$$

The mean Sherwood number is obtained by integrating the above expression from $x = 0$ to $x = \ell$,

$$Sh_{\ell} = 0.664\ Sc^{1/3}\ Re_{\ell}^{1/2} \tag{14}$$

The analogy between heat and mass transfer in this case can be easily visualized since the energy boundary layer equation (neglecting the thermal dissipation term) and the diffusion boundary layer equation are the same, and the only difference

is that for heat transfer the normal velocity at the wall is zero but for mass transfer it is greater than zero. They should have the same form of solution if the interfacial velocity in the mass transfer case is sufficiently small.

The Colburn analogy also holds for laminar boundary layer flow along a flat plate. The Colburn j-factors[20] are defined as

$$j_h = St_h Pr^{2/3}$$

$$j_m = St_m Sc^{2/3} \tag{15}$$

for heat and mass transfer, respectively. A comparison of Equations 9, 10, 13, and 15 gives the following simple relation

$$j_h = j_m = f/2 \tag{16}$$

The preceding formulas for heat and mass transfer are in good agreement with the measurements of Elias[21], Edwards and Furber[22], and Kestin, Maeder and Wang[23] for the transfer of heat from flat plates, and the measurements by Albertson[24] for the evaporation of water from a flat plate.

Transition

Since the celebrated experiment of Osborne Reynolds[15] it has been well known that the flow of a viscous fluid can be

classified into two basic hydrodynamic models, laminar flow and turbulent flow. At low Reynolds numbers, fluids flow along stream lines (laminar flow). In this regime, mass transfer in the direction normal to the flow depends only on the molecular diffusion. When the Reynolds number is increased, the flow undergoes a transition from the laminar to the turbulent regime, where mixing of fluid particles in various directions takes place. This macroscopic mixing is termed turbulence. In the turbulent regime, macroscopic mixing dominates the mass transfer process.

Since the mechanism of the transport process is distinctly different in these two regimes, the transition from the laminar to the turbulent flow is of fundamental importance in the study of momentum, heat, and mass transfer. It is a well known fact that for flow in a circular pipe, the transition occurs approximately between $Re = 2,000$ and $4,000$.

The flow in a boundary layer can also undergo transition, as shown in Figure 2. The process of transition in the boundary layer on a flat plate with a sharp leading edge has been studied by many investigators[26, 27, 28, 29, 30]. Near the leading edge the momentum boundary layer is always laminar, but becomes turbulent further down stream. On a flat plate with a sharp leading edge and in an air stream of the level of turbulence of the order of 0.5%, the transition takes place at

$$Re_x = 3.5 \times 10^5 \text{ to } 10^6 \tag{17}$$

Theoretical studies based on the method of small disturbances indicate that the point of instability of a laminar motion takes place at[1,31,32]

$$\left(\frac{U_\infty \delta^*}{\nu}\right)_{crit} = 420 \tag{18}$$

or

$$Re_{x,crit} = \left(\frac{U_\infty x}{\nu}\right)_{crit} = 6.0 \times 10^4 \tag{19}$$

for the boundary layer on a flat plate at zero incidence. At Reynolds numbers larger than this value, some disturbances may amplify themselves and make the laminar flow unstable. This point of instability (or the theoretical critical Reynolds number) gives the lower limit of the point of transition (or experimental critical Reynolds number).

The point of transition depends strongly on the experimental conditions. Using a special wind tunnel with a level of turbulence lower than 0.1%, Dryden and his coworkers[33,34] were able to maintain a laminar boundary layer for flow along a sharp-edged flat plate up to $Re_x = 2.8 \times 10^6$. They also found that when the level of turbulence was lower than 0.08% further decreases in the level of turbulence did not increase

the critical Reynolds number. Accordingly, there seems to exist an upper limit for the critical Reynolds number as well as a lower limit. A comprehensive review on the transition from laminar to turbulent flow has been given recently by Dryden[30].

In many experiments where the angle of incidence was not close to zero, transition at a Reynolds number of the order of 10^4 was observed. This is possible since the point of transition depends not only on the Reynolds number but also on other parameters. The most important ones are the level of turbulence of the main fluid flow, the pressure distribution in the external flow, and the roughness of the wall. The lowest Reynolds number employed in the mass transfer measurements of Maisel and Sherwood[13] was approximately 4×10^4, which was already in the turbulent boundary layer regime. The heat transfer measurements of Jacob and Dow[35] for axisymmetrical flow along a cylinder showed that the point of transition took place at Reynolds number as low as 5×10^4.

According to the Rayleigh theorem[36], the velocity profiles which possess a point of inflection are unstable. The pressure-distribution measurements by Sogin and Jacob[37] for a cylinder with a hemispheric nosepiece in axisymmetrical flow showed that there was a boundary layer separation immediately after the hemispheric nosepiece, and consequently there was a point of inflection. A hemispheric nosepiece will therefore accelerate the transition from the laminar to the

turbulent boundary layer. This was experimentally verified by Jacob and Dow[35]. They used a hemispherical nosepiece and a hemi-ellipsoidal nosepiece and found that in the former case there was a lower value of the critical Reynolds number.

Turbulent Boundary Layer

The theoretical treatment of the laminar boundary layer is rather straightforward, at least for flow along a flat plate, and agrees well with the experimental results. The theoretical analysis of the turbulent boundary layer has not been carried out with such great confidence due to the complex nature of turbulence which is not entirely understood. Mathematical analyses of the turbulent flow always involve some semi-empirical hypotheses. Since different investigators adopted different hypotheses in deriving theoretical formulas, the results often do not agree with each other. The agreement between experimental measurements and theoretical formulas has not been as good as in the laminar case. A detailed comparison of various results has been given by Christian and Kezios[38].

The classical method in the calculation of heat and mass transfer in a turbulent boundary layer takes as its starting point the Boussinesq expressions for shear stress and heat flux (or mass flux)[39,1], and assumes that the ratio between the shear stress and the heat flux, $\tau/\dot{q}$, remains constant across the boundary layer and the turbulent Prandtl number is

equal to a constant in the turbulent core. The resulting relation between the temperature gradient and the velocity gradient is then integrated to yield expressions for the heat flux. Additional assumptions concerning the velocity distribution across the boundary layer have to be made when the integration is being carried out. Consequently, different formulas have been obtained by various investigators due to different assumptions involved. The most widely accepted ones are those of Prandtl[40] and Taylor[41], von Kármán[42], van Driest[43], and Rubesin[44]. For the Prandtl number close to unity, the formulas by Prandtl and by von Karman can be approximated by the following simple expression with good accuracy[1]

$$Nu_x = 0.0296\ Pr^{1/3} Re_x^{0.8} \tag{20}$$

or

$$Nu_\ell = 0.037\ Pr^{1/3} Re_\ell^{0.8} \tag{21}$$

All the theoretical analyses indicate that the Nusselt number (or Sherwood number, for mass transfer) is approximately proportional to $Re_x^{0.8}$ for turbulent boundary layer along a flat plate, provided the Prandtl number is not too far from unity.

A new theoretical method for the analysis of heat transfer in a turbulent boundary layer has been developed recently by Spalding[45, 46, 47] by making use of the von Mises transformation[48]. The energy equation is transformed into a form

identical with the one-dimensional diffusion equation in which the coefficients are functions of the space coordinates. By assuming proper forms of the universal law of the wall[49] and of the turbulent Prandtl number, the equation can be integrated numerically to yield the heat transfer coefficient. This new approach is more exact and elegant in the mathematical sense, but the results are in the numerical form rather than the analytical form obtained by the classical method. It is therefore rather inconvenient for practical applications. A survey of the present status of knowledge concerning the transfer of heat by forced convection across incompressible turbulent boundary layers has been given by Kestin and Richardson[50].

The influence of the approach length on the rate of heat transfer through a turbulent boundary layer was first studied experimentally by Jacob and Dow[35]. They measured heat transfer from a 1.3-inch cylinder with a hemispheric nosepiece in axisymmetrical flow for various approach lengths from 0.075 to 1.026 feet and a heated length of 8 inches (x_o/ℓ = 0.101 to 0.606). Over a range of $Re_\ell = 2 \times 10^5$ to 1.5×10^6, the data were in good agreement with the empirical relation

$$Nu_\ell = 0.0280 \left[1 + 0.40(x_o/\ell)^{2.75}\right] Re_\ell^{0.80} \qquad (22)$$

Maisel and Sherwood[13] measured the mean mass transfer

coefficient* by evaporating water from a flat plate into a turbulent air stream for air velocities between 16 and 32 feet per second, with wetted lengths of 2.03, 4.06, and 6.09 inches, and approach lengths of 5.2, 10.4, 20.6, and 40.6 inches. Over the range of the Reynolds number from 6.5×10^4 to 6.5×10^5, the data were correlated by the following expression

$$Sh_\ell = 0.035\ Re_\ell^{0.8} \left[1 - (x_o/\ell)^{0.8}\right]^{-0.11} \tag{23}$$

with an uncertainty of ±15%. The approach-section functions of Maisel and Sherwood, and of Jacob and Dow agree fairly well for x_o/ℓ between 0 and 0.9. However, they behave completely differently as $x_o/\ell \rightarrow 1$:

$$1 + 0.4(x_o/\ell)^{2.75} \rightarrow 1.4 \tag{24}$$

$$\left[1 - (x_o/\ell)^{0.8}\right]^{-0.11} \rightarrow \infty \tag{25}$$

---

*Maisel and Sherwood claimed that "In the present case x_o is larger compared with x_w; with the 5.1 cm. wetted section and 103 cm. approach section j_m is essentially a point value and not an average over a wetted length ℓ." This is certainly not true in view of the strong dependence of the mass transfer coefficient on x_o/ℓ as $\ell \rightarrow x_o$, as one can see from Equation 23.

Spielman and Jacob[51] measured the mass transfer rate from a flat plate by evaporation of water into an air jet and concluded that the approach-section function of Maisel and Sherwood gave a better correlation. However, their results are somewhat doubtful in view of the high uncertainties (± 40%) involved. It has been pointed out by Tribus[51] in discussing Spielman and Jacob's paper that the boundary conditions required that the equation have a singularity at the point where the temperature or vapor pressure discontinuity occurred, therefore the formula by Maisel and Sherwood was more realistic than that of Jacob and Dow.

Theoretical formulas for the influence of the approach length have been obtained by Seban[52], Rubesin[53], and Reynolds et al.[54]. So far the experimental data are not extensive enough to make a clear choice among the various empirical and theoretical formulas. This is also due to the difficulty that the differences among the various formulas are of the same order of magnitude as the uncertainties involved in most experimental results.

Influence of Transverse Curvature

The presence of curvature normal to the flow direction affects the boundary layer structure, and hence the momentum, heat, and mass transfer. In general, a transverse curvature decreases the rates of heat and mass transfer in the case of flow in a pipe (concave curvature); whereas for flow outside an external surface, a transverse curvature (convex curvature) increases the rates of heat and mass transfer. This can be physically visualized since in the former case the surface area normal to the heat or mass flux decreases as it moves away from the solid-fluid interface, and the situation is reversed in the latter case.

The boundary layer equations for the axisymmetrical flow of a viscous fluid past a body of revolution were first derived by Boltze[55]. Millikan[56] solved these equations by using an approximate integral method and gave numerical results for an airship movel. Since the Boltze formulation is based on the assumption that the boundary layer thickness is much smaller than the radius of the transverse curvature, the method developed by Millikan does not apply when the influence of the transverse curvature on the structure of the boundary layer becomes important.

The influence of the transverse curvature on skin friction and heat transfer in a laminar boundary layer from a cylinder in axisymmetrical flow was first solved by Seban and Bond[8] in the form of series expansions in terms of the ratio of flat plate displacement thickness to radius curvature. Important numerical corrections to their work have been made by Kelly[57], and the resulting solution is referred to as the Seban-Bond-Kelly solution. For a Prandtl number of 0.715, the result for heat transfer can be expressed as follows

$$\frac{(Nu_x)_{cylinder}}{(Nu_x)_{plate}} = 1 + 2.30\left(\frac{x}{a}\right) Re_x^{-1/2} \qquad (26)$$

The leading term of the expansion is the corresponding flat plate expression, and the subsequent terms are corrections for the transverse curvature. Since the convergence of the solution is poor as the boundary layer becomes thick, the solution is valid only for the regime close to the leading edge of the cylinder. Since then, Mark[58], Stewartson[59], and Glauert and Lighthill[60] have obtained approximate solutions by means of the momentum integral method for the skin friction which cover the entire range from weak curvature effects close to the leading edge of the cylinder to strong curvature effects far downstream. Asymptotic solutions for the heat transfer rate in the regimes of strong and moderate curvature effects have also been obtained by Bourne and Davies[61], and Bourne, Davies and Wardle[62]. The combined

effects of transverse curvature and mass injection have been studied by Steiger and Bloom[63, 64], and Wanous and Sparrow[65]. The extension of the solutions to other bodies of revolution such as cones and parabolas have been discussed by Yasuhara[66] and Raat[9]. Christian and Kezios[38] measured the rate of mass transfer by sublimation from the outer surface of a hollow naphthalene cylinder in a parallel air stream. Their data indicated a smaller effect of curvature than any of the theoretical results discussed above. However, the range of their measurement was not extensive enough to lead to a decisive conclusion, particularly in view of the soundness of the theoretical analyses.

The picture for the turbulent boundary layer is still very obscure. No rigorous theoretical analysis is available. Most measurements in heat transfer from bodies of revolution in axisymmetrical flow have been carried out with large objects at high flow speeds by aeronautical engineers. Due to the small boundary layer thicknesses and large radii of curvature involved, little information concerning the influence of the transverse curvature on the rate of heat transfer has been gained from those measurements[67]. Theoretical analyses have been limited to approximate methods based on a number of assumptions which have been justified neither theoretically nor experimentally. Experimental studies have not been satisfactory due to the fact that experimental uncertainties involved in turbulent heat and mass transfer are usually of the same order as the effect of the transverse curvature.

Jacob and Dow[35] derived an expression for the influence of transverse curvature on the rate of heat transfer by means of an approximate integral method. In carrying out the integration they assumed that for both the flat plate and the cylinder the 1/7-th power velocity distribution law holds, and that the boundary layer thickness is the same on the cylindrical surface as on a plane for equal Reynolds numbers. This leads to the following result

$$\frac{(Nu_\ell)_{\text{cylinder}}}{(Nu_\ell)_{\text{plate}}} = 1 + 0.3\,\frac{\delta}{a} \tag{27}$$

The thickness of the turbulent boundary layer, δ, can be deduced from the 1/7-th power law,

$$\delta = 0.37\,x\,Re_x^{-1/5} \tag{28}$$

Since the influence of curvature is a second-order effect (in comparison with the first term which corresponds to heat transfer from a flat plate), the use of an approximate method which involves a number of unverified assumptions may give poor results. This can be seen when one uses Jacob and Dow's method to evaluate the influence of curvature on the heat transfer rate in a laminar boundary layer. This leads to

$$\frac{(Nu_x)_{\text{cylinder}}}{(Nu_x)_{\text{plate}}} = 1 + 3.94\left(\frac{x}{a}\right) Re_x^{-1/2} \tag{29}$$

A comparison of Equation 29 and the exact Seban-Bond-Kelly solution, Equation 26, shows that the influence of curvature obtained by Jacob and Dow's method is almost twice the exact solution. Another weak point of Equation 27 is that its convergence is poor. From Equations 20, 27, and 28, one obtains the following expression for heat transfer from a cylinder

$$\frac{\dot{q}}{t_s - t_a} = 0.0296\, k\, Pr^{1/3} \left(\frac{U_\infty}{\nu}\right)^{0.8} \frac{1 + 0.222 \left(\frac{U_\infty}{\nu}\right)^{-1/5} \frac{x^{0.8}}{a}}{x^{0.2}}$$

$$= 0.0296\, k\, Pr^{1/3} \left(\frac{U_\infty}{\nu}\right)^{0.8} \left[\frac{1}{x^{0.2}} + 0.222 \left(\frac{U_\infty}{\nu}\right)^{-1/5} \frac{x^{0.6}}{a}\right] \tag{30}$$

The $1/x^{0.2}$ term, which corresponds to the heat transfer from a flat plate, indicates that the local coefficient decreases with increasing x, as expected. But the second term, which is proportional to $x^{0.6}$, increases with x at a much higher rate and may overcome the decrease in the first term when the boundary layer thickness reaches a certain high value. In other words, the Jacob-Dow formula predicts that the rate of heat transfer at first decreases with x, reaches a minimum, and then increases with x. This phenomenon has never been observed experimentally and is difficult to conceive physically.

A method which removes the assumption that the boundary layer thickness is unaffected by curvature has been derived by

Landweber[68] and H. U. Eckert[69]. The results are expressed as the ratio of friction factors in terms of the boundary layer thickness and cylinder radius

$$\frac{f_{cylinder}}{f_{plate}} = \left(1 + \frac{1}{3}\,\frac{\delta}{a}\right)^{1/5} \tag{31}$$

$$\frac{\overline{f}_{cylinder}}{\overline{f}_{plate}} = \frac{1 + 0.30\,\frac{\delta}{a}}{\left(1 + \frac{1}{3}\,\frac{\delta}{a}\right)^{4/5}} \tag{32}$$

The boundary layer thickness, δ, is evaluated from

$$\delta = 0.37 \times Re^{-1/5}\left(1 + \frac{1}{3}\,\frac{\delta}{a}\right)^{4/5} \tag{33}$$

which is obtained by the momentum integral method and the 1/7-th power law.

The skin-friction measurements of Chapman and Kester[70] show that the influence of curvature is lower than the prediction of the Jacob-Dow analysis and higher than the prediction of the Landweber-Eckert analysis. No conclusion can be made from their experimental results concerning the relative merits of these two approaches.

Heat Transfer vs. Mass Transfer

In the above discussions we have considered heat and mass transfer as identical problems. This is approximately true since

the energy and diffusion boundary layer equations have the same form. However, it should be pointed out that heat transfer and mass transfer are not exactly analogous since in mass transfer the normal velocity at the phase interface is not zero, rather the interface serves as a sink or source of the diffusing component. This boundary condition makes the momentum boundary layer equation no longer independent but coupled with the diffusion boundary layer equation. The diffusion of a second component from the interface to the fluid (or vice versa) directly affects the boundary layer structure. In heat transfer the interfacial velocity remains zero. Temperature variations across the boundary layer can only change the velocity profile in an indirect way, namely by changing the properties of the fluid. When the temperature gradient is not very high, the momentum boundary layer equation can be treated independently of the heat transfer process.

Acrivos[71] has developed asymptotic expressions for mass transfer in laminar boundary layer flows in the two-dimensional case. No general and exact method is available to treat the problem of nonvanishing interfacial velocities.

EXPERIMENTAL EQUIPMENT

The principal parts of the equipment employed in this study were the porous cylinder, the liquid injection system, and the air supply system. Auxiliary equipment included devices for measuring temperature and humidity, pitot tube, and micro-manometers.

The one-inch porous cylinder with a hemispherical nose-piece was placed vertically above a square air jet. Liquid was supplied to the porous surface at predetermined rates from an injector. A photograph of the experimental equipment is shown in Figure 3.

Air Supply System

Figure 4 shows a schematic diagram of the air supply system. The equipment used in this work was essentially the same as that described by previous investigators in this laboratory[7,72], except that a square jet was used instead of the original rectangular jet. This open-circuit air tunnel was originally designed by Sage and coworkers for the measurement of heat and mass transfer rates from liquid drops, metal and porous spheres, at average air velocities from 4 to 32 feet per second at the opening of the converging jet.

Air was pressed by two blowers, A, over wire grid heaters, B, through a Venturi meter, V, into a system of 12-inch square ducts, and then into a converging jet which has a 6-inch square

opening. The air blowers were driven by a direct current motor. A glass-fiber filter was installed at the air inlet to the blowers to provide clean air to the system. The bends in the ductwork were equipped with vanes to reduce disturbances to the air stream due to sudden changes in the flow direction. The smoothly converging jet, shown in Figure 5, with a nozzle-contraction ratio of 4, and the screens at the bottom of this section, S, were used to reduce turbulence to a low value in the test region. They also provided a relatively flat velocity profile at the jet opening. According to Hsu[73], the level of turbulence of the air stream leaving the converging jet was approximately 1.3%.

The duct and the converging section were provided with heaters which could be regulated independently to control the temperature of the air stream. The reader is referred to Corcoran et al.[74] for details of the temperature control system.

Nine 36-gauge copper-constantan thermocouples were located in the duct and jet to measure the temperature. The air temperatures at the Venturi meter and at a point upstream of the converging section were determined by means of platinum resistance thermometers, shown at D and E, respectively, in Figure 4. The resistance of the platinum resistance thermometers was measured with a Mueller bridge, and the e.m.f. produced by the thermocouples was determined with a White potentiometer. The cold junctions of the thermocouples were maintained at the ice point. All temperature measurement devices were calibrated

by comparison with a standard platinum resistance thermometer which was calibrated by the National Bureau of Standards.

The pressure difference across the Venturi meter was used to establish the mass rate of air flow through the system. Kerosene and mercury manometers along with a precision cathetometer were used in the Venturi measurement. The moisture content in the air was measured by means of wet-and-dry bulb thermometers.

Porous Cylinder

The cylinder is shown in Figure 6 before assembly and in Figure 7 after assembly. It consisted of an approach section, a porous section, and a downstream section. All parts, with the exception of the porous section, were made of brass. The porous section was made of medium-grade diatomacious earth manufactured by the Allen Filter Corporation.

Four different lengths of approach section of 1.973, 4.973, 9.973, and 19.973 inches were used. By using different approach lengths, the Reynolds number could be varied independently of the air velocity and the influence of the approach length on the rate of mass transfer could also be studied.

Two porous sections of 0.500 inch and 0.715 inch were tested. The 0.500-inch porous section is shown in Figure 8. Due to its softness, the edges of the porous section tended to

become rounded. Though extreme care was taken during the machining and assembling, a discontinuous line with a width and depth of approximately 0.002 inch still existed between the approach section and the diatomacious earth. Fortunately, when liquid was fed into the porous earth, the liquid on the surface smoothed out this discontinuity.

Isothermal mass transfer was achieved by supplying energy from a heater coil placed in the helical grooves shown in Figure 8. The use of a coil instead of a straight wire provided more uniform heating and also made the assembly easier. The detailed specifications of the heater are described in Table I. The energy required was supplied by 6-volt batteries. A resistor was used to adjust the energy input to the heater.

The 18-inch downstream section provided a smooth air stream after the porous section and thus prevented deformation of the external flow by the cylinder support, shown in Figure 9. The 3-inch gutter which supported the cylinder from the top also contained the liquid line and the electrical wires. The downstream section had an inner passage of 1/8-inch diameter, which served as the liquid-supply line to the porous section. The thermocouple and heater leads were also passed through this passage.

The cylinder was carefully positioned so that the cylinder axis and the jet axis were on the same line. It was believed that the angle of attack was less than five tenths of a degree. This introduced a negligible correction to the mass transfer data,

as previous investigators[70] already showed that the skin friction was independent of the angle of attack variations up to the order of one degree.

Liquid Injection System

The evaporating component was supplied to the evaporating surface at a predetermined rate from a liquid injector. A method of control of a predetermined flow rate developed by Reamer and Sage[75] was employed. Figure 10 shows a photograph of the injector and some associated mechanisms. The speed of the motor which drove the injector was controlled by a quartz oscillator and a preset counter. For the details of the control circuit, the reader is referred to the original paper by Reamer and Sage. The liquid in the injector was maintained at a constant temperature of 100°F by means of an oil bath.

The liquid rate was so controlled that the evaporating surface was completely covered by a very thin liquid film, but no excess liquid was accumulated on the surface. In other words, the liquid injection rate was equal to the rate of evaporation at the porous surface. The attainment of this steady state was determined with a manometer with a small diameter of 0.025 inch.

Figure 11 shows schematically the liquid feeding system. Due to the rather small capacity of the injector (20 cc.), a large reservoir, R, of 5-inch inside diameter was used to supply the

liquid sample to the evaporating surface when no reading was being taken. The liquid level in the reservoir usually dropped by less than 3 mm. during a test period of one hour. The relatively constant liquid level and the fact that liquid was raised to the evaporating surface mainly by the capillary force enabled the maintenance of a constant flow rate from the reservoir to the evaporating surface and kept the system at a steady state. The liquid level (relative to the porous section) in the large reservoir could be adjusted conveniently by a traversing gear which moved the reservoir in the vertical direction.

As shown in Figure 11, two manometers were used. Manometer M_1, which was taped close to the porous cylinder, was used to determine the correct injection rate as described above. The second manometer M_2, which was taped close to the reservoir R, was used along with M_1 to determine the pressure drop of the liquid from the reservoir to the cylinder. The difference in the liquid levels in M_1 and M_2 provided an approximate value of the flow rate from which one could estimate the injector speed to be used.

The whole liquid injection system was evacuated by means of a vacuum pump before it was filled with liquid. This ensured that the liquid in the system was free of air bubbles. The liquid sample was purified and deaerated before adding to the injector and the reservoir. To avoid the accumulation of impurities on the evaporating surface, the porous section was washed periodically

with purified sample. When no test was being made, a test tube was used to surround the porous surface. The slight loss of liquid due to diffusion into the stagnant air was continuously compensated by filling from the reservoir. The rather tedious liquid filling process did not have to be repeated unless leakage was discovered.

Measurement of Evaporating Surface Temperature

The measurement of surface temperature is always an important and difficult matter in heat and mass transfer experiments. In heat transfer, the temperature difference between the solid-fluid interface and the free stream is used directly to establish the heat transfer coefficient. In mass transfer, due to the strong dependence of vapor pressure on temperature, accurate measurement of the surface temperature is equally important. The dependence of the vapor pressure on temperature for the samples used in this experiment was not as strong as for most liquids, such as water, but still amounted to 2.5% for n-heptane and 2.8% for n-octane, per degree Fahrenheit. The evaporation of a liquid on the porous surface essentially formed an energy sink at the interface, which established a large temperature gradient at the neighborhood of the evaporating surface. This made accurate measurements even more difficult. The position of the thermocouple became a very important problem in this experiment.

The direct extension of thermocouple wires from the inside

of the cylinder to the outer surface would not be satisfactory for two reasons. First, it is difficult to locate the junction at the correct position. Secondly, the large temperature gradient inside the porous earth would affect the reading of the thermocouple. The thermocouple wires must travel through a distance of a constant temperature region before they reach the junction in order to obtain accurate measurements.

During the construction of the porous cylinder, 0.003-inch copper and constantan wires were passed from the inside of the cylinder and extended to the surface at an angle of 45°. The wires traveled through an equal distance on the surface to meet at the junction which was soft soldered. A groove had been cut beneath the wires so that about one half of the wire diameter was under the surface. With this arrangement, the error in the temperature reading due to the heat conduction along the thermocouple wires was essentially eliminated. This fixed thermocouple was located midway between the edges of the porous section.

The thermocouple as arranged above was not sufficient to determine the surface temperature. The temperature of the evaporating surface varied in the flow direction due to different local evaporating rates and due to heat conduction between the porous section and the neighboring parts. It was necessary to use a traversing thermocouple to measure the surface temperature at different positions in the flow direction. The readings were then

averaged to obtain the surface temperature to be used in the calculation of the experimental results.

Figure 12 shows the traversing thermocouple and its probe at a measuring position. When a reading was being taken, the thermocouple was pressed against the porous surface to form an arc. This provided isothermal regions on both sides of the junction to minimize errors due to heat conduction along the wires. The traversing thermocouple was also made of 0.003-inch copper and constantan wires. The thermocouple probe was mounted on a traversing gear, which located the position of the thermocouple to within 0.001 inch in the direction of the axis of the cylinder.

Local Velocity Measurement

Local velocities were measured by means of a pitot tube and a micromanometer. The micromanometer was attached to a traversing mechanism which was able to determine the vertical position of the liquid level to an accuracy of 0.0005 inch.

MATERIALS AND THEIR PROPERTIES

N-heptane and n-octane

N-heptane and n-octane were chosen as the diffusing components for the following reasons:

1. Their vapor pressures at room temperature are typical in many chemical processes. They are of the same order as the vapor pressure of water. The use of hydrocarbons instead of water also avoids the uncertainties involved in the measurement of the moisture content in the air stream.
2. The dependence of their vapor pressures on temperature is small compared to other compounds. This reduces the experimental error due to the uncertainty involved in the measurement of the temperature of the evaporating surface.
3. Physical properties required for the correlation of experimental data are available in the literature.
4. High-purity samples can be obtained at relatively low cost.
5. Small amounts of the sample present in the air do not give any unpleasant odor or harmful affects.

The samples used were pure-grade n-heptane and n-octane obtained from the Phillips Petroleum Company. They had purities better than 99% according to the manufacturer. The sample was first distilled through a laboratory-scale distillation column before being placed in the deaerating system described in Appendix I. The liquid fed to the porous surface was free of air and had an esti-

mated purity greater than 99.8%. The 0.2% impurities probably introduced little error to the final experimental results due to the fact that they have approximately the same vapor pressure and molecular weight as the main component. Therefore, for the purpose of this work the samples could be considered as pure substances.

The properties of n-heptane and n-octane used in correlating the experimental data were as follows:

1. Vapor Pressures: The vapor pressures were calculated from the Antoine equations and the constants given by Rossini[76]

$$\log p = A - \frac{B}{C + t}$$

for n-heptane:

A = 5.21016

B = 2439.227

C = 345.131

for n-octane:

A = 5.18879

B = 2282.607

C = 358.420

2. Diffusivities: The diffusivity of n-octane in air was calculated from the following equation taken from the International Critical Tables[77]:

$$D_{F,k} = 1.1274 \times 10^{-4} \left(\frac{T}{428}\right)^{2.00} \left(\frac{14.696}{P}\right) \quad ft^2/sec$$

The diffusivity of n-heptane in air was taken from the data of Schlinger et al.[78] and was fitted into the following equation:

$$D_{F,k} = 0.8336 \times 10^{-4} \left(\frac{T}{560}\right)^{1.64} \left(\frac{14.696}{P}\right) \quad ft^2/sec$$

for $520^\circ R \leq T \leq 660^\circ R$.

3. Specific Volumes: The specific volumes of liquid n-heptane and n-octane were taken from Rossini[76]. At $100^\circ F$ and 1 Atm.,

$V = 0.02388\ ft^3/lb$ for n-heptane

$V = 0.02374\ ft^3/lb$ for n-octane

Air

Air was considered as a single component in this work since its composition was uniform. The specific volume of air was calculated from the pressure, temperature and humidity. The viscosity of air was taken from Hsu and Sage[79].

EXPERIMENTAL RESULTS

Flow Conditions

The first step during each test was to bring the air stream to the desired flow rate and temperature. In order to ensure the steady-state operation of the equipment during the course of the measurement, the air flow was started at the desired velocity about 4 hours before data were taken. During the stabilization period, measurements of the temperatures in the air duct and jet and of the pressure difference across the Venturi were made periodically. Those measurements along with the atmospheric pressure, room temperature and humidity measurements were used to establish the flow rate. The average air velocity at the jet opening was calculated from the following equation

$$U_{avg} = \frac{\dot{m}_a}{A} \cdot \frac{ZbT}{P} \tag{34}$$

The weight flow rate and average velocity were not directly used to evaluate the Reynolds number, but were important for the establishment of flow conditions. The measurements of the flow conditions were made also before and after each test to ensure that steady-state conditions were maintained throughout the test period. Table II presents the conditions under which the experimental data were taken.

All tests were made at an air temperature of $100^{\circ}F$, with a maximum uncertainty of $\pm 0.3^{\circ}F$. The weight rate of the

air flow was kept within 0.3% of the desired value throughout each test. The average velocity ranged from 4 to 32 feet per second.

Velocity Distribution at Jet Opening

Although the smoothly converging jet with a high nozzle-contraction ratio and the turbulence-damping screens succeeded in providing a flat velocity profile at the opening of the air jet, the velocity of the air stream at the central core was considerably higher than the average velocity measured by the Venturi meter. This was inevitable because the flow of a viscous fluid requires that the velocity at the wall be zero. Consequently, there were large velocity gradients close to the wall.

The velocity distribution in the air jet was measured by using a pitot tube at a plane 1/4 inch below the jet opening. The results for the average velocity at 32 and 8 feet per second are shown in Figures 13 and 14, respectively. The velocity at the central core was 4.5% higher than the average velocity measured by the Venturi meter at an average velocity of 32 ft/sec, and 14.5% at 8 ft/sec. We shall call the air velocity at the central core of the jet as U_∞ for reasons to be discussed in the next section. Figure 15 shows the values of U_∞/U_{avg} as a function of the average velocity. The dotted line represents extrapolated values. Higher flow rates gave flatter velocity profiles as expected.

The velocity distributions were integrated over the entire cross-sectional area and compared with the Venturi measurements.

The average velocity obtained by integration agreed with the Venturi measurement to within 0.5% for U_{avg} = 32 ft/sec, and 1.5% for U_{avg} = 8 ft/sec. The deviations mainly resulted from the difficulty in measuring velocities at positions close to the wall. The velocities at the corners of the square jet were very low. This phenomenon was also observed by Prandtl[80] and Nikuradse[81].

Reynolds Number

Since the boundary layer thickness for flow along a plate or a cylinder increases in the flow direction, the correct length parameter should be the distance along the interface from the stagnation point as has been verified both theoretically and experimentally[1]. In this work, the Reynolds number will be defined as

$$Re_{\ell} = \frac{U_{\infty} \ell}{\nu} \tag{35}$$

where ℓ is the sum of the approach length and the wetted length, $\ell = x_o + x_w$. The equivalent length of the nosepiece is assumed equal to the length of a cylindrical section with the same external surface area. For a hemispherical nosepiece, this equivalent length happens to be equal to its radius. Figure 16 shows the relevant coordinate system used in this work.

The air stream which emerged from the air jet had a nearly constant-velocity core of approximately 5-inch diameter, as shown

in Figures 13 and 14. During each test, a pitot tube was placed parallel to the cylinder axis just outside the boundary layer at the wetted section to measure the velocity of the external flow. It was found that this velocity, U_∞, was essentially independent of the distance from the jet opening, except for the test made at $x_o = 19.973$ inches and $U_\infty = 8.93$ ft/sec. During that test it was found that the velocity at the edge of the boundary layer was 3% lower than the correct value. When a thermocouple was placed in the boundary layer, temperature fluctuations larger than $1^\circ F$ were observed. It appeared that an interaction between the boundary layer on the wall and the free jet mixing region occurred in this particular test. This was not observed in other tests. The boundary layer on the cylinder wall remained well within the potential core of the free air jet, with the one exception just mentioned, and the velocity of the external flow could be taken as equal to the air velocity at the potential core leaving the converging jet.

A series of three or more tests was made at different air velocities at a fixed approach length. After the completion of each series of tests, the approach section was changed to a different length and the position of the cylinder was readjusted to ensure that the stagnation point was at the jet opening.

Four approach lengths of 1.973, 4.973, 9.973 and 19.973 in. were used. The Reynolds number ranged from 5,000 to 310,000.

Temperature of Evaporating Surface

When the air flow was adjusted to the desired conditions and remained steady-state, the test tube surrounding the porous section was removed and electric energy was supplied from the batteries to the heater inside the porous section. One or two 6-volt batteries were used depending on the rate of evaporation. Usually, it took 30 to 60 minutes for the surface temperature to reach a steady value of 100°F as indicated by the fixed thermocouple at the middle of the porous section. Suitable adjustment of the resistor kept the surface temperature to within 0.1°F of the desired value for the duration of the test being carried out.

Tests were also made without energy supply from the heater inside the porous section. Under this condition, the energy required for the evaporation of the liquid from the porous surface came from the air stream and the neighboring parts in contact with the porous section. When steady-state conditions were reached, the surface temperature was 10 to 15 degrees lower than the temperature of the main air stream, depending on the rate of evaporation and the position of the porous section. These tests will be referred to as "nonisothermal evaporation," and the tests made under nearly-isothermal conditions will be referred to as "isothermal evaporation."

Immediately after the evaporation rate was determined, temperatures at 9 or more points along the porous surface in the longitudinal direction were measured with the traversing thermo-

couple for the purpose of evaluating the average surface temperature. The method of evaluating the average surface temperature is described in Appendix II.

The traversing thermocouple agreed with the fixed thermocouple to within 0.2°F when they were within 0.005 inch. This indicated that the temperature measurement by the traversing thermocouple was reliable. It was also found that the presence of this traversing thermocouple did not have any appreciable influence on the rate of evaporation of the liquid. In other words, the thermocouple did not affect the boundary layer to a degree sufficient to introduce errors to the measurement. Tests were made to determine the dependence of the average surface temperature on the angular positions. The difference in the average surface temperature at different angular positions had a maximum of only 0.1°F, and could be neglected for practical purposes.

In spite of all the precautions, the uncertainties involved in the measurement of the evaporating surface temperature probably contributed the major share of errors to the final experimental results, due to the inherent difficulties. It was estimated that the uncertainty in the average surface temperature was probably up to 0.4°F, mainly due to the errors in the measurement and in the averaging process.

Rate of Evaporation

After the air flow, evaporation rate, and evaporating surface temperature had reached steady-state conditions, the liquid injector was started at a speed estimated from the pressure drop between the liquid reservoir and the porous cylinder shown in Figure 11. The valve to the reservoir was then closed. The liquid level in Manometer M_1 was used as an indicator for adjusting the liquid injection rate to the correct value by means of the preset counter. The measurement was continued for approximately 20 minutes to ensure that the injection rate was correct and that the experimental conditions were steady. The preset counter as well as the fixed thermocouple were read at about 3-minute intervals. They agreed exactly except when mechanical or electronic failures occurred. At the end of the measurement the valve to the liquid reservoir was opened and the injector was re-filled with liquid from a liquid loading system described in Appendix I.

It was observed that when the liquid rate was at the vicinity of the desired value, the liquid level in Manometer M_1, shown in Figure 11, was very sensitive to the feed rate. A liquid rate of 0.3% higher than the correct value would cause the evaporating surface to flood with excess liquid and the liquid level in the manometer would rise by more than 1 cm. On the other hand, if the liquid rate was 0.3% lower than the correct value, the liquid would retreat from the evaporating surface and the liquid

level in the manometer would drop by more than 1 cm. This sensitive method provided an accurate measurement of the injection rate. It appeared that when the liquid sample was injected at the correct rate, the evaporating surface was completely covered by a very thin liquid film but no excess liquid was accumulated on the surface. This phenomenon is independent of the porosity of the porous material, provided that the material has a sufficiently high porosity and the pore diameters are small enough to give a high capillary pressure[†‡].

The results of this measurement are shown in Table III. The reproducibility of the liquid rate measurement was better than 1%, with a few exceptions.

Sherwood Number

From the rate of evaporation, the surface temperature, and physical properties of air and the diffusion substance, one can calculate the Sherwood number from the following expression

$$Sh_{\ell}^{*} = \frac{\dot{m}_k b_k T\ell}{2\pi a x_w D_{M,k} \ln\left(\frac{p_{j\infty}}{p_{js}}\right)} \tag{36}$$

[†] This method has been used by Sage and coworkers for measurements of mass transfer rates from porous spheres. See, e.g., references (79) and (83).

[‡] Assuming that the diatomacious earth has pore radii of the order of 1 micron, the surface tension will give a capillary pressure of 5 psi, which is sufficient to raise the liquid to a height of 15 feet against the gravitational force. This high capillary pressure accounts for the high sensitivity of the method used.

which is derived in detail in Appendix III. The logarithmic term in Equation 36 results from the net flow due to the diffusion of one component into a second component. We shall call the Sherwood number defined by Equation 36 the "modified Sherwood number" since it does not come directly from the conventional definition. The validity of this expression will be discussed in a later section.

Equation 36 represents the average modified Sherwood number because the average weight rate of evaporation was used in the calculation. The partial pressure of the diffusing component at the solid-air interface was assumed equal to the vapor pressure of the liquid at the interface. The results of this calculation are also shown in Table III.

Theoretically, fugacity difference instead of partial pressure difference may be the more logical choice as the driving force for mass transfer[82]. However, the concentration of the diffusing component in this experiment was low, thus the difference between the fugacity and the partial pressure was small. The consistent use of partial pressure throughout this work should introduce few errors. The use of partial pressure also comes from the practical reason that diffusivities obtained from the literature are based on partial pressure rather than the fugacity.

A summary of the range of experimental data is given in Table IV.

Remarks on Variable Physical Properties

Since the diffusion boundary layer was thin relative to the momentum boundary layer and the concentration of the diffusing component was small, the mass transfer process had little effect on the boundary layer flow. The physical properties of the free stream air were used to calculate the Reynolds number. On the other hand, the Sherwood number and the Schmidt number are directly related to the mass transfer process, and were therefore evaluated at the mean temperature:

$$t_m = 1/2(t_a + t_s) \tag{37}$$

The influence of the diffusing component on the kinematic viscosity is not known and was neglected in the calculations.

DISCUSSION OF RESULTS

Influence of the Interfacial Velocity

The mass transfer problem differs from the corresponding heat transfer problem by the fact that the normal velocity at the phase boundary is not zero. The evaporation and transfer of a liquid into an air stream create an additional net flow in the gas phase. The chemical engineer usually incorporates this net flow into the Sherwood number by considering the diffusion of a second component through a stagnant gas. With this method the average Sherwood number, which we call the average modified Sherwood number, can be expressed by Equation 36[†] on page 44, for the particular system in this work. This method does not take into account the influence of the interfacial velocity in an exact way since we are dealing with a convective system, but it gives a good approximation when the concentration of the diffusion component is much smaller than that of the main stream fluid. This method is useful in engineering work because of its simplicity and usefulness in the direct comparison of various results for heat and mass transfer.

If the interfacial velocity in mass transfer is neglected, the average Sherwood number assumes the following form

---

[†] A similar expression has been used by Sage for mass transfer from porous spheres. See, e.g., references (72) and (83).

$$Sh_{\ell} = \frac{\dot{m}_k b_k TP\ell}{2\pi a x_w D_{M,k}(p_{j\infty} - p_{js})} \qquad (38)^{\dagger}$$

which is analogous to the Nusselt number in the heat transfer case. A comparison of Equations 36 and 38 gives the following relationship between the average modified Sherwood number, Sh_{ℓ}^{*}, and the average Sherwood number, Sh_{ℓ}:

$$\frac{Sh_{\ell}}{Sh_{\ell}^{*}} = \frac{P}{p_{jm}} \qquad (39)$$

where

$$p_{jm} = \frac{p_{j\infty} - p_{js}}{\ln \frac{p_{j\infty}}{p_{js}}} \qquad (40)$$

that is, the log mean value of $p_{j\infty}$ and p_{js}.

In order to determine the relative merits of Equations 36 and 38 in this experiment, a series of tests (Series A, Table III) was made with n-heptane as the diffusing component. The results were compared with the measurements with n-octane as the diffusing component under the same experimental conditions.

Table V shows the results expressed in $Sh_{\ell}^{*}/Sc^{1/3}$ and in $Sh_{\ell}/Sc^{1/3}$. When the modified Sherwood number is used, the

---

†See Appendix III for the details of the derivation.

results for n-heptane and n-octane have excellent agreement at low Reynolds numbers. At higher Reynolds numbers the agreement is not so good and deviations up to 9.5% are obtained. Over the whole range of the experiment, the use of the unmodified Sherwood number, Equation 38, gives poor agreement between the results for n-heptane and n-octane, with deviations from 2.5 to 14%. For all the tests shown in Table V, the use of Sh_ℓ^* gives better results than the use of Sh_ℓ. This indicates that the modified Sherwood number as expressed by Equation 36 should be used in correlating the results of this experiment.

The larger deviations at higher Reynolds numbers mentioned above are probably because those data are in the transition region, as will be discussed in the next section.

We have assumed that the Sherwood number is proportional to the one-third power of the Schmidt number in the above analysis. This relationship is nearly true when the Schmidt number is not far from unity according to Schlichting[1]. Since the Schmidt numbers for the n-heptane-air system (2.18) and for the n-octane-air system (2.28) are quite close, any deviation from this assumption would not affect the conclusion made above.

Transition from Laminar to Turbulent Boundary Layer

The transition of the boundary layer from the laminar to the turbulent regime can be observed from mass transfer data. In

the laminar regime the Sherwood number is approximately proportional to the one-half power of the Reynolds number, and in the turbulent regime approximately to the eight-tenths power. When the Sherwood number is plotted against the Reynolds number with log-log scales a change in the slope of the curve from 0.5 to 0.8 indicates a transition from the laminar to the turbulent boundary layer.

In this experiment, the transition was observed only when the porous section was at the lowest position, i.e., $x_o = 1.973$ inches. Figures 17, 18, and 19 show evidence of the occurrence of transition in three groups of data. It appears that the transition took place at $Re_\ell = 10^4$ to 1.5×10^4. This relatively low critical Reynolds number, as was also observed by Jacob and Dow[35], was probably due to the use of a hemispherical nosepiece.

Isothermal vs. Nonisothermal Evaporation

The results for both isothermal and nonisothermal evaporation are shown in Table III. The physical properties used in calculating the average modified Sherwood number and the Schmidt number were taken at an average temperature defined by Equation 37, page 46, that is, the average of the temperatures of the free air stream and the evaporating surface.

With a few exceptions, the results for both cases agree remarkably well.

Empirical Correlation of Experimental Data

In Figure 20 the average modified Sherwood numbers are plotted versus the Reynolds number for various ratios of the unwetted approach length to the total length, x_o/ℓ. A theoretical curve by Schlichting[1] for mass transfer from a flat plate is shown in the same figure for comparison. The slope for each series of data taken at a fixed value of x_o/ℓ varies from 0.76 to 0.8 for $Re_\ell > 15,000$. The slight deviations from the well-known relation for the turbulent boundary layer

$$Sh_\ell^* \sim Re_\ell^{0.8} \tag{41}$$

are probably partially due to the influence of the transverse curvature. This is understandable since at low velocities the boundary layer thickness is greater and the influence of transverse curvature on the mass transfer rate is accordingly greater, as discussed in detail on page 18. In other words, one expects higher mass transfer rates at low velocities than the prediction of Equation 41. The effect of transverse curvature will be discussed further in the next section.

From the scattering of the data shown in Figure 20, one can see that the length of the unwetted approach section apparently had an influence on the Sherwood number. In the presence of an approach length the diffusion boundary layer does not begin at the same position as the momentum boundary layer. It is physically clear

that if x is close to x_o, the presence of this section will noticeably increase the rate of mass transfer from the wetted surface to the air stream due to the large concentration gradient.

Several approach-length functions were tested. It was found that the following formula

$$\frac{Sh_\ell^*}{(Sh_\ell^*)_{x_o=0}} = \frac{1}{[1 - (x_o/\ell)^{0.8}]^{0.11}} \tag{42}$$

obtained by Maisel and Sherwood[13] from their mass transfer data for the evaporation of water from a flat plate gave a good correlation for the present data.

The experimental results of Maisel and Sherwood indicate that Equation 42 is applicable for $x_o/\ell = 0.45$ to 0.95. This formula also gives good correlation with the heat transfer measurements of Jacob and Dow[35] for $x_o/\ell = 0.101$ to 0.606. In this work the range of data is $x_o/\ell = 0.734$ to 0.975. Since as $x_o/\ell \to 0$ the effect of the approach length becomes very small, it appears that Equation 42 is applicable for $x_o/\ell = 0$ to 0.975.

Combining Equations 41 and 42 and assuming that the Sherwood number is proportional to $Sc^{1/3}$, one obtains an empirical

formula of the following form:

$$Sh_\ell^* = C\, Sc^{1/3} Re_\ell^{0.8} \frac{1}{[1 - (x_o/\ell)^{0.8}]^{0.11}} \tag{43}$$

By fitting this formula to the experimental data, the constant C was found to be 0.048. Thus we have the following empirical relation

$$Sh_\ell^* = 0.048\, Sc^{1/3} Re_\ell^{0.8} \frac{1}{[1 - (x_o/\ell)^{0.8}]^{0.11}} \tag{44}$$

for $Re_\ell > 15,000$. Equation 44, along with the experimental data, is plotted in Figure 21.

As mentioned on page 40, an interaction between the boundary layer on the cylinder surface and the mixing region of the air jet[84] was observed for the test made at $x_o = 19.973$ inches and $U_\infty = 8.93$ ft/sec. For this test, the mass transfer rate was about 20% higher than expected and was excluded from the above correlation.

For $Re_\ell < 10,000$, the data agree well with the laminar boundary layer relation

$$Sh_\ell^* \sim Re_\ell^{1/2} \tag{45}$$

and therefore appear to be in the laminar boundary layer regime. The application of the approach-length function, Equation 42, made

the data fall nicely on a single curve represented by the following expression

$$Sh_{\ell}^{*} = 0.75\, Sc^{1/3} Re_{\ell}^{1/2} \frac{1}{[1 - (x_o/x)^{0/8}]^{0.11}} \qquad (46)$$

for Re_{ℓ} = 5,000 to 10,000, as shown in Figure 21.

The dependence of the Sherwood number on the Schmidt number has been assumed to be $Sh_{\ell}^{*} \sim Sc^{1/3}$. This was not tested experimentally in this work since the difference between the Schmidt numbers of n-heptane and n-octane was only 4.7% and was not sufficient to arrive at a meaningful conclusion.

Comparison with Previous Work

A. Laminar Boundary Layer

Mass transfer from a flat plate with a step-function variation of surface concentration has been solved by means of an approximate integral method[3, 17]. The results can be expressed by the following equation:

$$Sh_{x}^{*} = 0.332\, Sc^{1/3} Re_{x}^{1/2} \frac{1}{[1 - (x_o/x)^{0.75}]^{1/3}} \qquad (12)$$

In order to compare the data of this work with the theoretical prediction, Equation 12 was integrated to obtain the average Sherwood number

$$Sh_\ell^* = 0.664\, Sc^{1/3} Re_\ell^{1/2} \left\{ \frac{\sqrt{\ell}}{2x_w} \int_{x_o}^{\ell} \frac{dx}{x^{1/2}[1 - (x_o/\ell)^{0.75}]^{1/3}} \right\} \quad (47)$$

$$\frac{Sh_\ell^*}{(Sh_\ell^*)_{x_o=0}} = \frac{\sqrt{\ell}}{2x_w} \int_{x_o}^{\ell} \frac{dx}{x^{1/2}[1 - (x_o/\ell)^{0.75}]^{1/3}} \quad (48)$$

The integration was carried out by a numerical method to give the following results:

for $x_o = 1.973$ inches, $x_w = 0.500$ inch

$$\frac{Sh_\ell^*}{(Sh_\ell^*)_{x_o=0}} = 1.441 \quad (49)$$

for $x_o = 1.973$ inches, $x_w = 0.715$ inch

$$\frac{Sh_\ell^*}{(Sh_\ell^*)_{x_o=0}} = 1.321 \quad (50)$$

Equations 49 and 50 were used to extrapolate the experimental data in the laminar regime to $x_o = 0$. The results of this calculation are compared with the exact solution of Pohlhausen, Equation 14, and the empirical correlation, Equation 46, as shown in Figure 22. It is seen that the empirical formula gives an excellent correlation.

The use of the theoretical expression, Equation 12, results in a deviation of 4% between the two different wetted lengths. Moreover, the average Sherwood numbers for $x_w = 0.500$ inch are lower than the corresponding flat plate case. This is in contradiction to the fact that the transverse curvature should increase the mass transfer rate.

Although the rather narrow range of the experimental data in the laminar boundary layer regime in this work, $Re_\ell = 5,000$ to 10,000, makes one hesitate to draw a definite conclusion, the inconsistency between the experimental data and the theoretical prediction does suggest that the validity of the theoretical expression, Equation 12, for mass transfer from a flat plate with a step-function variation of surface concentration is questionable and requires further experimental verification.

B. Turbulent Boundary Layer

While the relation

$$Sh_\ell^* \sim Sc^{1/3} \tag{51}$$

has been well justified both theoretically and experimentally for the laminar boundary layer mass transfer, the picture is far from clear in the turbulent regime. This presents great difficulties in comparing measurements with different Schmidt numbers. Difficulties also exist in comparing experimental data with theoretical analyses since the turbulent boundary layer equations can not be

solved exactly and all theoretical analyses involve some assumptions which have not been fully justified. In this work, we have additional complexities introduced by the presence of the unwetted approach length and the transverse curvature. Therefore, the following discussions can only be regarded as qualitative comparisons of various results.

In Figure 23 the empirical formula obtained in this work is compared with the theoretical expression of Schlichting[1] for heat transfer from a flat plate at zero incidence, Maisel and Sherwood's measurements[13] for the evaporation of water (Sc = 0.6) from a flat plate in an air tunnel, Jacob and Dow's measurements[35] for heat transfer from a 1.3-inch cylinder to an air jet (Pr = 0.71), and Tessin and Jacob's measurements[85] for heat transfer from a 0.624-inch cylinder. All the above results were based on the assumption that the Sherwood number was proportional to the one-third power of the Schmidt number. This comparison shows that the results of this work are 15% higher than the data of Maisel and Sherwood and 30% higher than the theoretical prediction of Schlichting. The higher mass transfer rates obtained in this work are probably partially due to the influence of the transverse curvature and partially due to the inaccuracy in assuming $Sh \sim Sc^{1/3}$.

The results of Jacob and Dow are lower than results for a flat plate. This is difficult to understand since the convex transverse curvature can only increase the rate of heat transfer from the wall to the fluid stream.

In Figure 24 the data of this work are compared with the theoretical formulas of Prandtl and Taylor[86] and von Karman[87], which do not assume $Sh \sim Sc^{1/3}$. For the convenience of comparison Equation 44 is extrapolated to $x_o = 0$ and differentiated to obtain the local Sherwood number

$$Sh_x^* = 0.0384\, Sc^{1/3}\, Re_x^{0.8} \tag{52}$$

The comparison is made with $Sc = 2.28$ (n-octane-air system). The experimental data are 5 to 10% higher than the prediction of the Prandtl and Taylor equation, and 10 to 20% higher than the von Karman equation. This comparison again shows that the presence of a transverse curvature increases the mass transfer rate.

In order to reach a more quantitative conclusion concerning the influence of the transverse curvature on the rate of mass transfer, it is suggested that cylinders of different diameters be tested. A clearer picture may be obtained if the cylinder is wetted from the leading edge to eliminate the complication due to the unwetted approach length.

SUMMARY

Mass transfer from wetted surfaces on one-inch cylinders was studied by means of the evaporation of n-octane and n-heptane into an air stream in axisymmetrical flow. The porous sections had lengths of 0.500 and 0.715 inch with the ratio of the approach length to the total length varying from 0.734 to 0.975. The air stream ejected from a 6-inch square jet had velocities from 4.5 to 33.4 feet per second and the range of the Reynolds number was from 5,000 to 310,000. The results were expressed in terms of the Sherwood number as a function of the Reynolds number, the Schmidt number, and the ratio of the approach length to the total length.

The transition from the laminar to the turbulent boundary layer was observed to occur at Reynolds numbers between 10,000 to 15,000. The influence of the approach length on the Sherwood number was in good agreement with the empirical formula of Maisel and Sherwood[13]. The data for the turbulent boundary layer regime were correlated well by the following empirical expression

$$Sh_{\ell}^{*} = 0.048\ Sc^{1/3} Re_{\ell}^{0.8}\ \frac{1}{[1 - (x_o/\ell)^{0.8}]^{0.11}} \qquad (44)$$

for Re_{ℓ} = 15,000 to 310,000. For the laminar boundary layer regime, the data were in good agreement with the following

empirical correlation

$$Sh_{\ell}^{*} = 0.75\, Sc^{1/3} Re_{\ell}^{1/2} \frac{1}{[1 - (x_o/\ell)^{0.8}]^{0.11}} \qquad (46)$$

The data of this experiment did not agree with the theoretical formula by Eckert for the laminar boundary layer mass transfer from a flat plate with a step-function variation of surface concentration.

The mass transfer rates were higher than the experimental measurements and theoretical results by previous investigators. This was interpreted as due to the influence of the transverse curvature.

NOMENCLATURE

a	radius of cylinder, ft
b_k	specific gas constant of the diffusing component, $(ft)(lb_f)/(lb_m)(^oR)$
c_k	Maxwell coefficient of component k, $(lb)(sec)(ft)^2/lb\text{-mole}$
c_p	isobaric heat capacity, $Btu/(lb)(^oF)$
$D_{F,k}$	Fick diffusivity of component k, ft^2/sec
$D_{M,k}$	Maxwell diffusivity of component k, lb/sec
f	local skin-friction factor, $2g_c\tau_o/U_\infty^2\rho$
$\bar{f}$	average skin-friction factor, $2g_c\bar{\tau}_o/U_\infty^2\rho$
h_m	local mass transfer coefficient, ft/sec
g_c	conversion factor, $32.17(lb_m)(ft)/(lb_f)(sec^2)$
j_h	heat transfer j-factor, defined by Eq. 15
j_m	mass transfer j-factor, defined by Eq. 15
k	thermal conductivity, $Btu/(sec)(ft)^2(^oF/ft)$
ℓ	total length from leading edge of cylinder to the downstream edge of wetted section, ft
$\dot{m}_a$	total air flow rate, lb/sec
$\dot{m}_k$	local material flux of component k, $lb/(ft)^2(sec)$
$\dot{\bar{m}}_k$	total material transfer rate of component k, lb/sec
M_k	molecular weight of component k, lb/lb-mole
Nu_x	local Nusselt number
Nu_ℓ	average Nusselt number
p_k	partial pressure of diffusing component, lb_f/ft^2
p_j	partial pressure of main stream fluid, lb_f/ft^2

P	total pressure, lb_f/ft^2
Pr	Prandtl number
$\dot{q}$	heat flux, $Btu/(sec)(ft)^2$
r	radial distance from centerline of cylinder, ft or in.
Re_x	local Reynolds number, $U_\infty x/\nu$
Re_ℓ	total Reynolds number, $U_\infty \ell/\nu$
Sc	Schmidt number, $\nu_a/D_{F,k}$
Sh_ℓ	average Sherwood number
Sh_x	local Sherwood number
Sh_ℓ^*	average modified Sherwood number
Sh_x^*	local modified Sherwood number
St_h	heat transfer Stanton number, Nu/(Re)(Pr)
St_m	mass transfer Stanton number, Sh/(Re)(Sc)
t	temperature, ^oF
t_a	temperature of free stream air, ^oF
t_m	mean temperature, defined by equation 37, ^oF
t_s	temperature of evaporating surface, ^oF
T	temperature, ^oR
u	velocity in x-direction, ft/sec
U_{avg}	average velocity, ft/sec
U_∞	velocity of free stream, ft/sec
v	velocity in y- or r-direction, ft/sec
V	specific volume, ft^3/lb
x	distance from the leading edge of cylinder in the direction parallel to cylinder axis, ft or in.
x_o	unwetted approach length, ft or in.

x_w wetted length, ft or in.

y distance from solid surface in the direction normal to the surface, ft or in.

z compressibility factor

δ boundary layer thickness, ft

δ^* displacement thickness, ft

δ_d diffusion boundary layer thickness, ft

ν kinematic viscosity, ft^2/sec

ρ density, lb/ft^3

σ molal concentration, $lb\text{-}mole/ft^3$

τ local shear stress, $lb_m/(ft)(sec)^2$ or lb_f/ft^2

$\overline{\tau}$ average shear stress, $lb_m/(ft)(sec)^2$ or lb_f/ft^2

Subscripts:

a air

k diffusing component

j main stream fluid

s evaporating surface

∞ free stream

REFERENCES

1. Schlichting, H., "Boundary Layer Theory," 4th edition, translated by J. Kestin, McGraw-Hill Book Company, Inc., 1962.

2. Goldstein, S., ed., "Modern Developments in Fluid Dynamics," vols. I and II, Clarendon Press, Oxford, 1938.

3. Levich, V. G., "Physicochemical Hydrodynamics," Prentice-Hall, Inc., Englewood Cliffs, N. J., 1962.

4. Galloway, T. R. and B. H. Sage, Int. J. Heat Mass Transfer, 7, 283 (1964).

5. Venezian, E., M. J. Crespo and B. H. Sage, A. I. Ch. E. Journal, 8, 383 (1962).

6. Kutateladze, S. S., "Fundamentals of Heat Transfer," Academic Press Inc., N. Y., 1963.

7. Cuffel, R. F., Ph. D. Thesis, California Institute of Technology, Pasadena, California, 1964.

8. Seban, R. A. and R. Bond, J. Aero. Sci., 18, 671 (1951).

9. Raat, J., NOLTR 63-68 (1964).

10. McAdams, W. H., "Heat Transmission," 3rd ed., McGraw-Hill Book Company, Inc., N. Y., 1954.

11. Knudson, J. G. and D. L. Katz, "Fluid Dynamics and Heat Transfer," McGraw-Hill Book Company, Inc., N. Y., 1958.

12. Sage, B. H., A. I. Ch. E. Journal, 5, 331 (1959).

13. Maisel, D. S. and T. K. Sherwood, Chem. Eng. Progr., 46, 131 (1951).

14. Blasius, H., Z. Math. u. Phys., 56, 1 (1908); Engl. transl. in NACA Tech. Memo No. 1256.

15. Pohlhausen, E., ZAMM, 1, 115 (1921).

16. See Reference (3), p. 104.

17. Eckert, E. R. C., "Heat and Mass Transfer," 2nd ed., McGraw-Hill Book Company, Inc., 1959, p. 173.

18. Lighthill, M. J., Proc. Roy. Soc., A 202, 359 (1950).

19. Tribus, M. and J. Klein, Heat Transfer Symposium, University of Michigan, 1953, p. 211.

20. Colburn, A. P., Trans. A. I. Ch. E., 29, 174 (1933).

21. Elias, F., ZAMM, 9, 434 (1929), and 10, 1 (1930).

22. Edwards, A. and B. N. Furber, Proc. Inst. Mech. Eng., 170, 941 (1956).

23. Kestin, J., P. F. Maeder and H. E. Wang, Int. J. Heat Mass Transfer, 3, 133 (1961).

24. Albertson, M. L., Heat Transfer and Fluid Mechanics Institute, Reprints of Papers (1951), Stanford University Press, Stanford, California, p. 243.

25. Reynolds, O., Phil. Trans. Roy. Soc., 174A, 935 (1883).

26. Burgers, J. M., Proc. of the First Int. Congress for Applied Mechanics, Deft (1924), p. 113.

27. Dryden, H. L., Proc. Fourth Int. Congress for Applied Mechanics, Cambridge (1934), p. 175.

28. Dryden, H. L., J. Aero. Sci., 6, 85 and 101, (1939).

29. Dryden, H. L., NACA TN 1168 (1947).

30. Dryden, H. L., Transition from Laminar to Turbulent Flow, in "Turbulent Flows and Heat Transfer" edited by C. C. Lin, Princeton University Press, Princeton, N. J., 1959.

31. Tollmién, W., Nachr. Wiss Göttingen, Math. Phys. Klasse 21-44 (1929); Engl. transl. in NACA TM No. 609 (1931).

32. Lin, C. C., "The Theory of Hydrodynamic Stability," Cambridge University Press, 1955.

33. Dryden, H. L., Zeitschrift Für Flugwissenshaften, 4, 89 (1956).

34. Schubauer, G. B. and H. K. Shramstad, J. Aero. Sci., 14, 69 (1947).

35. Jacob, M. and W. Dow, Trans. ASME, 68, 123 (1946).

36. See, e.g., Reference (1), p. 389.

37. Sogin, H. H. and M. Jacob, Heat Transfer and Fluid Mechanics Institute, Reprints of Papers (1953), Stanford University Press, Stanford, California, p. 5.

38. Christian, W. J. and S. P. Kezios, IIT H. T. Lab., Office of Ordnance Research Project No. 940-Ren, 1957.

39. Bonssinesq, J., Mem. Prep. par. div. sav. 23, Paris (1877).

40. Prandtl, L., Phys. Zeitschr., 11, 1072 (1910).

41. Taylor, G. E., Brit. Aeronaut. Comm., Rept. and Memo., 272, 423 (1919).

42. Kármán, Th. von, Trans. ASME, 61, 705 (1939).

43. Driest, E. R. van, "Fifty Years of Boundary Layer Research," edited by H. Görtler and W. Tollmien, Braunschweig, 1955, p. 257.

44. Rubesin, M. W., NACA TN 2917 (1953).

45. Spalding, D. B., Proceedings of the 1961-62 International Heat Transfer Conference, ASME, p. 439.

46. Spalding, D. B., Int. J. Heat Mass Transfer, 7, 743 (1964).

47. Hatter, A. P., Int. J. Heat Mass Transfer, 7, 875 (1964).

48. Mises, R. von, AZMM, 7, 425 (1927).

49. Coles, D., "Fifty Years of Boundary Layer Research," edited by H. Görtler and W. Tollmien, Braunschweig, 1955,

50. Kestin, J. and P. D. Richardson, Int. J. Heat Mass Transfer, 6, 147 (1963).

51. Spielman, M. and M. Jacob, Trans. ASME, 75, 385 (1953).

52. Seban, R., Theory reported in M. S. Thesis by S. Scesa, University of California, Berkeley, 1951.

53. Rubesin, M. W., NACA TN 2345, 1951.

54. Reynolds, W. C., W. M. Kays and S. J. Kline, NASA Memo 12-2-58 W (1958).

55. Boltze, E., Dissertation Göttingen 1908; see, e. g., Reference (1), p. 185.

56. Millikan, C. B., Trans. ASME, 54, 29 (1932).

57. Kelly, H. R., J. Aero. Sci., 634 (1954).

58. Mark, R. M., CIT Guggenheim Aero. Lab, Hypersonic Wind Tunnel Memo No. 21, July, 1954.

59. Stowartson, K., Quart. Appl. Math., 13, 113 (1955).

60. Glauert, M. B. and M. J. Lighthill, Proc. Roy. Soc., A 230, 188 (1955).

61. Bourne, D. E. and D. R. Davis, Quart. J. Mech. Appl. Math., 11, 52 (1958).

62. Bourne, D. E., Davis and S. Wardl, Quart. J. Mech. Appl. Math., 12, 257 (1959).

63. Steiger, M. H. and M. H. Bloom, Poly. Inst. of Brooklyn, Aero. Research Lab., 6, Dec. 1960.

64. Steiger, M. H. and M. H. Bloom, Int. J. Heat Mass Transfer, 5, 513 (1962).

65. Wanous, D. J. and E. M. Sparrow, AIAA Journal, 3, 147 (1965).

66. Yasuhara, M., J. Aero. Sci., 29, 667 (1962).

67. Weistein, I., NASA TN D-1503 (1962).

68. Landweber, L., David W. Taylor Model Basin, Report No. 689 (1949).

69. Eckert, H. U., J. Aero. Sci., 19, 23 (1952).

70. Chapman, D. R. and R. H. Kester, NACA TN 3097 (1954).

71. Acrivos, A., A. I. Ch. E. Journal, 6, 410 (1960).

72. Sato, K., Ph. D. Thesis, California Institute of Technology, Pasadena, California, 1955.

73. Hsu, N. T., Ph. D. Thesis, California Institute of Technology, Pasadena, California, 1956.

74. Corcoran, W. H., F. Page Jr., W. G. Schlinger, and B. H. Sage, Ind. Eng. Chem., 44, 410 (1952).

75. Reamer, H. H. and B. H. Sage, Rev. Sci. Inst., 24, 362 (1953).

76. Rossini, F. D., et al., "Selected Values of Physical and Thermodynamic Properties of Hydrocarbons and Related Compounds," Carnegie Press, Pittsburgh, 1953.

77. "International Critical Tables," vol. 5, p. 63, McGraw-Hill Book Company, Inc., N. Y., 1929.

78. Schlinger, W. G., H. H. Reamer, B. H. Sage, and W. N. Lacey, Fundamental Research on Occurrence and Recorvery of Petroleum (Biennial Volume 1952-53), API, p. 70.

79. Hsu, N. T. and B. H. Sage, A. I. Ch. E. Journal, 3, 405 (1957).

80. Prandtl, L., Proc. Int. Congr. Appl. Mech., 2nd congr., Zurich (1927), p. 62.

81. Nikuradse, J., Ing. Arch., 1, 306 (1930).

82. Opfell, J. B. and B. H. Sage, Ind. Eng. Chem., 47, 918 (1955).

83. Brown, R. A. S. and B. H. Sage, J. Chem. & Eng. Data, 6, 355 (1961).

84. Pai, S. I., "Fluid Dynamics of Jets," D. van Nostrand Company, Inc., N. Y., 1954.

85. Tessin, W. and M. Jacob, Trans. ASME, 75, 473 (1953).

86. See Reference (17), p. 215.

87. See Reference (1), p. 496.

88. Longwell, P. A. and B. H. Sage, A. I. Ch. E. Journal, 11, 46 (1965).

FIGURES

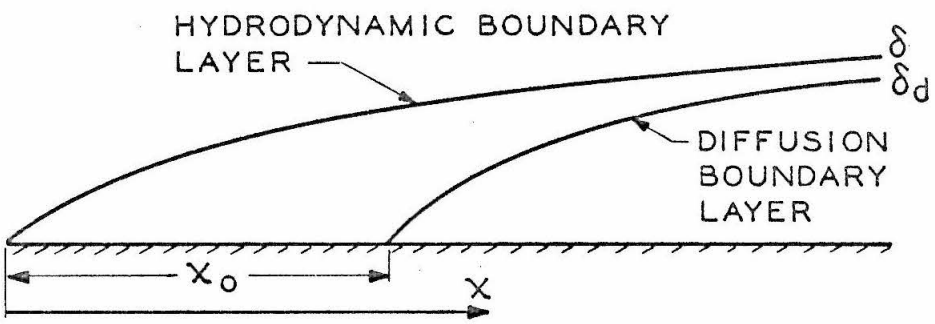

Fig. 1. Hydrodynamic and Diffusion Boundary Layers.

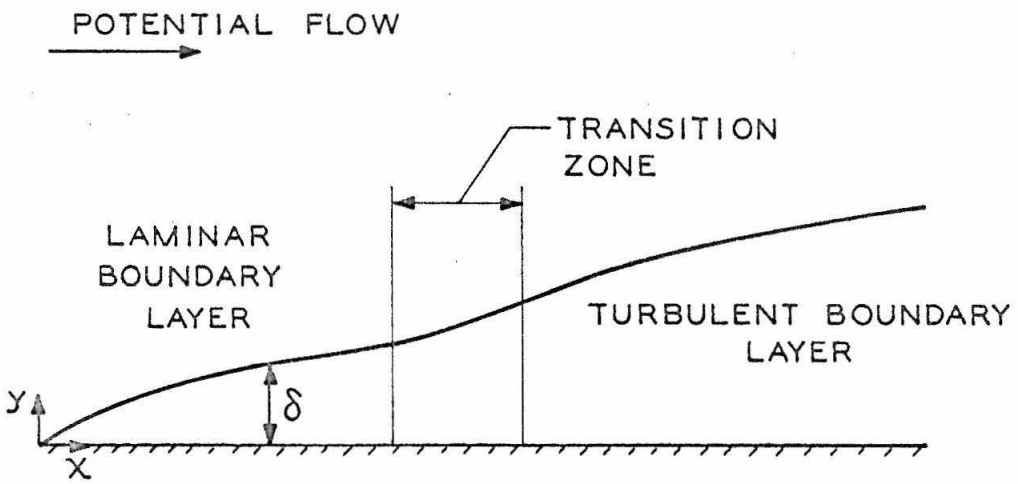

Fig. 2. Laminar and Turbulent Boundary Layers

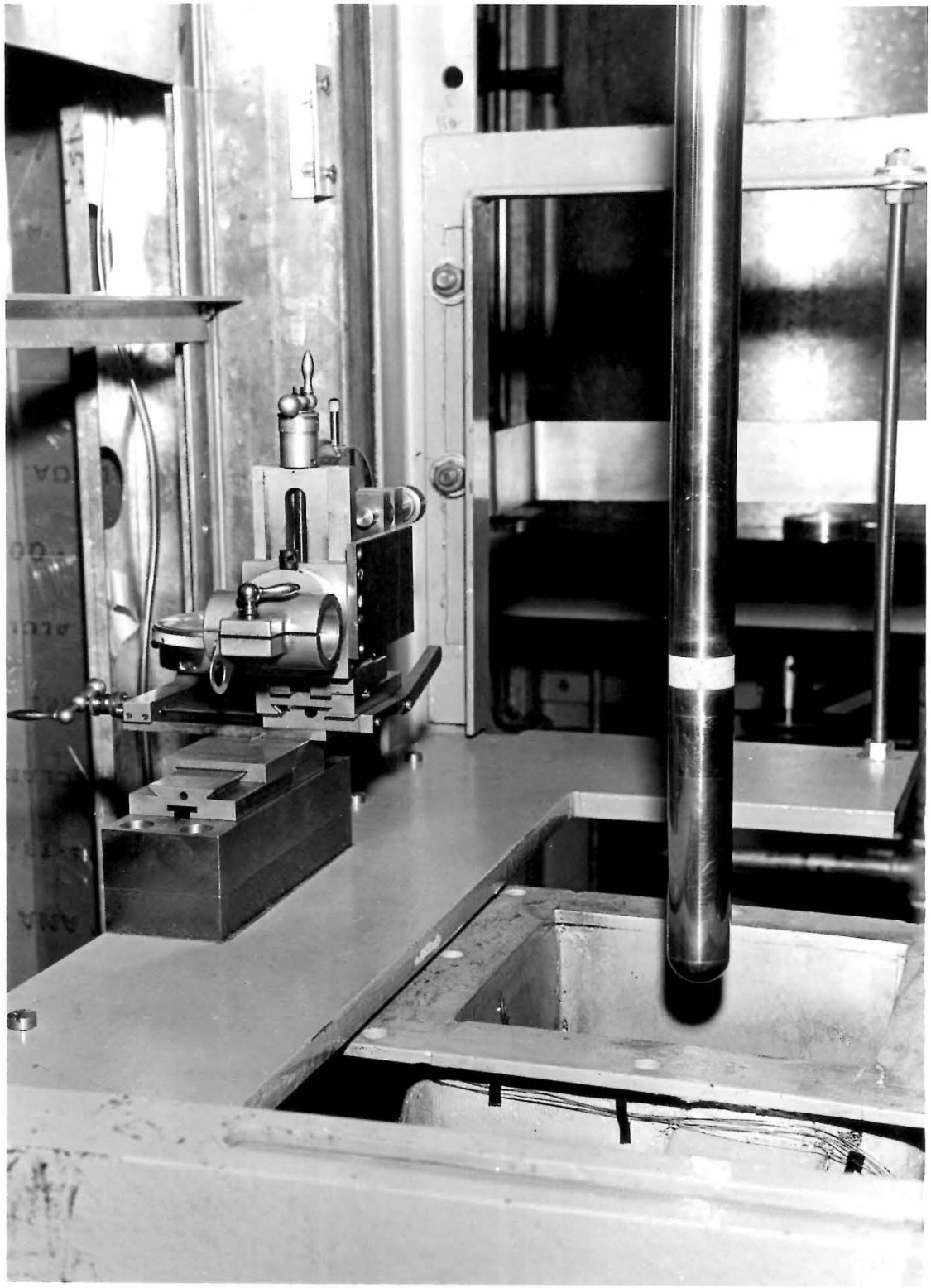

Fig. 3. Porous Cylinder, Air Jet, and Traversing Gear

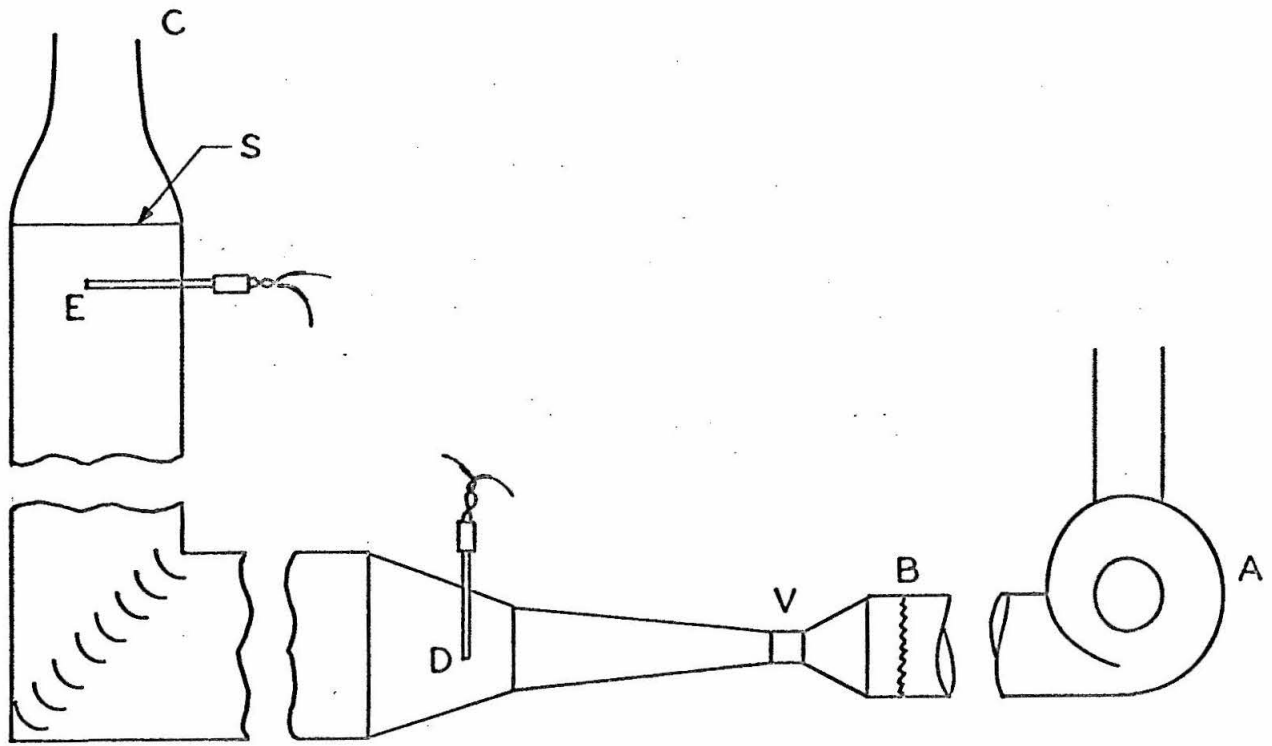

Fig. 4. Air Supply System

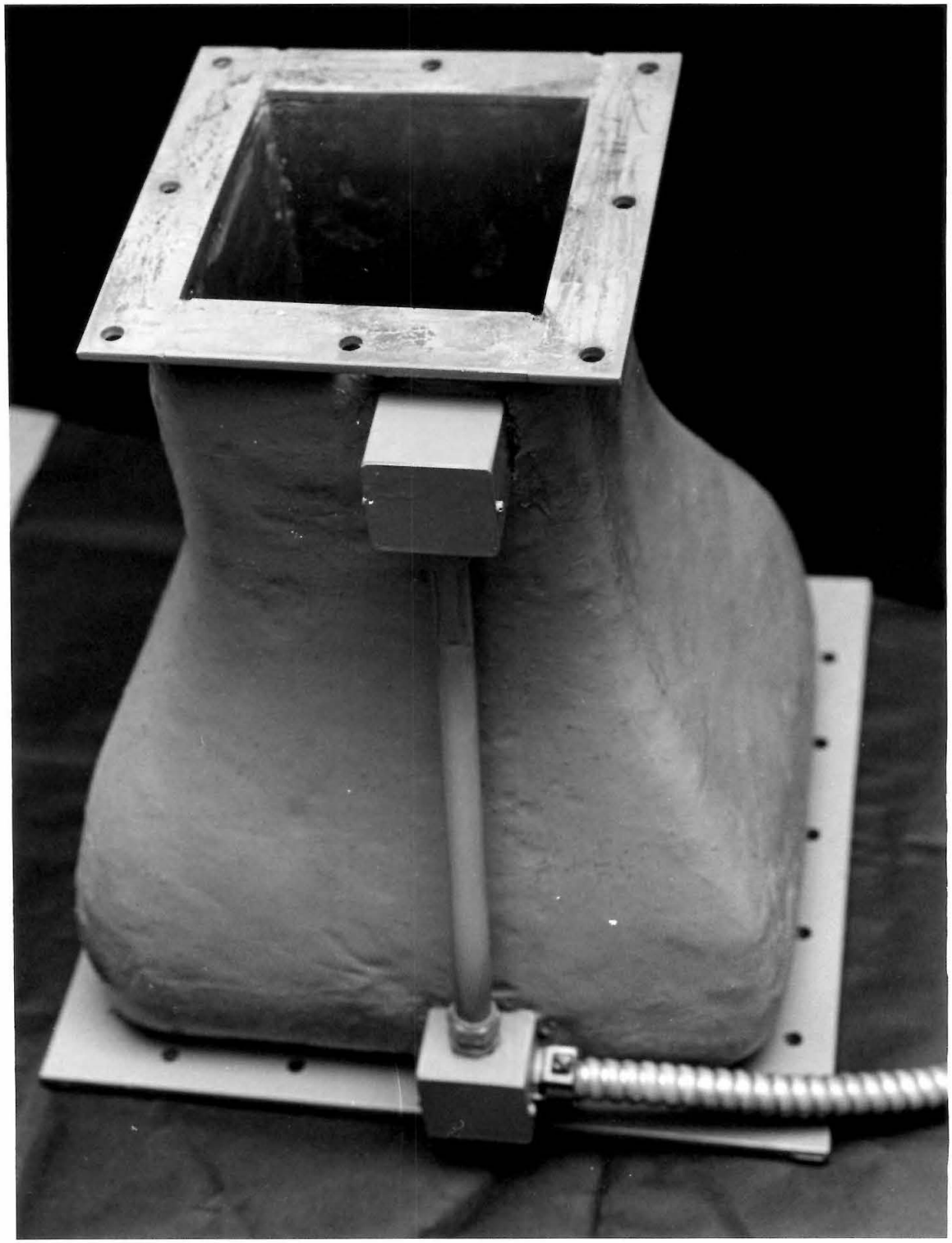

Fig. 5. Converging Air Jet

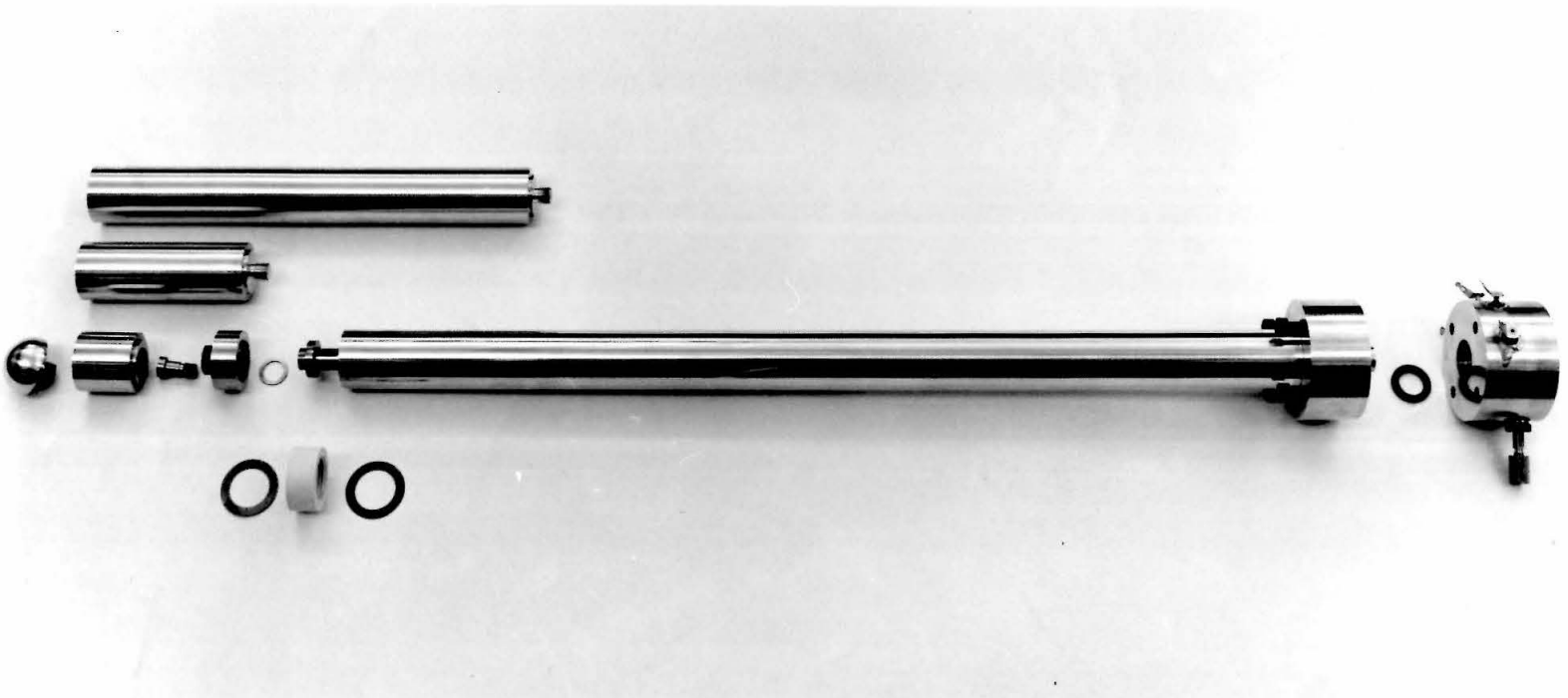

Fig. 6. Cylinder Before Assembly

Fig. 7. Cylinder After Assembly

diameter = 1 inch
length = 0. 500 inch

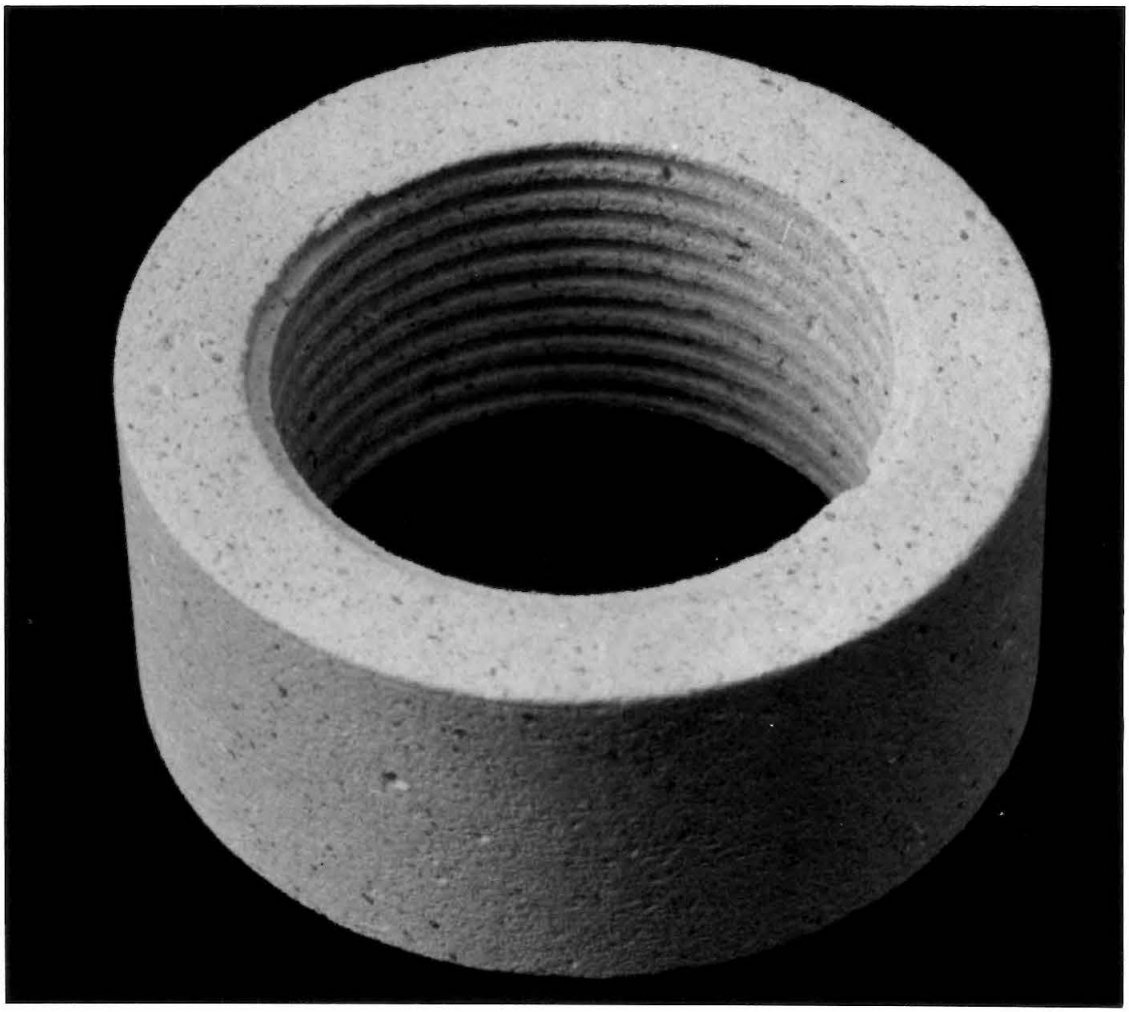

Fig. 8. Porous Section

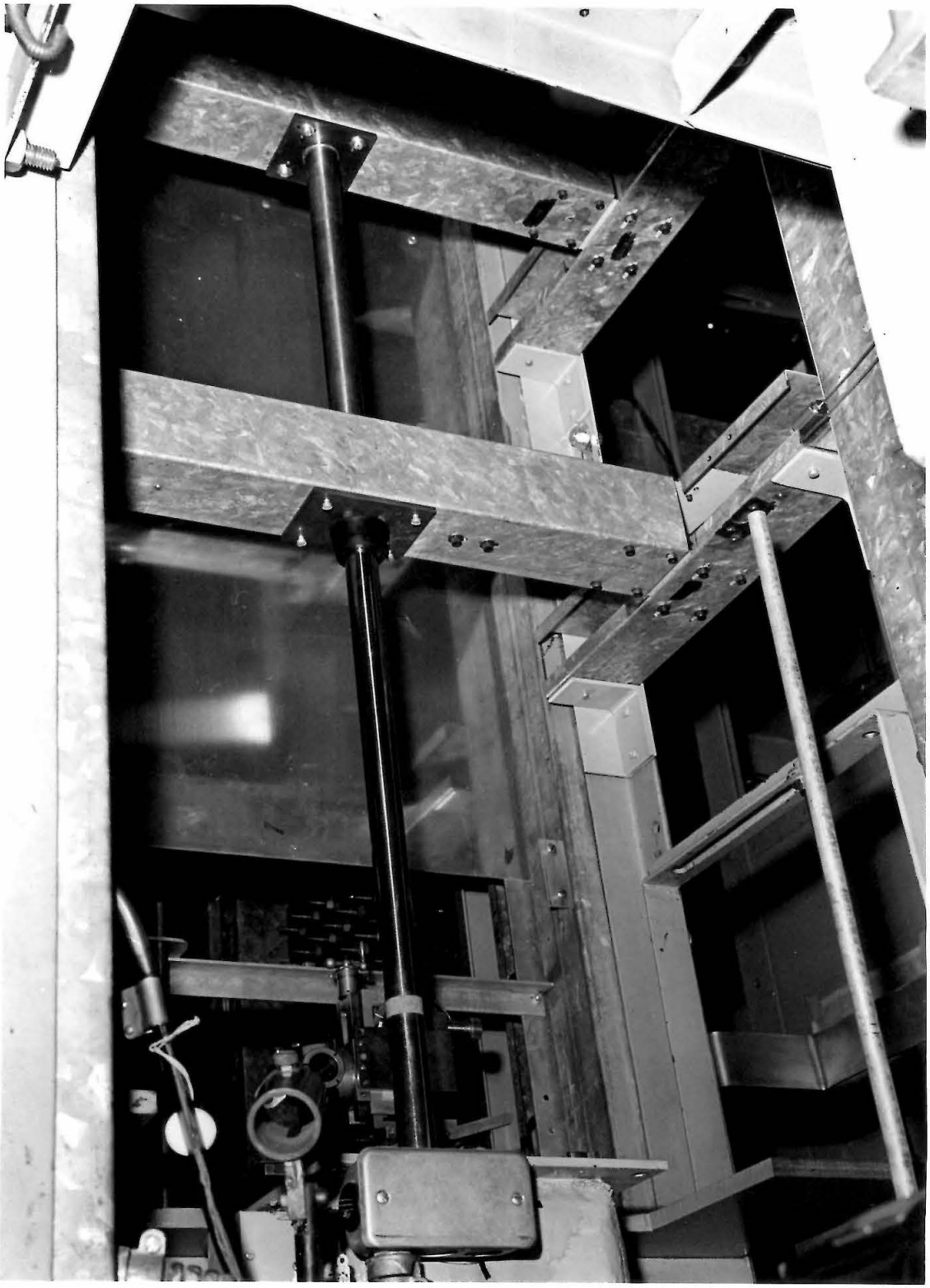

Fig. 9. Cyliner and Its Support

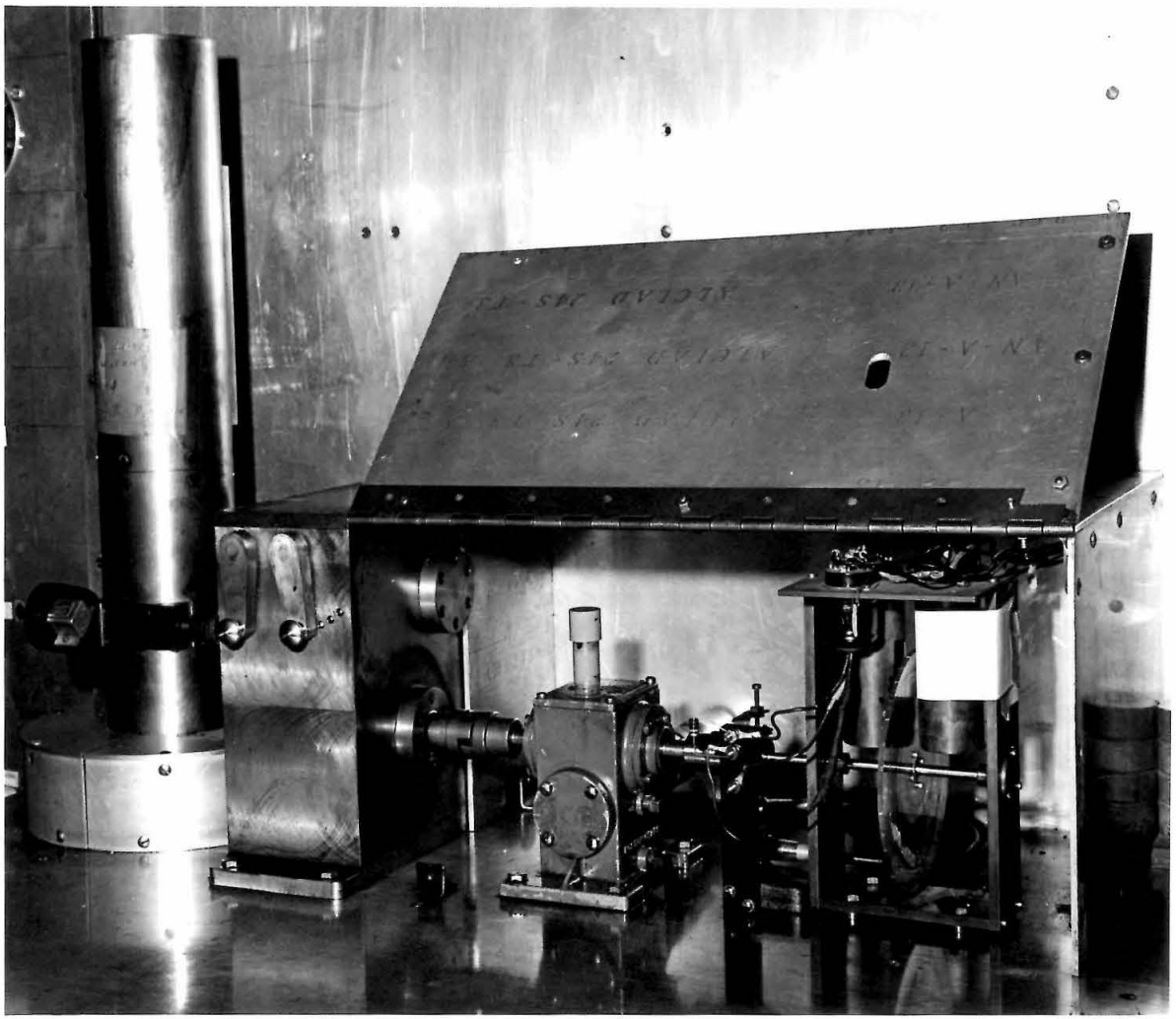

Fig. 10. Liquid Injector and Associated Mechanisms

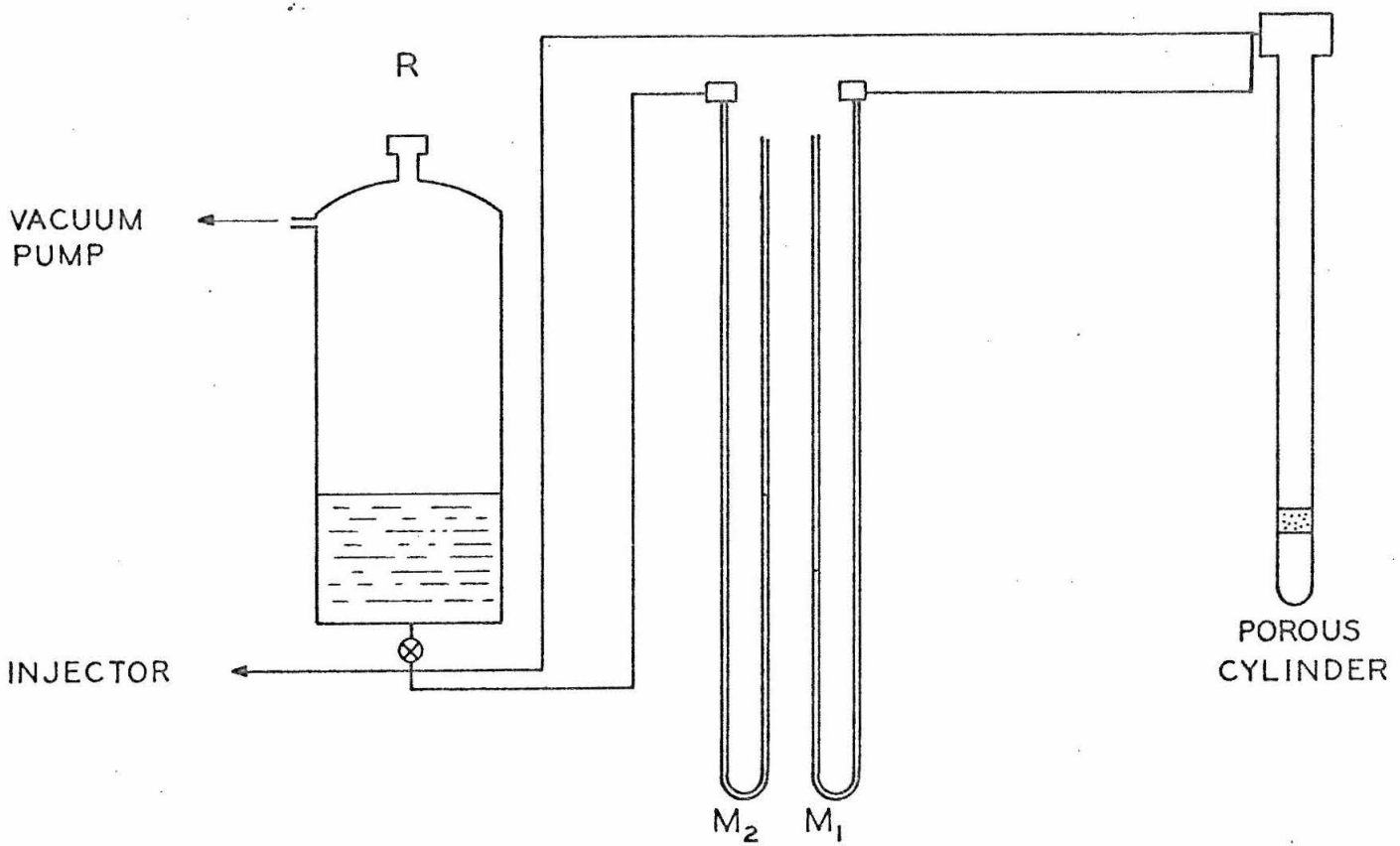

Fig. 11. Liquid Injection System

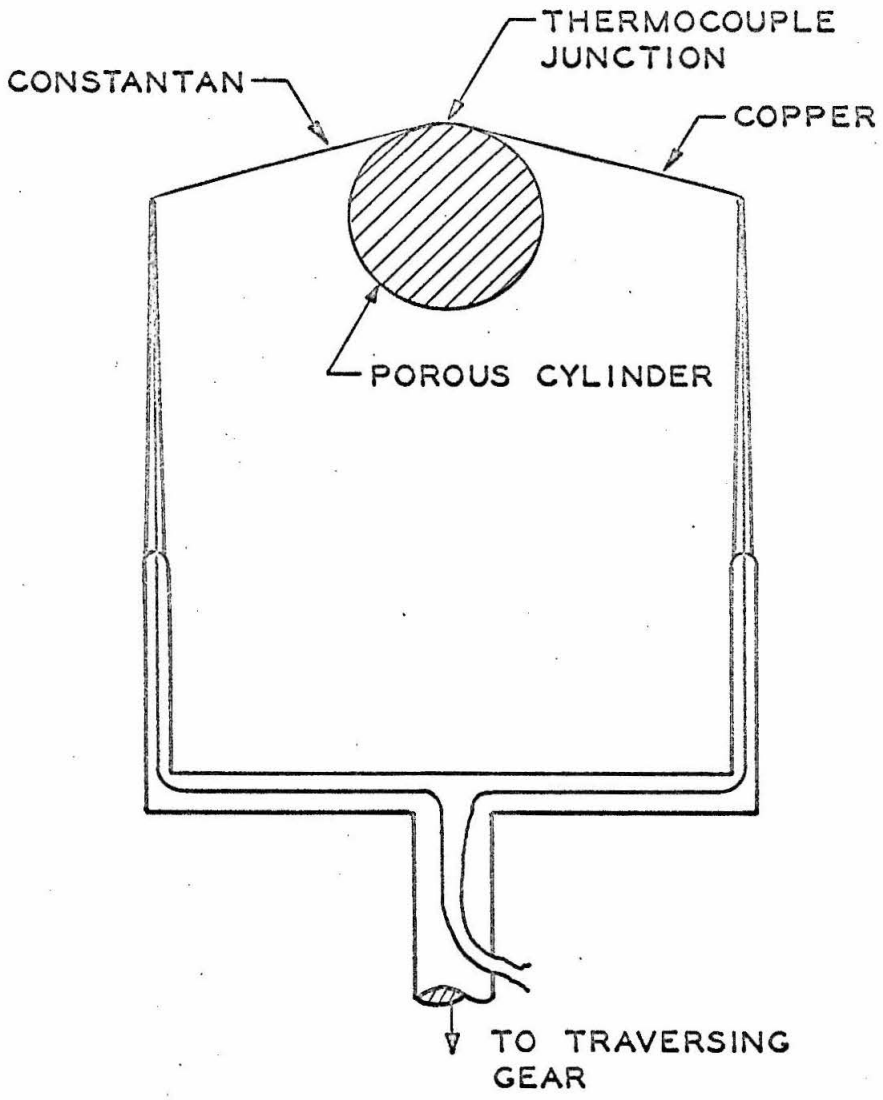

Fig. 12. Traversing Thermocouple at Measuring Position

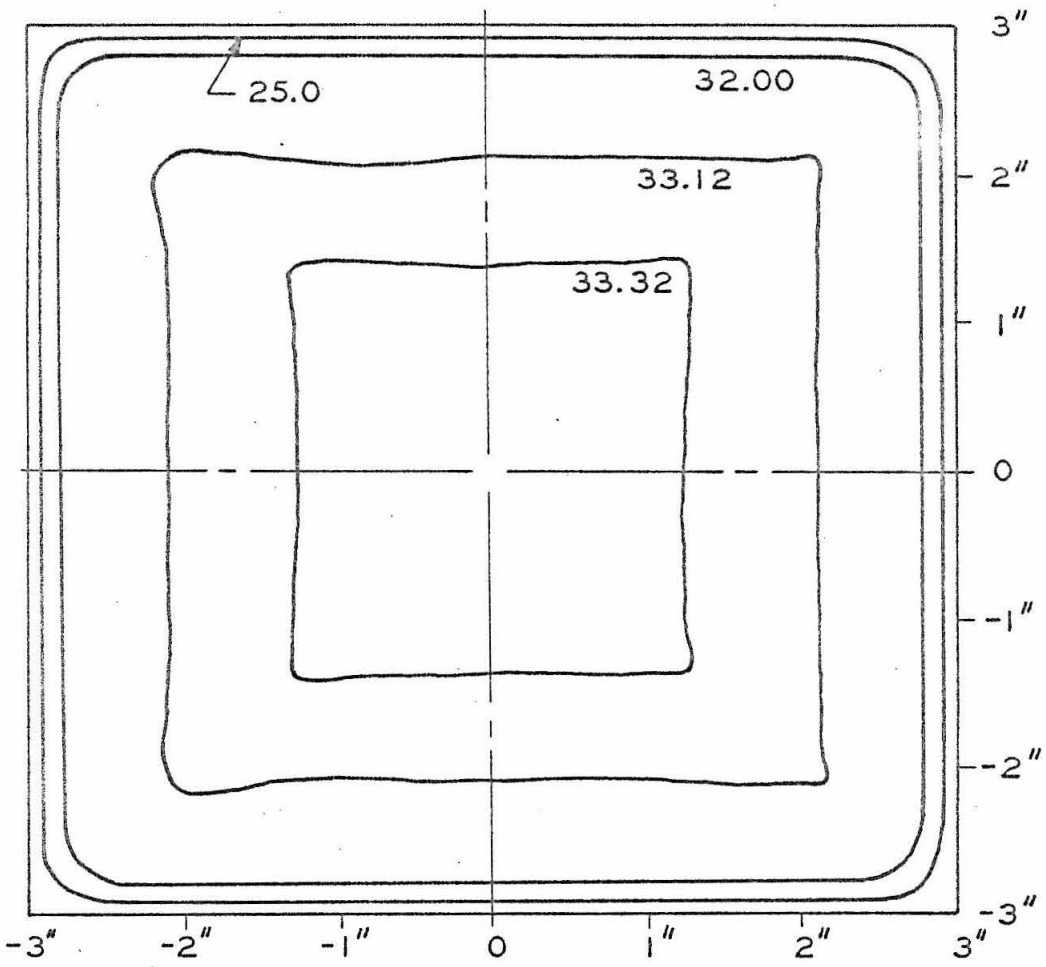

U_{avg} = 32.08 ft/sec by Venturi measurement

= 32.23 ft/sec by integration

Fig. 13. Velocity Distribution in Air Jet at 1/4-in. Below Jet Opening

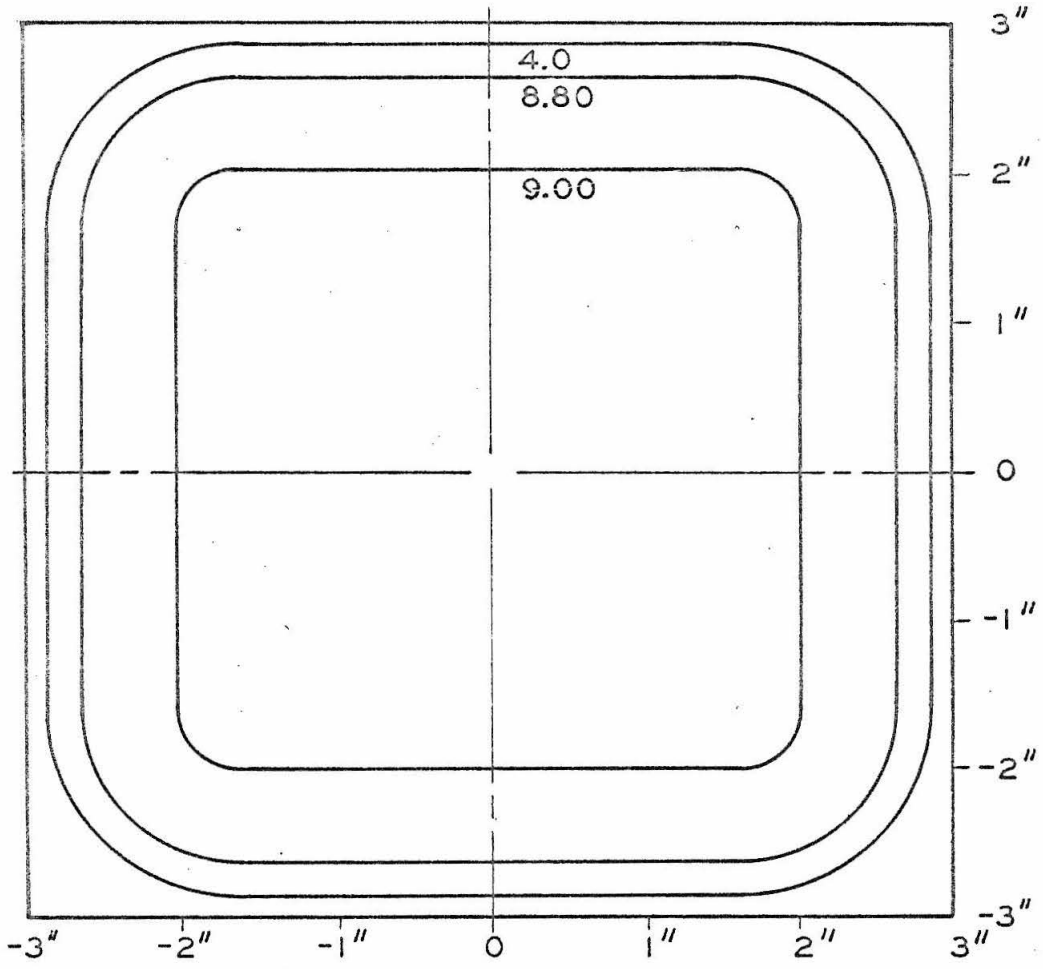

U_{avg} = 7.84 ft/sec by Venturi measurement

= 7.96 ft/sec by integration

Fig. 14 . Velocity Distribution in Air Jet at 1/4-in. Below Jet Opening

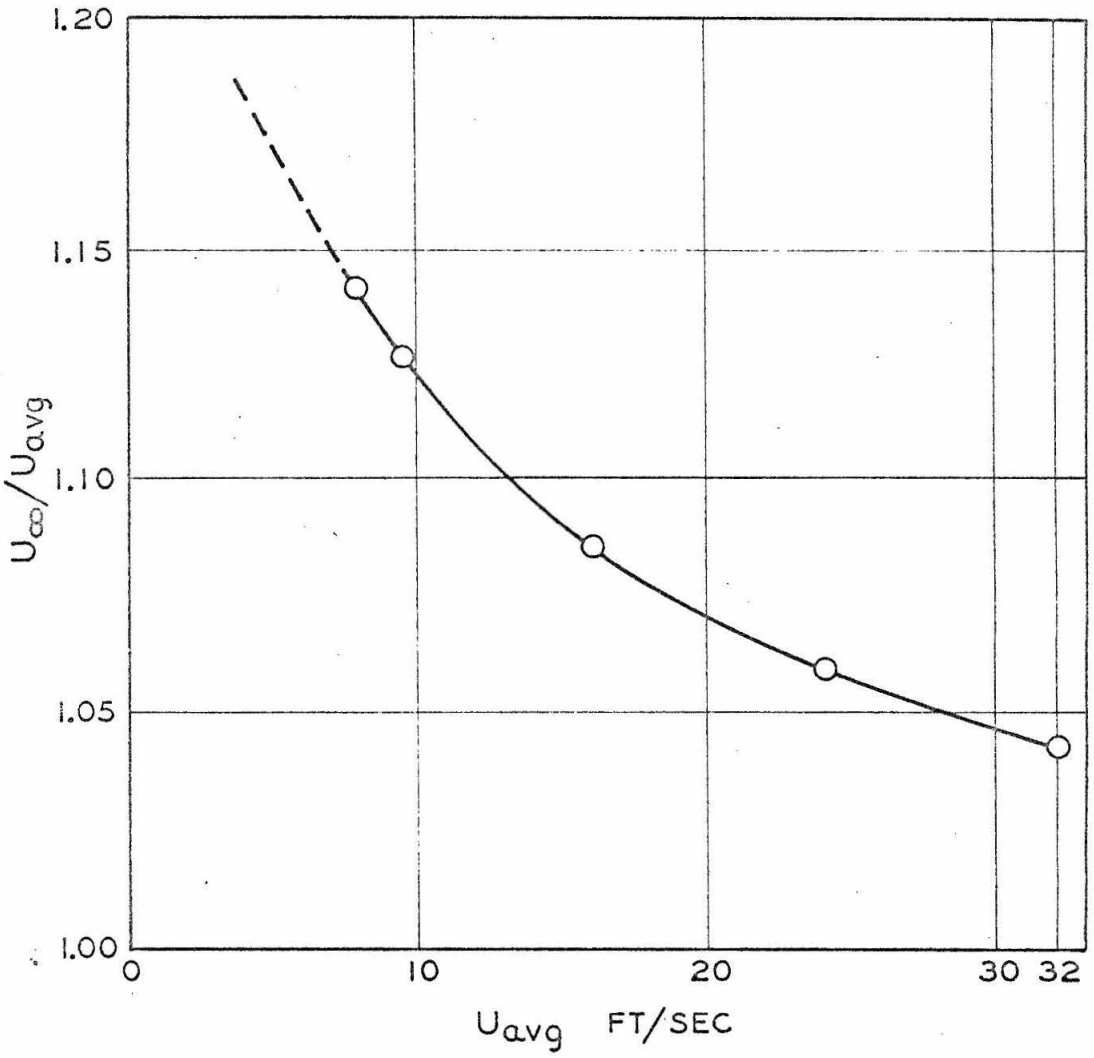

Fig. 15. U_∞/U_{avg} as a Function of U_{avg}

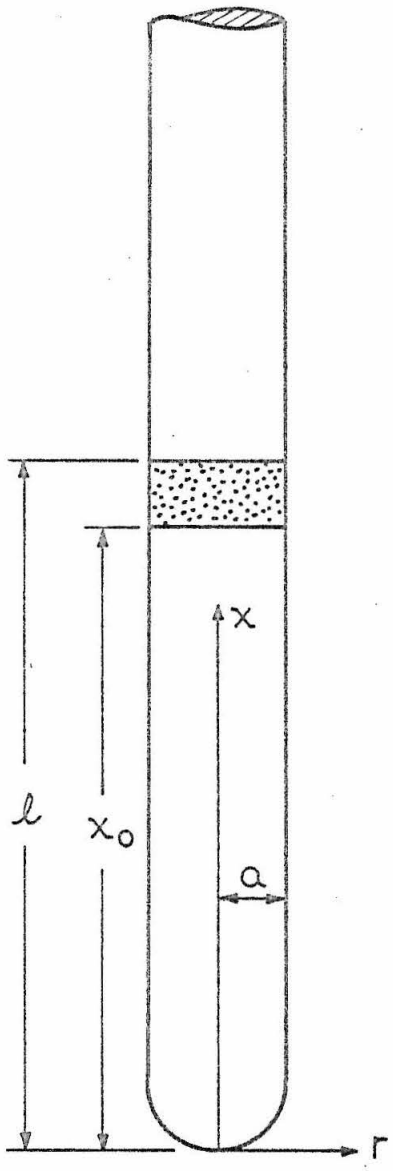

Fig. 16. Coordinate System

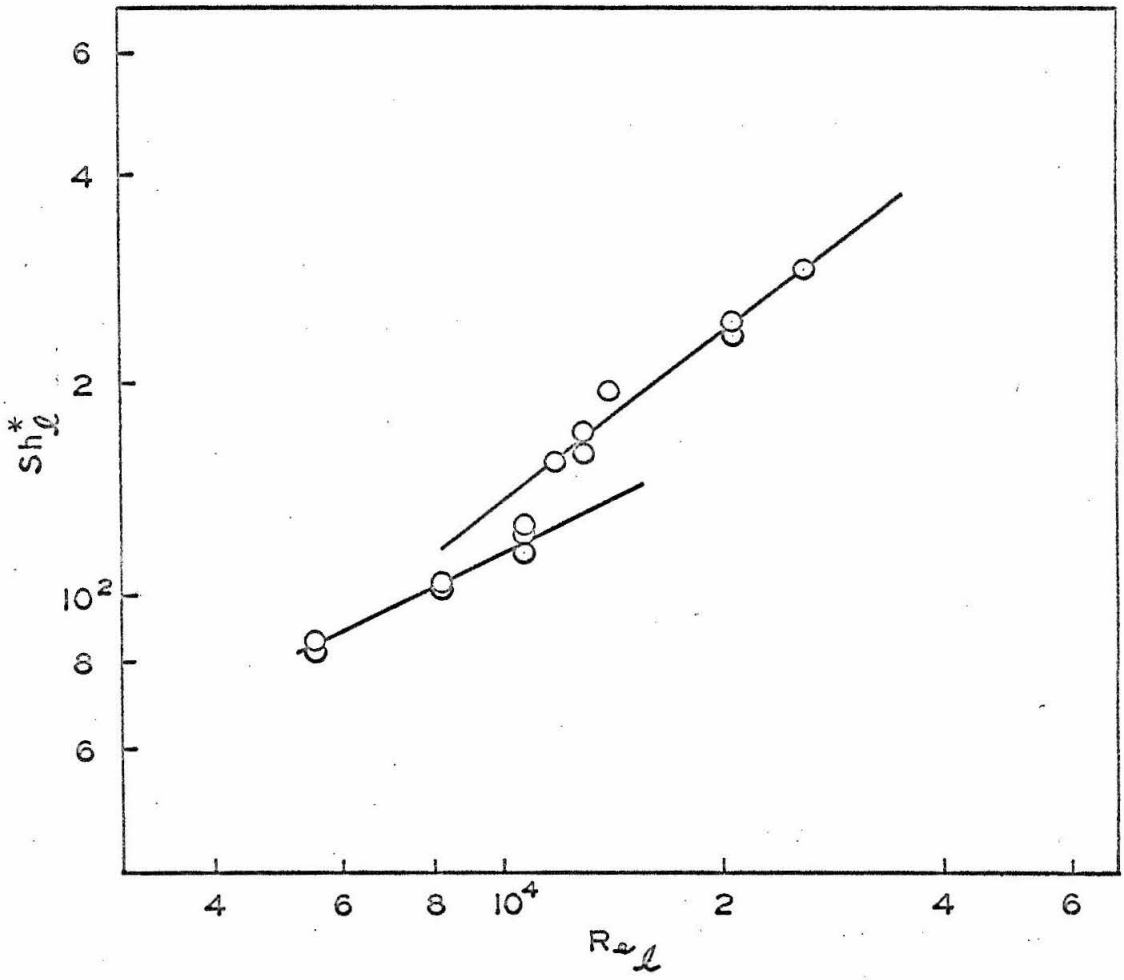

Fig. 17. Experimental Results for x_o = 1.973 in., x_w = 0.715 in., n-heptane

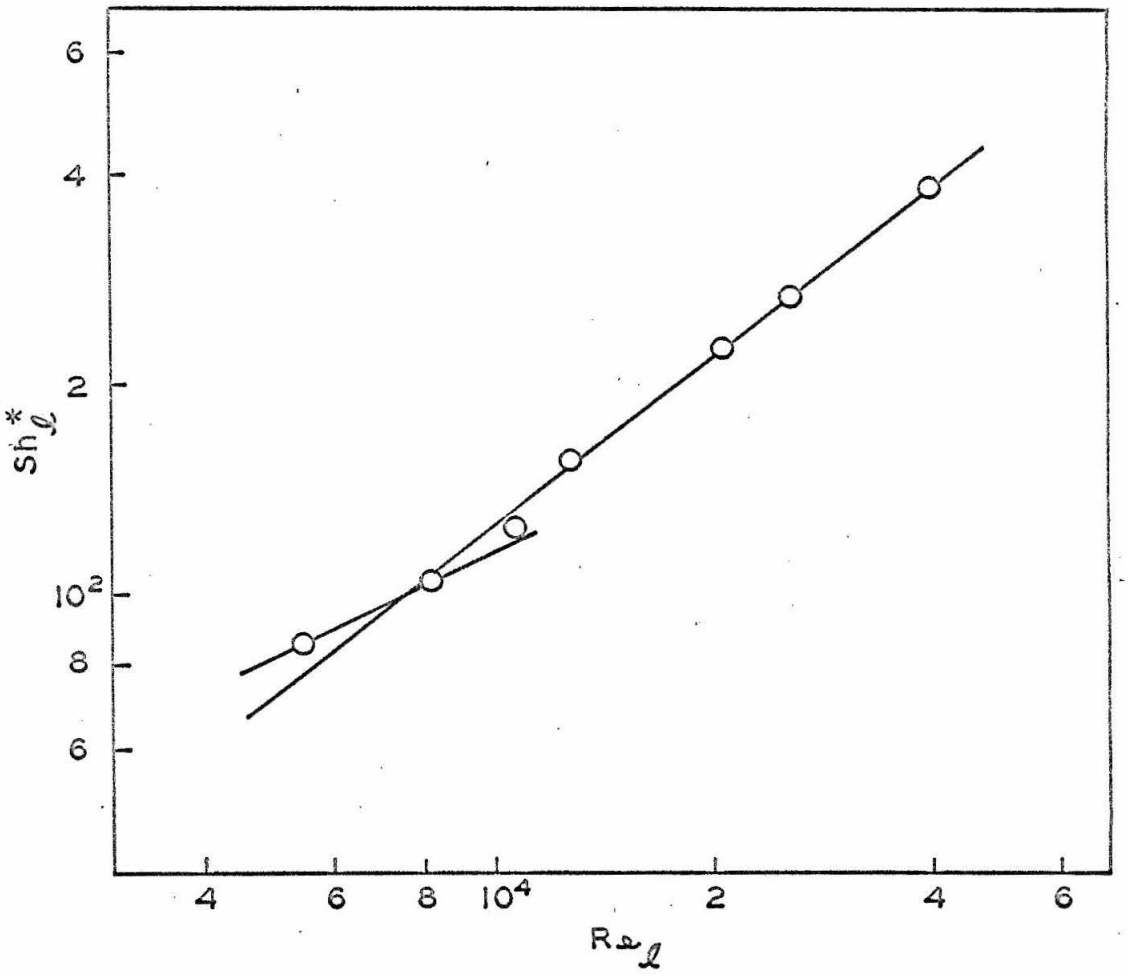

Fig. 18. Experimental Results for x_o = 1.973 in., x_w = 0.715 in., n-octane

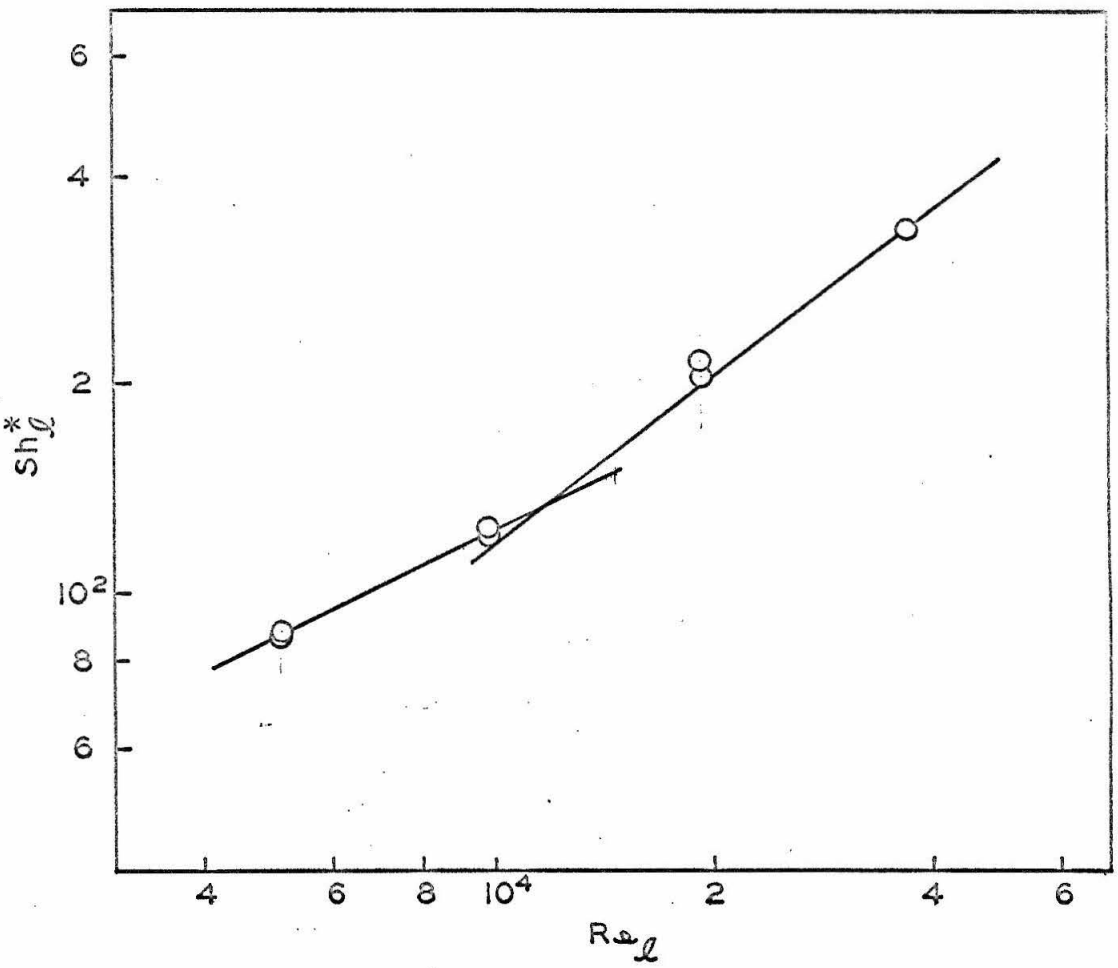

Fig. 19. Experimental Results for x_o = 1.973 in., x_w = 0.500 in., n-octane

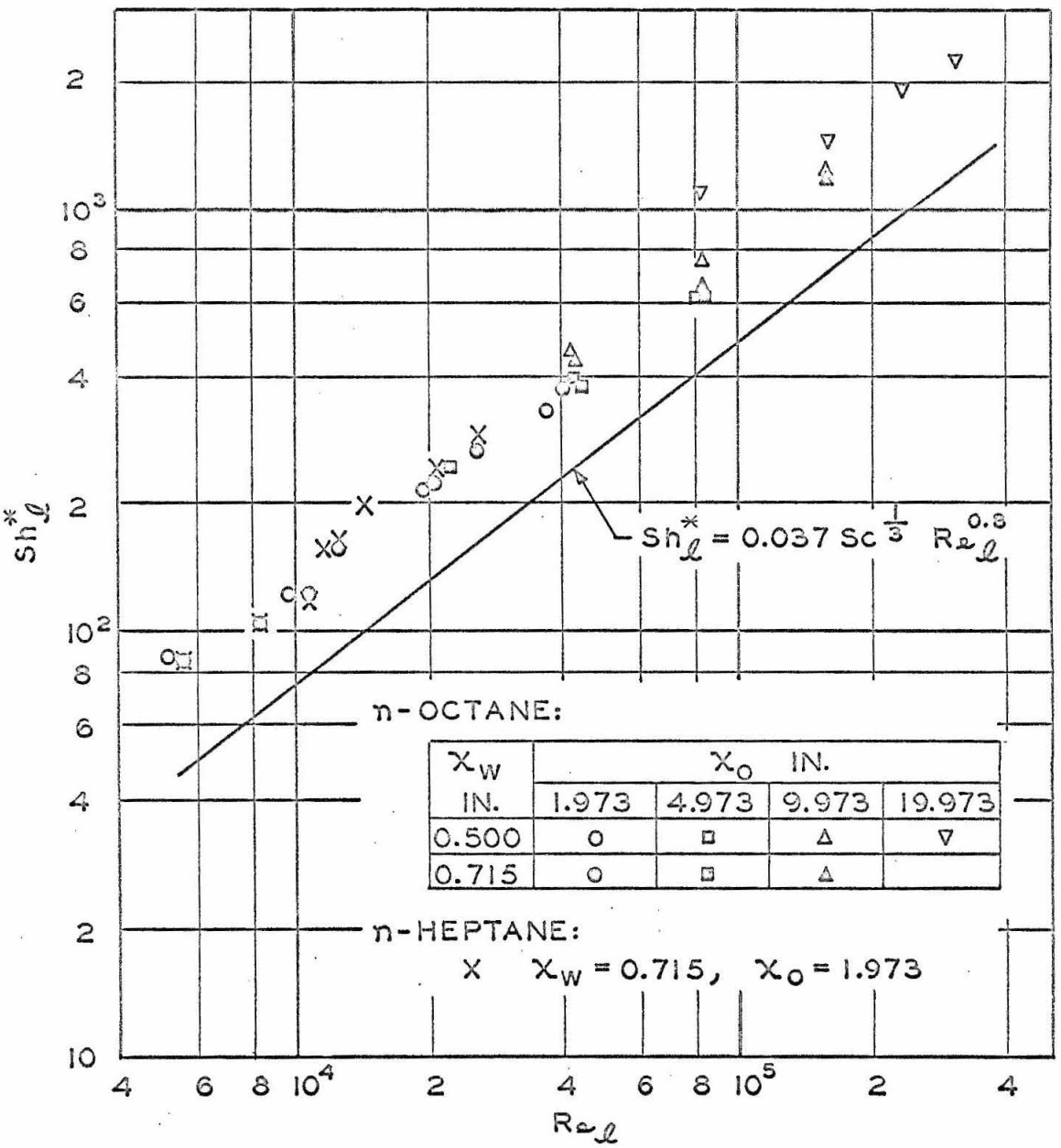

X_W IN.	X_O IN. 1.973	4.973	9.973	19.973
0.500	o	□	△	▽
0.715	o	▣	△	

Fig. 20. Experimental Results Uncorrected for Unwetted Approach Lengths

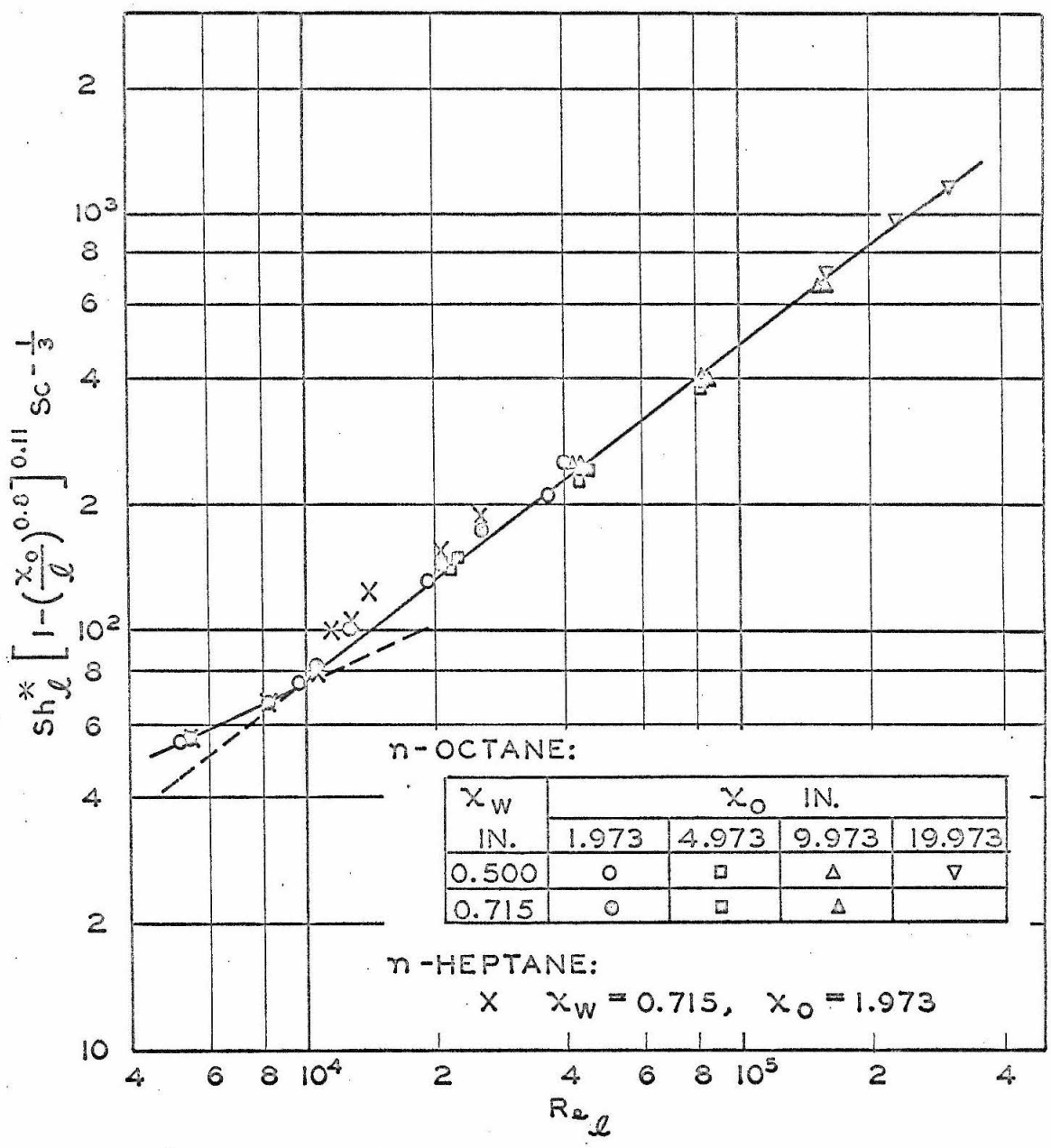

Fig. 21. Correlation of Experimental Data

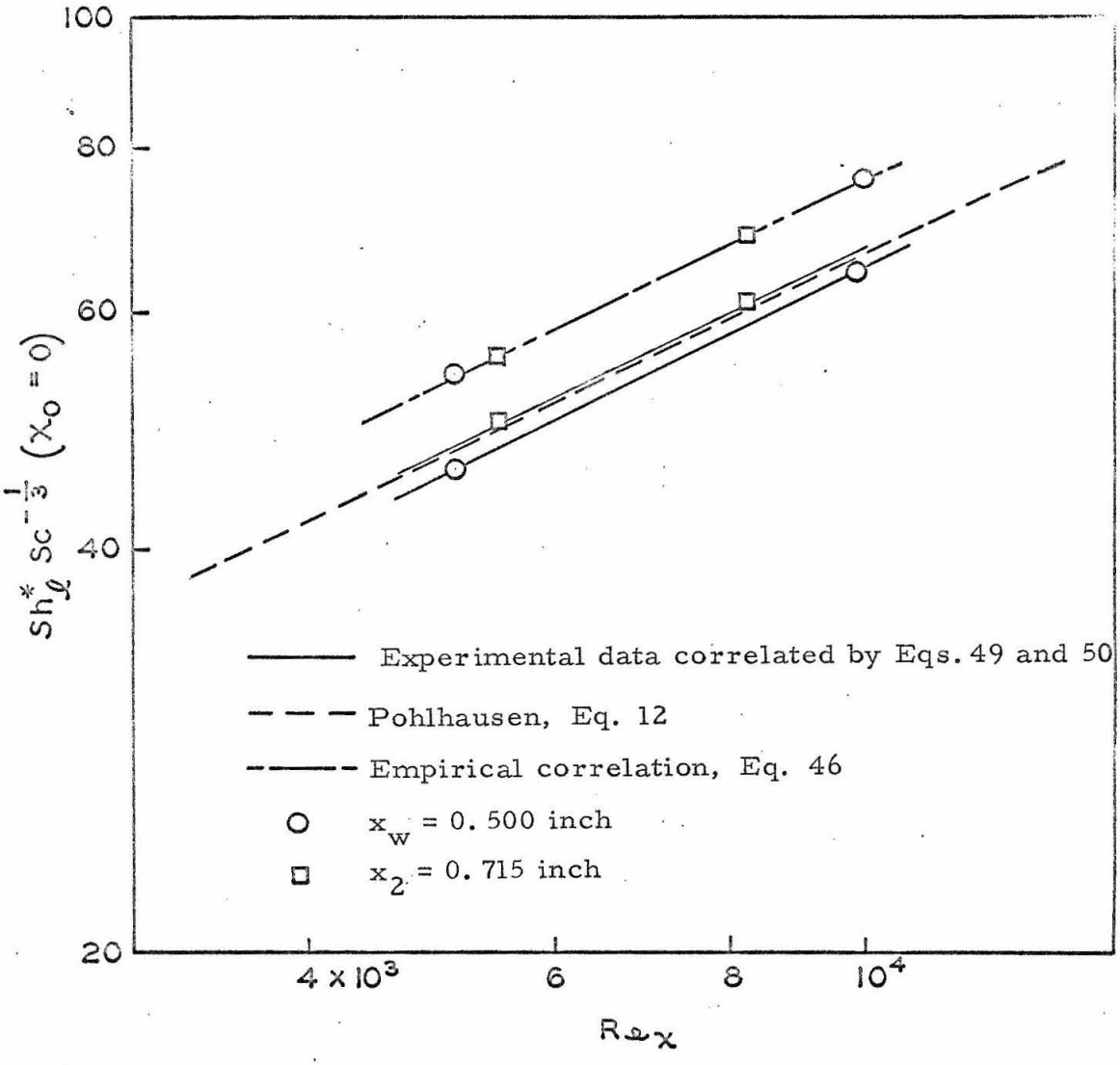

Fig. 22. Comparison of Results with Theoretical Work for Laminar Boundary Layer

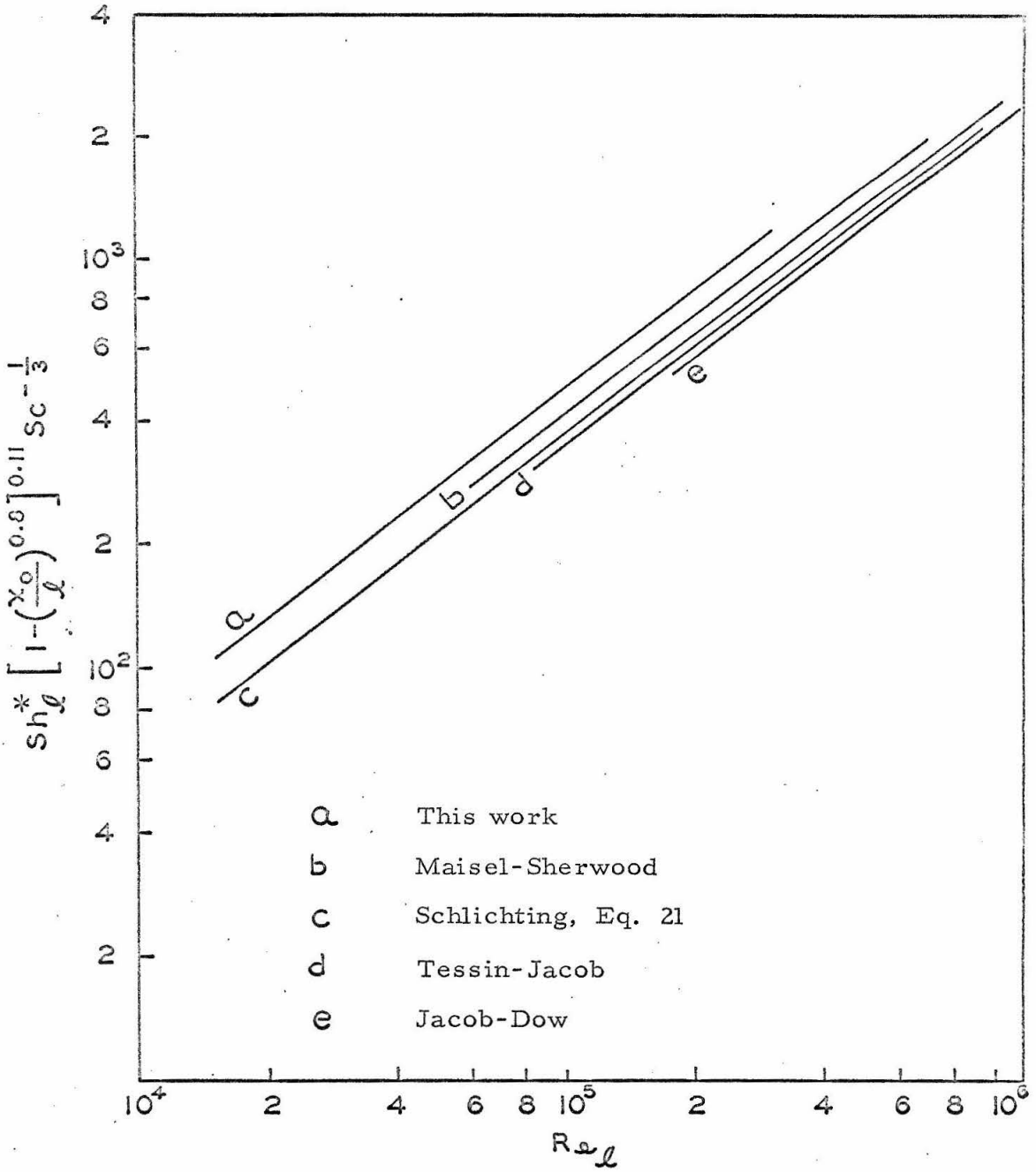

Fig. 23. Comparison of Results with Previous Measurements for Turbulent Boundary Layer

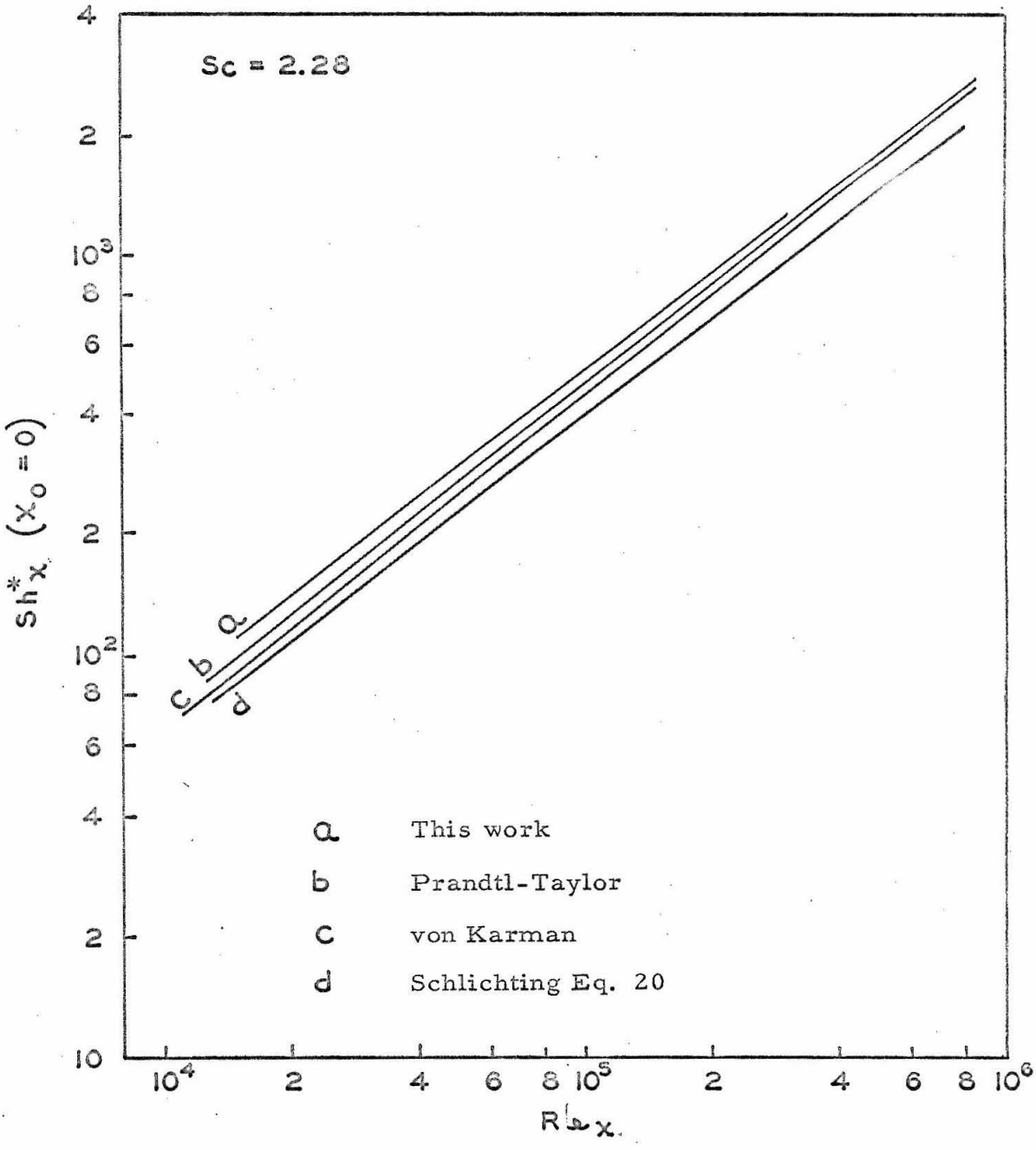

Fig. 24. Comparison of Results with Theoretical Work for Turbulent Boundary Layer

TABLES

TABLE I. SPECIFICATIONS OF HEATERS FOR POROUS SECTIONS

	Unit	0.500-inch porous section	0.715-inch porous section
Material		platinum	constantan
Diameter of wire	in.	0.005	0.010
Resistance	ohm/ft	2.56	2.99
Length of wire	in.	38.5	35.0
Inner diameter of coil	in.	0.014	0.018
Outer diameter of coil	in.	0.024	0.038
Length of coil	in.	20.0	11.5
Total resistance	ohm	8.21	8.72
Pitch of coil	in.	0.026 - 0.032*	0.031 - 0.034*

*The pitch was increased from one end to another. The denser end was placed on the lower side of the porous section for higher local evaporation rates.

TABLE II

EXPERIMENTAL OPERATING CONDITIONS

Test No.	Pressure psia	Weight fraction water	Air stream temp °F	Average air velocity ft/sec
562	14.33	0.0051	100.02	7.79
564a	14.32	0.0066	100.10	9.58
564b	14.23	0.0068	100.23	9.61
565	14.36	0.0045	99.94	7.76
566	14.30	0.0071	99.89	3.86
567	14.40	0.0080	100.13	5.88
568	14.34	0.0062	100.06	9.56
569	14.30	0.0077	99.96	16.00
570	14.37	0.0084	100.08	20.18
571	14.26	0.0079	100.00	10.56
572	14.26	0.0065	100.20	8.75
573	14.32	0.0066	100.09	7.79
587	14.30	0.0114	100.21	7.82
588	14.26	0.0125	99.98	3.86
589	14.25	0.0124	100.06	32.10
590	14.25	0.0125	99.98	16.08
591a	14.26	0.0139	99.97	20.22
591b, c	14.27	0.0135	100.23	20.22
594	14.27	0.0128	100.14	9.59
595	14.27	0.0125	99.99	5.94
612	14.45	0.0051	99.89	7.69
613	14.36	0.0053	99.90	15.98
614	14.35	0.0052	100.07	31.86

TABLE II (Continued)

Test No.	Pressure psia	Weight fraction water	Air stream temp °F	Average air velocity ft/sec
615	14.36	0.0088	99.96	32.00
616	14.30	0.0070	100.01	15.96
617	14.37	0.0090	99.87	7.78
618	14.39	0.0040	100.12	15.89
619	14.31	0.0061	100.10	31.95
620	14.41	0.0057	99.88	15.86
621	14.39	0.0053	99.99	7.74
622	14.34	0.0063	99.90	7.76
623	14.27	0.0060	100.21	16.03
624	14.30	0.0044	99.96	31.92
625	14.37	0.0054	99.92	31.86
626	14.37	0.0066	99.84	16.05
627	14.33	0.0076	100.13	3.86
628	14.31	0.0088	100.13	7.81
629	14.32	0.0080	100.14	7.80
630	14.31	0.0087	99.65	16.04
631	14.35	0.0096	100.07	32.02
632	14.30	0.0080	100.14	24.04

TABLE III

EXPERIMENTAL RESULTS (Series A)

x_o = 1.973 inches, x_w = 0.715 inch, $[1 - (x_o/\ell)^{0.8}]^{0.11}$ = 0.8462, Sample: n-heptane

Test No.	t_s °F	t_m °F	U_∞ ft/sec	Re_ℓ	$\dot{m}_k \times 10^6$ lb/sec	Sh_ℓ^*	Sc	$\frac{Sh_\ell^*}{Sc^{1/3}}[1 - (x_o/\ell)^{0.8}]^{0.11}$
566a	99.20	99.55	4.60	5,520	14.10	85.8	2.18	56.0
566b	99.07	99.48	4.60	5,520	13.99	83.8	2.18	54.7
567a	98.89	99.51	6.82	8,260	17.02	103.1	2.18	67.6
567b	98.81	99.47	6.82	8,260	17.14	104.1	2.18	68.3
562	99.41	99.72	8.92	10,750	21.13	125.6	2.18	82.0
565	99.28	99.61	8.89	10,750	19.26	114.9	2.18	74.9
573	99.11	99.60	8.92	10,730	20.41	122.4	2.18	79.9
572a	99.92	100.06	9.83	11,780	26.48	154.4	2.18	100.8
572b	99.58	99.89	9.83	11,780	26.33	155.0	2.18	101.0
564a	99.15	99.62	10.79	12,980	26.62	159.3	2.18	103.9
564b	99.17	99.70	10.81	12,940	26.72	158.6	2.18	103.5
568	98.76	99.41	10.75	12,940	27.41	166.0	2.18	108.3
571a	98.89	99.45	11.80	14,140	32.57	195.5	2.18	125.0
571b	98.94	99.47	11.80	14,140	32.48	194.6	2.18	124.4
569a	98.98	99.47	17.39	20,890	41.08	246.6	2.18	160.9
569b	99.36	99.66	17.37	20,970	40.05	237.9	2.18	155.2
569c	99.54	99.75	17.37	20,970	40.33	238.4	2.18	155.5
570a	99.20	99.64	20.18	26,090	48.63	291.6	2.18	190.3
570b	99.20	99.60	20.18	26,090	48.63	292.6	2.18	190.9
570c	99.11	99.62	20.18	26,090	48.63	292.3	2.18	190.7

TABLE III (Continued)

EXPERIMENTAL RESULTS (Series B)

x_o = 1.973 inches, x_w = 0.715 inch, $[1 - (x_o/\ell)^{0.8}]^{0.11}$ = 0.8462, Sample: n-octane

Test No.	t_s °F	t_m °F	U_∞ ft/sec	Re_ℓ	$\dot{m}_k \times 10^6$ lb/sec	Sh_ℓ^*	Sc	$\frac{Sh_\ell^*}{Sc^{1/3}}[1 - (x_o/\ell)^{0.8}]^{0.11}$
588	98.77	99.36	4.60	5,490	4.92	85.4	2.28	54.9
595	98.59	99.27	6.89	8,240	6.01	105.0	2.28	67.6
587	99.73	99.47	8.95	10,730	7.16	124.6	2.28	80.1
594a	98.34	99.24	10.80	12,900	8.85	155.6	2.28	100.1
594b	98.41	99.28	10.80	12,900	8.89	156.1	2.28	99.7
590a	97.99	99.07	17.46	20,800	12.79	226.8	2.28	145.8
590b	98.68	99.41	17.46	20,800	13.08	227.4	2.28	146.2
591a	97.76	98.87	21.66	25,800	15.07	269.5	2.28	173.3
591b	97.48	98.86	21.66	25,800	14.93	269.5	2.28	173.3
591c	97.62	98.93	21.66	25,800	14.93	268.2	2.28	172.5
589a	97.76	98.91	32.10	40,000	21.56	384.9	2.28	247
589b	97.85	98.96	32.10	40,000	21.61	385.2	2.28	247
589c	97.94	98.96	32.10	40,000	21.51	382.3	2.28	246

TABLE III (Continued)

EXPERIMENTAL RESULTS (Series C)

x_o = 4.973 inches, x_w = 0.715 inch, $[1 - (x_o/\ell)^{0.8}]^{0.11}$ = 0.7779 Sample: n-octane

Test No.	t_s °F	t_m °F	U_∞ ft/sec	Re_ℓ	$\dot{m}_k \times 10^6$ lb/sec	Sh_ℓ^*	Sc	$\frac{Sh_\ell^*}{Sc^{1/3}}[1 - (x_o/\ell)^{0.8}]^{0.11}$
612a	98.77	99.33	8.81	22,700	6.77	250.9	2.28	148.3
612b	98.77	99.33	8.81	22,700	6.73	250.6	2.28	148.1
612N†	89.09	94.49	8.81	22,700	4.97	248.6	2.30	146.5
613a	97.81	98.86	17.35	44,400	10.63	404	2.28	239
613b	97.81	98.86	17.35	44,400	10.34	394	2.28	233
613c	97.81	98.86	17.35	44,400	10.39	395	2.28	234
613N	87.22	93.56	17.35	44,400	7.27	383	2.30	228
614a	97.58	98.83	33.23	84,900	17.26	661	2.28	390
614b	97.62	98.85	33.23	84,900	17.24	659	2.28	390
614N	85.96	93.02	33.23	84,900	11.61	635	2.30	375

†Test numbers ended with N indicate nonisothermal evaporation

TABLE III (Continued)

EXPERIMENTAL RESULTS (Series D)

x_o = 9.973 inches, x_w = 0.715 inch, $[1-(x_o/\ell)^{0.8}]^{0.11}$ = 0.7252 Sample: n-octane

Test No.	t_s °F	t_m °F	U_∞ ft/sec	R_ℓ	$\dot{m}_k \times 10^6$ lb/sec	Sh_ℓ^*	Sc	$\frac{Sh_\ell^*}{Sc^{1/3}}[1-(x_o/\ell)^{0.8}]^{0.11}$
617a	98.22	99.04	8.91	42,700	6.28	444	2.28	245
617b	98.22	99.04	8.91	42,700	6.31	446	2.28	246
617N	89.04	98.46	8.91	42,700	4.74	442	2.30	244
616a	97.81	98.91	17.33	83,100	9.73	693	2.28	382
616b	97.85	98.93	17.33	83,100	9.75	695	2.28	383
616N	87.27	93.63	17.33	83,100	7.00	689	2.30	379
615a	97.62	98.79	33.38	159,400	17.23	1,239	2.28	683
615b	97.62	98.79	33.38	159,400	17.22	1,239	2.28	683
615N	85.96	92.96	33.38	159,400	11.49	1,177	2.30	649

TABLE III (Continued)

EXPERIMENTAL RESULTS (Series E)

x_o = 1.973 inches, x_w = 0.500 inch, $[1-(x_o/\ell)^{0.8}]^{0.11}$ = 0.8204 Sample: n-octane

Test No.	t_s °F	t_m °F	U_∞ ft/sec	Re_ℓ	$\dot{m}_k \times 10^6$ lb/sec	Sh_ℓ^*	Sc	$\frac{Sh_\ell^*}{Sc^{1/3}}[1-(x_o/\ell)^{0.8}]^{0.11}$
627	99.03	99.58	4.59	5,090	3.81	86.6	2.28	54.0
627N	90.07	94.99	4.59	5,090	2.94	87.7	2.30	54.5
628	99.03	99.58	8.94	9,880	5.30	120.5	2.28	75.2
628N	89.70	94.92	8.94	9,880	4.08	123.1	2.30	76.5
626a	99.04	99.64	17.43	19,360	9.48	216.3	2.28	134.9
626b	99.04	99.64	17.43	19,360	9.46	215.9	2.28	134.7
626N	86.57	93.20	17.43	19,360	6.09	203.4	2.30	126.4
625a	98.79	99.36	33.23	37,000	14.69	338	2.28	211
625b	98.79	99.36	33.23	37,000	14.68	337	2.28	210
625N	85.63	92.78	33.23	37,000	9.71	334	2.30	208

TABLE III (Continued)

EXPERIMENTAL RESULTS (Series F)

x_o = 4.973 inches, x_w = 0.500 inch, $[1-(x_o/\ell)^{0.8}]^{0.11}$ = 0.7507 Sample: n-octane

Test No.	t_s °F	t_m °F	U_∞ ft/sec	Re_ℓ	$\dot{m}_k \times 10^6$ lb/sec	Sh_ℓ^*	Sc	$\frac{Sh_\ell^*}{Sc^{1/3}}[1-(x_o/\ell)^{0.8}]^{0.11}$
622	98.93	99.59	8.89	21,800	4.85	245	2.28	140.0
622N	90.07	94.77	8.89	21,800	3.72	246	2.30	139.9
623a	98.57	99.39	17.41	42,500	7.96	405	2.80	231
623b	98.57	99.39	17.41	42,500	7.96	405	2.80	231
623N	88.16	94.19	17.41	42,500	5.71	399	2.30	227
624a	98.31	99.41	33.29	81,600	12.79	657	2.28	375
624b	98.31	99.14	33.29	81,600	12.79	657	2.28	375
624N	86.85	93.41	33.29	81,600	9.02	659	2.30	375

TABLE III (continued)

EXPERIMENTAL RESULTS (Series G)

x_o = 9.973 inches, x_w = 0.500 inch, $[1 - (x_o/\ell)^{0.8}]^{0.11}$ = 0.6987 Sample: n-octane

Test No.	t_s °F	t_m °F	U_∞ ft/sec	Re_ℓ	$\dot{m}_k \times 10^6$ lb/sec	Sh_ℓ^*	Sc	$\frac{Sh_\ell^*}{Sc^{1/3}}[1 - (x_o/x_\ell)^{0.8}]^{0.11}$
621a	99.00	99.50	8.86	41,800	4.81	466	2.28	248
621b	99.00	99.50	8.86	41,800	4.81	466	2.28	248
621N	90.58	95.29	8.86	41,800	3.74	468	2.30	248
620	98.86	99.37	17.22	81,400	7.71	752	2.28	399
620N	88.76	94.32	17.22	81,400	5.63	770	2.30	407
618N	86.27	94.00	17.26	81,500	5.59	761	2.30	403
619	98.08	99.09	33.32	156,300	12.73	1,261	2.27	670
619N	86.27	93.19	33.32	156,300	8.86	1,262	2.30	668

TABLE III (Continued)

EXPERIMENTAL RESULTS (Series H)

x_o = 19.973 inches, x_w = 0.500 inch, $[1-(x_o/x_\ell)^{0.8}]^{0.11}$ = 0.6489 Sample: n-octane

Test No.	t_s °F	t_m °F	U_∞ ft/sec	Re_ℓ	$\dot{m}_k \times 10^6$ lb/sec	Sh_ℓ^*	Sc	$\frac{Sh_\ell^*}{Sc^{1/3}}[1-(x_o/\ell)^{0.8}]^{0.11}$
629	98.68	99.36	8.93	81,800	5.78	1,099	2.28	542
629N	89.42	94.73	8.93	81,800	4.40	1,110	2.30	546
630	98.77	99.21	17.42	159,500	7.56	1,434	2.28	707
630N	88.53	94.11	17.42	159,500	6.60	1,551	2.30	764
632a	96.58	98.36	25.46	233,000	9.47	1,916	2.28	945
632b	96.58	98.39	25.46	233,000	9.42	1,906	2.28	940
632N	87.88	94.02	25.46	233,000	7.34	1,940	2.30	954
631a	96.10	98.09	33.40	306,000	11.08	2,285	2.28	1,127
631b	96.10	98.12	33.40	306,000	11.08	2,285	2.28	1,127
631N	87.18	93.63	33.40	306,000	8.43	2,286	2.30	1,124

TABLE IV. RANGE OF EXPERIMENTAL DATA

Item	Symbol	Unit	Minimum	Maximum
Wetted length	x_w	in.	0.500	0.715
Approach length	x_o	in.	1.973	19.973
Total length	ℓ	in.	2.473	20.473
Length ratio	x_o/ℓ		0.734	0.975
Air velocity	U_∞	ft/sec	4.59	33.38
Reynolds number	Re_ℓ		5,090	306,000
Partial pressure of diffusion component at interface	p_{ks}	psia	0.3528	1.617
Modified average Sherwood number	Sh_ℓ^*		54.0	1,127
Schmidt number	Sc		2.18	2.30

TABLE V. COMPARISON OF EXPERIMENTAL RESULTS EXPRESSED IN Sh_ℓ^* AND IN Sh_ℓ

(x_o = 1.973 inches, x_w = 0.715 inch)

Re	$Sh_\ell^*/Sc^{1/3}$			$Sh_\ell/Sc^{1/3}$		
	n-octane	n-heptane	% deviation†	n-octane	n-heptane	% deviation†
5,490	64.9	65.2	0.5	66.1	69.1	4.5
8,240	79.8	79.8	0.0	81.3	84.5	3.9
10,730	94.7	93.2	- 1.6	96.5	98.8	2.4
12,900	118.4	123.9	4.6	120.6	131.3	8.9
20,800	172.6	185.0	7.2	175.8	196.1	11.6
25,900	204.5	224.0	9.5	208.2	237.2	13.9

† % deviation = $\dfrac{(Sh_\ell^*/Sc^{1/3})_{c_7} - (Sh_\ell^*/Sc^{1/3})_{c_8}}{(Sh_\ell^*/Sc^{1/3})_{c_8}}$ or $\dfrac{(Sh_\ell/Sc^{1/3})_{c_7} - (Sh_\ell/Sc^{1/3})_{c_8}}{(Sh_\ell/Sc^{1/3})_{c_8}}$

APPENDICES

APPENDIX I

LIQUID LOADING SYSTEM

The principal function of the liquid loading system was to deaerate the liquid sample. It also improved the purity of the liquid injected to the evaporating surface. Complete deaeration of the sample was necessary for the accurate measurement of the liquid injection rate since dissolved air might generate bubbles between the liquid injector and the porous surface.

The arrangement of this unit is shown in Figure AI. The sample, which had already been purified by distillation, was loaded into Boiler C_1 and the top was sealed. The sample was then deaerated with vacuum until no further bubbles were generated in the liquid. The first 10% distillate was discarded, and the next 80% was trapped in C_2 by using liquid nitrogen as the cooling medium. The deaeration was continued during this step so that complete deaeration of the sample was ensured. After the sample in C_2 was liquified, it was transferred to ampule D by cooling with a trichlorethylene-dry ice mixture in a large beaker around ampule D, at a temperature just above the freezing point of the sample. By keeping the temperature in C_2 slightly higher than that in C_1, it was possible to retain a constant liquid level in C_1. Therefore the second distillation step essentially involved only Boiler C_2 and Ampule D. After this step was completed, valve 1 was closed and valve 5 was opened, and part of the sample flowed

into the injector which had been evacuated beforehand. The pressure in Ampule D was maintained slightly higher than the atmospheric pressure by adjusting the level of the mercury leg B on the end open to the atmosphere. The capacity of ampule D was 250 cc. and the injector 20 cc.

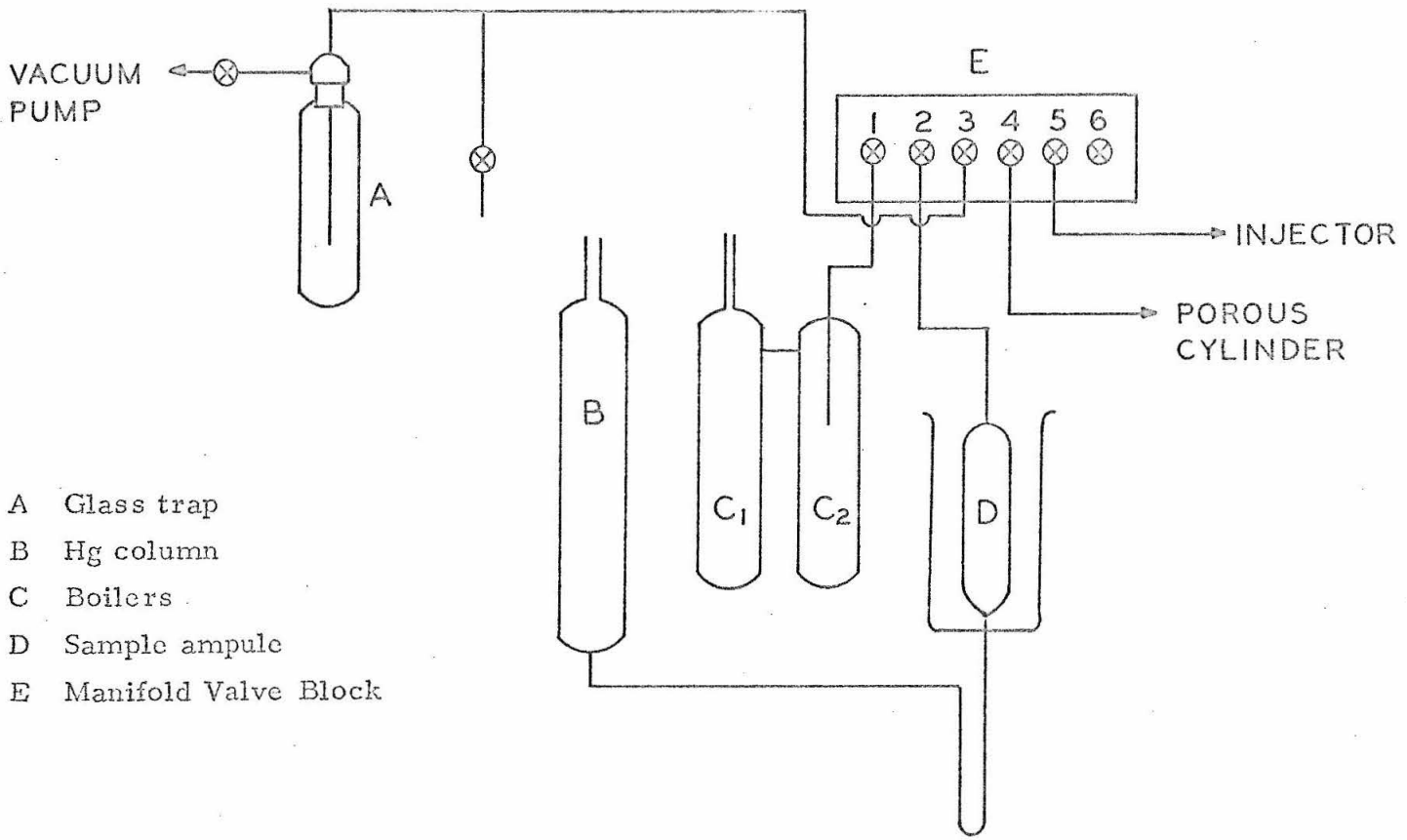

Fig. AI. Liquid Loading System

APPENDIX II

METHOD OF AVERAGING THE EVAPORATING SURFACE TEMPERATURE

Due to the different local rates of evaporation in the flow direction and heat conduction between the porous section and the neighboring parts, it was difficult to maintain the evaporating surface at a uniform temperature. Typical temperature distributions on the evaporating surface are shown in Figure AII-1 and AII-2 for isothermal and non-isothermal evaporation, respectively.

A difference of $1^{\circ}F$ in temperature gives a difference of 2.8% in the vapor pressure of n-octane and 2.5% in the vapor pressure of n-heptane. An error of $1^{\circ}F$ in the temperature measurement therefore would introduce an error of 2.8% or 2.5% to the final results. It is therefore very important to use the correct surface temperature for the calculation of the Sherwood number.

As a first approximation the arithmetic average value of the surface temperature was used to calculate the Sherwood number. The results were then used to obtain an empirical expression of the form of Equation 43. The surface was then divided into intervals of 0.100 inch, and different weighing factors according to the empirical equation and the relation between the Sherwood number and the mass transfer rate, Equation 36, were used to calculate a new average surface temperature. The experimental data were then recalculated by using this average surface temperature. It was

found that these two averaging methods agreed with each other to within 0.1°F, which would contribute an error of only less than 0.3% to the final results. Therefore, it is relatively unimportant which averaging process was used.

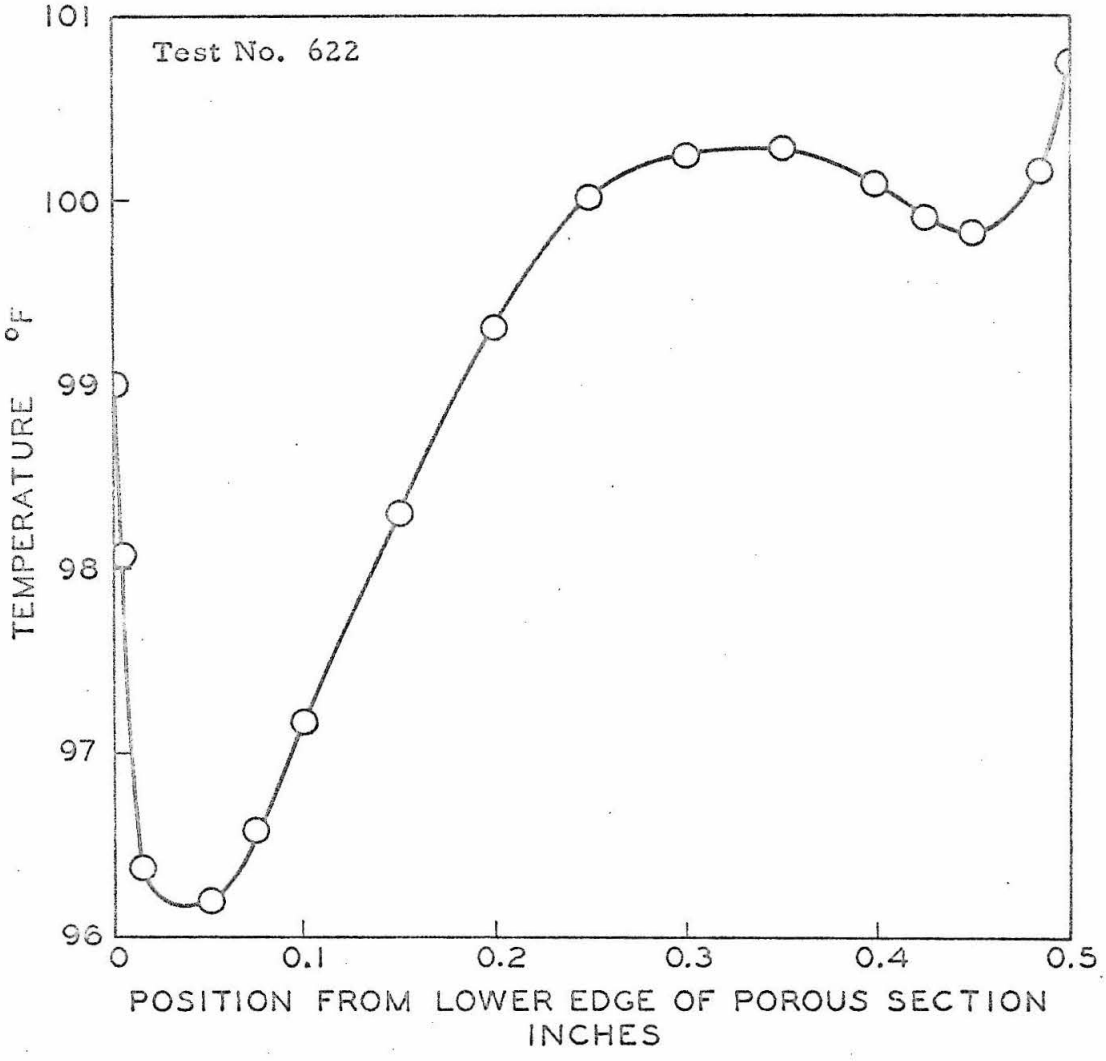

Fig. AII-1. Temperature Distribution Along Porous Surface, Isothermal Case

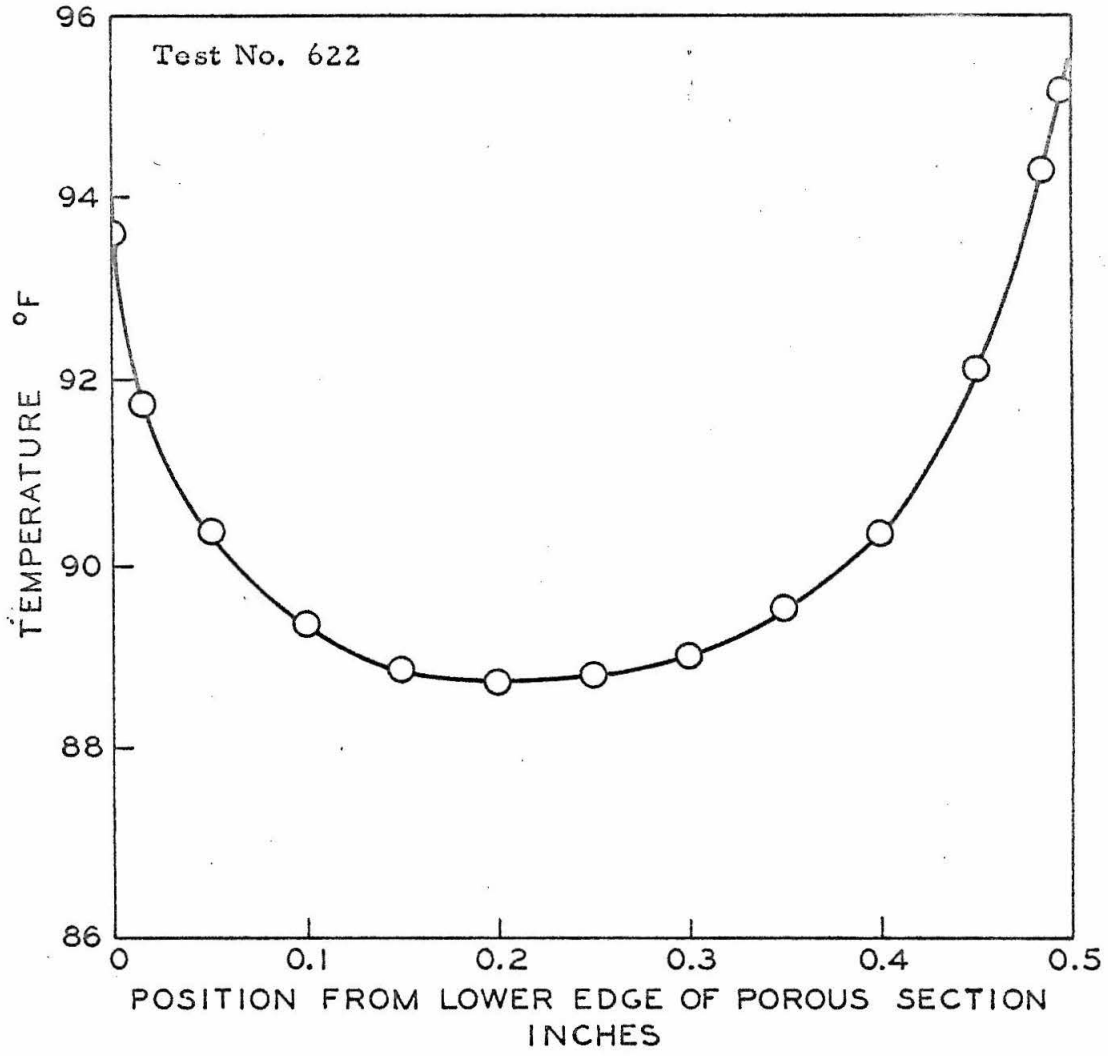

Fig. AII-2. Temperature Distribution Along Porous Surface, Nonisothermal Case

APPENDIX III

DERIVATION OF THE MODIFIED SHERWOOD NUMBER

Using partial pressure as the driving force, the Maxwell theory for the diffusion of gas k through gas j can be expressed as

$$\frac{\partial p_k}{\partial r} + c_k \sigma_{\cdot k} \sigma_{\cdot j} u_k = 0 \qquad \text{(AIII-1)}$$

Assuming an ideal gas, the molal concentrations can be written as

$$\sigma_{\cdot j} = \frac{p_j}{RT}$$

$$\sigma_{\cdot k} = \frac{p_k}{RT} \qquad \text{(AIII-2)}$$

The mass flux of component k is, by definition

$$\dot{m}_k = M_k \sigma_{\cdot k} u_k \qquad \text{(AIII-3)}$$

Combining Equations 1, 2, and 3, one obtains

$$\dot{m}_k = - \frac{M_k \left(\frac{\partial p_k}{\partial r} \right)}{\frac{c_k}{RT} p_j} \qquad \text{(AIII-4)}$$

The Maxwell diffusion coefficient is defined as

$$D_{M,k} = \frac{R^2 T^2}{c_k} \qquad \text{(AIII-5)}$$

Equation 4 becomes

$$\dot{m}_k = - \frac{D_{M,k} M_k \left(\frac{\partial p_k}{\partial r}\right)}{RTp_j} = \frac{D_{M,k} \left(\frac{\partial p_j}{\partial r}\right)}{b_k T p_j} \qquad \text{(AIII-6)}$$

Upon integration from the solid-gas interface to the boundary layer edge, one obtains

$$\dot{m}_k = \frac{D_{M,k}}{b_k T} \frac{\ln \frac{p_{j\infty}}{p_{js}}}{\Delta r} = \frac{D_{M,k}}{b_k T \Delta r} \frac{p_{j\infty} - p_{js}}{p_{jm}} \qquad \text{(AIII-7)}$$

The log mean value of $p_{j\infty}$ and p_{js} is defined as

$$p_{jm} = \frac{p_{j\infty} - p_{js}}{\ln \frac{p_{j\infty}}{p_{js}}} \qquad \text{(AIII-8)}$$

For the case where the concentration of the diffusing component is small, i. e. $p_{js}/p_{j\infty} \approx 1$, Equation AIII-7 reduces to

$$\dot{m}_k = \frac{D_{M,k}}{b_k T \Delta r} \frac{p_{ks} - p_{k\infty}}{P} \qquad \text{(AIII-9)}$$

The mass transfer coefficient is conventionally defined by

$$\dot{m}_k = h_m (\sigma_{ks} - \sigma_{k\infty}) = h_m \frac{p_{ks} - p_{k\infty}}{b_k T} \qquad \text{(AIII-10)}$$

The Sherwood number can be expressed as

$$Sh_x = \frac{h_m x}{D_{F,k}/P} = \frac{\dot{m}_k x b_k TP}{D_{M,k}(p_{ks} - p_{k\infty})} \qquad \text{(AIII-11)}$$

The above expression is applicable when the interfacial velocity and the net flow resulting from diffusion are very small.

From Equations AIII-9 and AIII-10, one obtains the following relation

$$h_m = \frac{D_{M,k}}{P\Delta r} \qquad \text{(AIII-12)}$$

A comparison of Equations AIII-11 and AIII-7 gives the following expression for the mass transfer coefficient for the general case of non-vanishing interfacial velocities

$$h_m = \frac{\dot{m}_k b_k T}{P \ln \frac{p_{j\infty}}{p_{js}}} \qquad \text{(AIII-13)}$$

The modified Sherwood number can then be expressed as

$$Sh_x^* = \frac{\dot{m}_k x b_k T}{D_{M,k} \ln \frac{p_{j\infty}}{p_{js}}} \qquad \text{(AIII-14)}$$

and the average modified Sherwood number as

$$Sh_{\ell}^{*} = \frac{\dot{m}_k \ell b_k T}{2\pi a x_w D_{M,k} \ln \frac{P_{j\infty}}{P_{js}}} \qquad \text{(AIII-15)}$$

which is the expression used in this work.

It should be pointed out that the use of the modified Sherwood number does not give an exact solution for convective mass transfer, but rather gives an approximate method to take account of the non-vanishing interfacial velocity.

PROPOSITIONS

PROPOSITION I

It is proposed that the solution obtained by Chu and Hougen[1] for the effect of adsorption on the effectiveness factor of catalyst pellets can be simplified by properly grouping the dimensionless parameters*.

One of the disadvantages of the numerical solution of differential equations is the lack of generality. In order to partially overcome this weak point, one usually obtains a spectrum of solutions which covers a wide range of values of each parameter involved. While this does not cause much difficulty when only two or three parameters are involved, it becomes impractical when there are more than three parameters, owing to the large amount of time needed for the computation and the space required for presenting the solutions in graphical form. Therefore, it is important to group the variables and parameters in proper forms and reduce them to a minimum number before the computation is carried out. We shall consider here an important example in the heterogeneous catalytic process.

The effectiveness factor of a catalyst particle is defined as the ratio of the actual rate of reaction to the rate which would exist if the concentrations in the interior of a porous particle

---

*This proposition was formulated in 1962. A similar treatment appeared in a recent paper by Krasuk and Smith[2].

were the same as the concentrations in the bulk fluid bathing the particles. This concept was first developed by Thiele[3] and later discussed in detail by many authors[4]. It was pointed out recently by Chu and Hougen[1] that Thiele's derivation was based on the faulty assumption that the same reaction model applied to the surface-catalyzed reaction as for the corresponding homogeneous reaction. They took the effect of adsorption into consideration and developed new mathematical results for the following irreversible first-order reaction

$$A \rightarrow Q \tag{1}$$

catalyzed by porous flat plates. By assuming that the surface reaction is the rate-controlling step, the rate equation for the disappearance of component A is

$$r_A = \frac{kK_A p_A}{(1 + K_A p_A + K_Q p_Q)} \tag{2}$$

where K_A and K_Q are adsorption equilibrium constants and k is the surface reaction rate constant. From the definition of the effective diffusivity, D_e, we obtain the molar flux of A as

$$N_A = D_e \frac{dC_A}{dx} \tag{3}$$

A material balance of component A leads to

$$\frac{d^2 y_A}{dx^2} = \alpha^2 \frac{y_A}{(1 - z)y_A + \zeta} \tag{4}$$

where

y_A = molal fraction of component A = $C_A v$

$z = K_Q / K_A$

$\zeta = z + \frac{1}{K_A P}$

$\alpha = \sqrt{\frac{kv}{D_e}}$

v = molal volume

Equation 4 was solved numerically by Chu and Hougen[1] with the boundary conditions

$$y_A = y_{As} \qquad \text{at } x = L/2$$

$$\frac{dy_A}{dx} = 0 \qquad \text{at } x = 0 \text{ (center of slab)} \tag{5}$$

The resultant effectiveness factor is given by

$$E = E(y_{As}, z, \zeta, M) \tag{6}$$

The modulus M is defined as

$$M = \frac{L}{2} \alpha \tag{7}$$

The presentation of the effectiveness factor in terms of four parameters, as shown in Equation 6, in a graphical or a numerical form is highly impractical.

Equations 2 and 5 can be simplified by using the following

parameters

$$u = y_A/y_{As} \quad ; \quad t = x/(L/2)$$

$$\beta = \frac{a(L/2)}{\sqrt{\zeta}} \quad ; \quad \xi = \frac{\sqrt{y_{As}(1-z)}}{a(L/2)} \tag{8}$$

The differential equation becomes

$$\frac{d^2u}{dt^2} = \frac{u}{\xi^2 u + \frac{1}{\beta^2}} \tag{9}$$

with the boundary conditions

$$u = 1 \quad \text{at} \quad t = 1$$

$$\frac{du}{dt} = 0 \quad \text{at} \quad t = 0 \tag{10}$$

The solution of Equations 9 and 10 can be expressed as

$$u = u(t, \beta, \xi) \tag{11}$$

By definition, the effectiveness factor can be written as

$$E = \frac{N_{As}}{r_{As}(L/2)} = \frac{\frac{D_e}{v}\left(\frac{dy_A}{dx}\right)_{x=L/2}}{\frac{ky_{As}}{(1-z)y_{As}+\zeta}\ (L/2)} \tag{12}$$

$$E = \left(\xi^2 + \frac{1}{\beta^2}\right)\left(\frac{du}{dt}\right)_{t=1} \tag{13}$$

or

$$E = E(\beta, \xi) \tag{14}$$

Thus, the results can be presented in a single chart by plotting the effectiveness factor E vs. β for various values of ξ. This has been done by Krasuk and Smith[2].

For $z = 1$, the problem reduces to Thiele's formulation and the solution is simple:

$$E = \frac{\tanh \beta}{\beta} \tag{15}$$

and β becomes the conventional Thiele modulus. The transformations used in this proposition also have the advantage that the problem reduces automatically to the Thiele case for $z = 1$. The results of Chu and Hougen for $z = 1$ differ from the Thiele solution by a factor and are not convenient for a direct comparison.

References:

1. Chu, C. and O. A. Hougen, Chem. Eng. Sci., 17, 167 (1962).

2. Krasuk, J. H. and J. M. Smith, I&EC Fundamentals, 4, 103 (1965).

3. Thiele, G. W., Ind. Eng. Chem., 31, 916 (1938).

4. See, e.g., O. A. Hougen and K. M. Watson, "Chemical Process Principles," part III, John Wiley & Sons, Inc., N.Y., 1947, and A. Wheeler, in "Catalysis," vol. II, pp. 105-165, Reinhold Publishing Corporation, N.Y., 1955.

PROPOSITION II

A mathematical analysis of the kinetics of the following competitive-consecutive reaction system

$$A \xrightarrow{k_1} B \qquad (1)$$

$$A + B \xrightarrow{k_2} C \qquad (2)$$

is proposed.

Rate constants of chemical reactions are usually not obtained directly from measurements, but rather the concentrations are observed as functions of time. It is therefore necessary to integrate the differential rate equations into integrated forms in order to determine the rate constants. Moreover, even if this step is accomplished, difficulties still exist in fitting the experimental data to the integrated equations which are often complicated in form. Experiments must be designed based on mathematical analyses in order to arrive at accurate results. A general method for the determination of the rate constants of complex first-order reactions from proper experimental data has been developed recently by Wei and Prater[1]. This was possible because the problem of solving first-order kinetic equations can be reduced to the problem of finding the eigenvalues and eigenfunctions of matrices. Since this method depends on the linearity of the kinetic equations, it is not applicable to reactions other than the

first order. No general method is available for the solution of higher-order kinetic equations, and each case has to be solved individually. The solutions to some rate equations which can be solved in terms of elementary functions have been compiled by Moelwyn-Hughes[2]. Some irreversible consecutive reactions have been solved by Chien[3] and Pearson et al.[4] in terms of transcendental functions. A system of two competitive-consecutive reactions have been solved by Frost and Schwemer[5, 6]. Here we propose to study mathematically the system of competitive-consecutive reactions represented by Equations 1 and 2 and discuss methods for fitting experimental data to the integrated equations to obtain the rate constants.

The rate equations for this system of equations can be written as

$$\frac{dA}{dt} = - k_1 A - k_2 AB \tag{3}$$

$$\frac{dB}{dt} = k_1 A - k_2 AB \tag{4}$$

$$\frac{dC}{dt} = k_2 AB \tag{5}$$

where A, B, and C represent the molar concentrations of the corresponding chemical species. If the initial concentration of A is A_o and no B and C are present at the beginning of the reaction, a material balance gives

$$A + B + 2C = A_o \tag{6}$$

Introducing the following dimensionless variables

$$\tau = k_1 t \; ; \quad \kappa = k_2 A_o / k_1 \; ;$$

$$\alpha = A/A_o \; ; \quad \beta = B/A_o \; ; \quad \gamma = C/A_o \tag{7}$$

Equations 3, 4, 5, and 6 become

$$\frac{d\alpha}{d\tau} = -\alpha - \kappa\alpha\beta \tag{8}$$

$$\frac{d\beta}{d\tau} = \alpha - \kappa\alpha\beta \tag{9}$$

$$\frac{d\gamma}{d\tau} = \kappa\alpha\beta \tag{10}$$

$$\alpha + \beta + 2\gamma = 1 \tag{11}$$

Solving the above equations, we obtain

$$\tau = \int_o^\beta \frac{d\beta}{(1 - \kappa\beta)\left[1 + \beta + \frac{2}{\kappa}\ln(1 - \kappa\beta)\right]} \tag{12}$$

$$\alpha = 1 + \beta + \frac{2}{\kappa}\ln(1 - \kappa\beta) \tag{13}$$

It does not appear feasible to integrate Equation 12 in terms of known functions, but the numerical integration is fairly simple. The results, expressed in α, β, and γ as functions of τ for various values of κ, are plotted in Figures 1, 2, and 3.

The above analysis can be used for the determination of the rate constants k_1 and k_2. We first tabulate the values of τ as a function of κ and α as shown in Table 1, and then the time ratios calculated from the first table as shown in Table 2. The τ-ratios are equal to the time ratios according to the definition $\tau = k_1 t$. We can then determine the values of κ for a particular experiment by comparing the experimental time ratios with Table 2. Once κ is determined, the rate constant k_1 can be obtained from the relation $\tau = k_1 t$ and Table 1. The second rate constant, k_2, can be evaluated from the definition $\kappa = k_2 A_o / k_1$.

Due to the nature of the reaction system, α and β approach different constant values for different values of κ as $t \rightarrow \infty$. This particular phenomenon also can be used to determine the value of κ.

The writer was unable to find an actual system which follows the mechanism considered above. Nevertheless, it is hoped that the analysis might be found useful for some organic reactions.

References:

1. Wei, J. and C. D. Prater, The Structure and Analysis of Complex Reaction Systems, in "advances in Catalysis," vol. 13, pp. 203-392, Academic Press, N. Y., 1962.

2. Moelwyn-Hughes, E. A., "Physical Chemistry," 2nd edition, Pergamon Press, N. Y., 1961.

3. Chien, J., J. Am. Chem. Soc., 70, 2256 (1948).

4. Pearson, Q. G., L. C. King, and S. H. Langer, J. Am. Chem. Soc., 73, 4147 (1951).

5. Frost, A. A. and W. C. Schwemer, J. Am. Chem. Soc., 73, 4541 (1951).

6. Frost, A. A. and R. G. Pearson, "Kinetics and Mechanism," 2nd edition, John Wiley & Sons, Inc., N. Y., 1961.

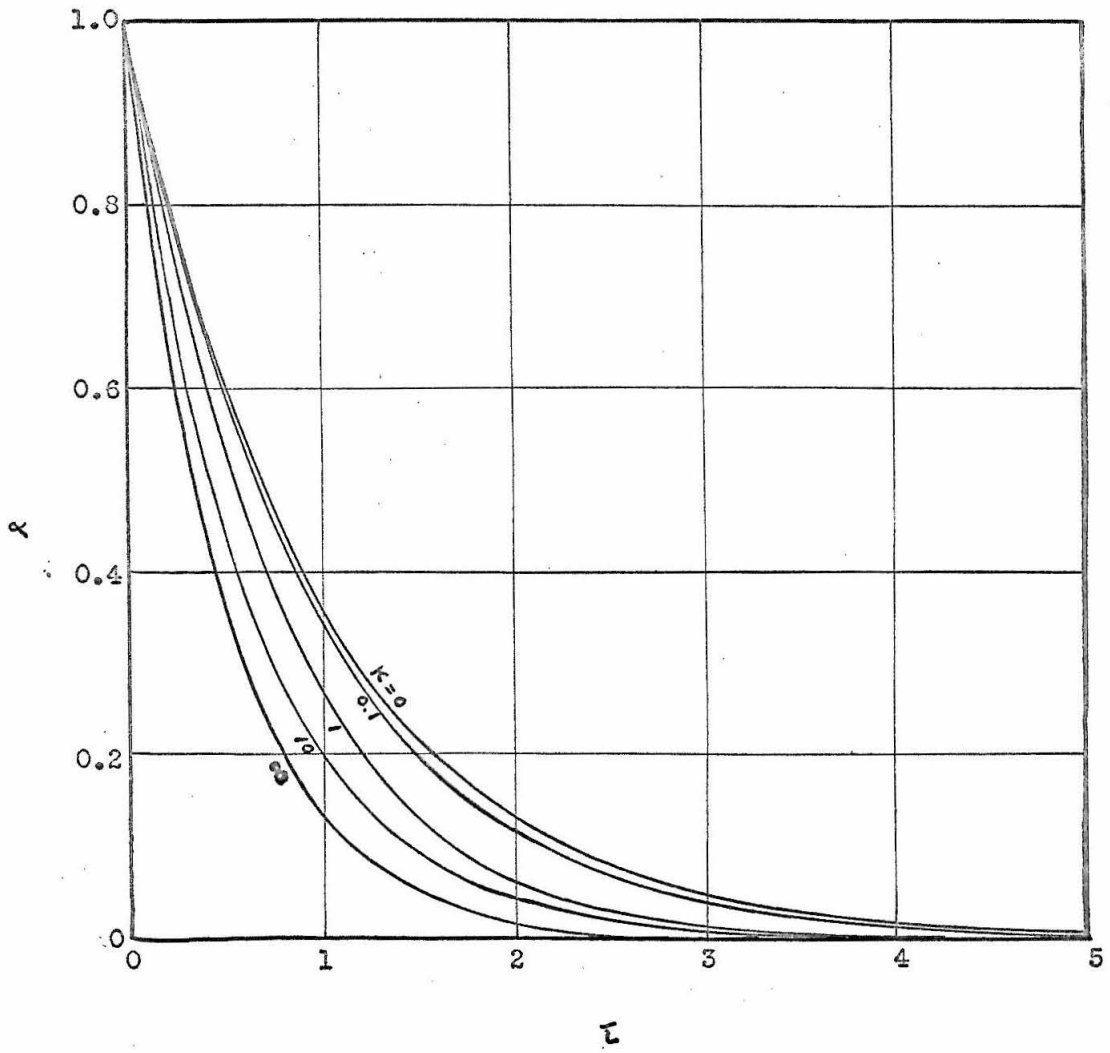

Figure 1

α vs. τ

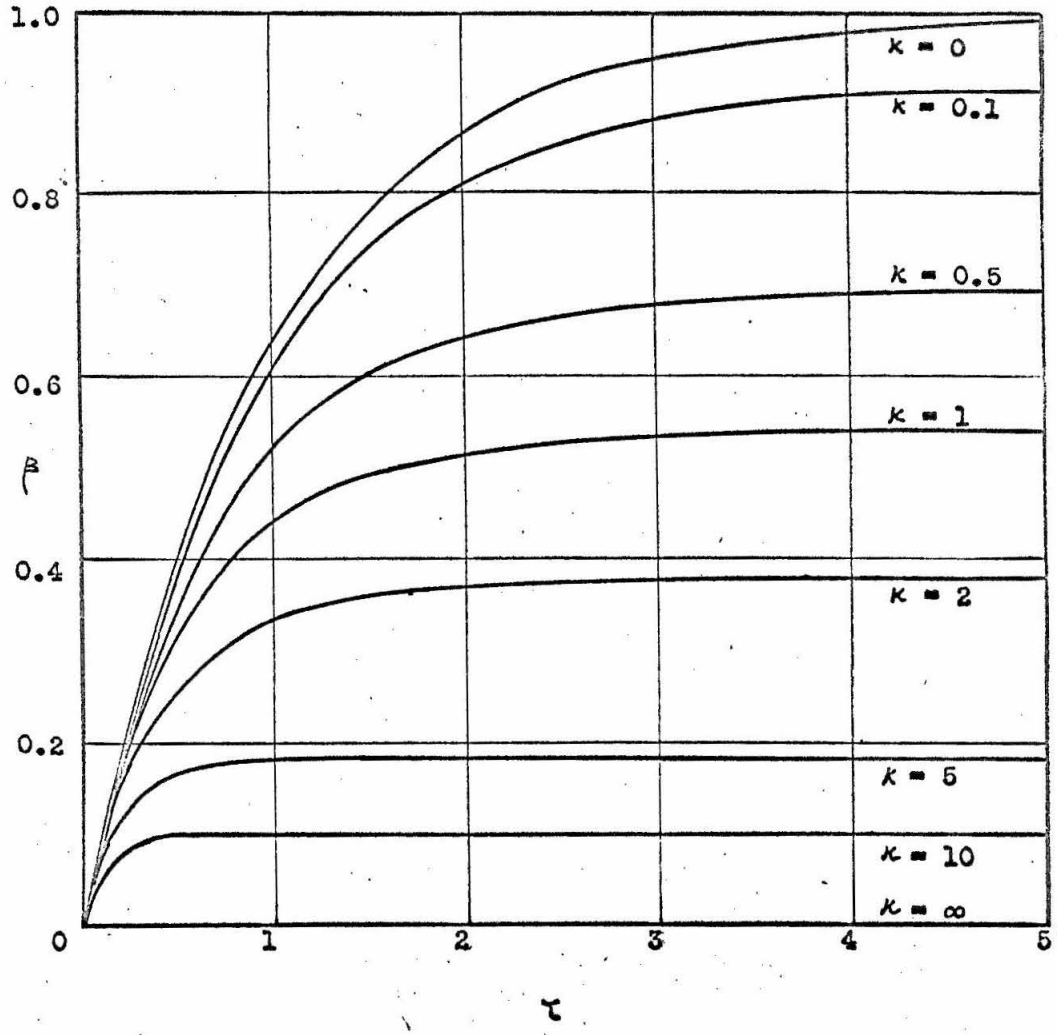

Figure 2

β vs. τ

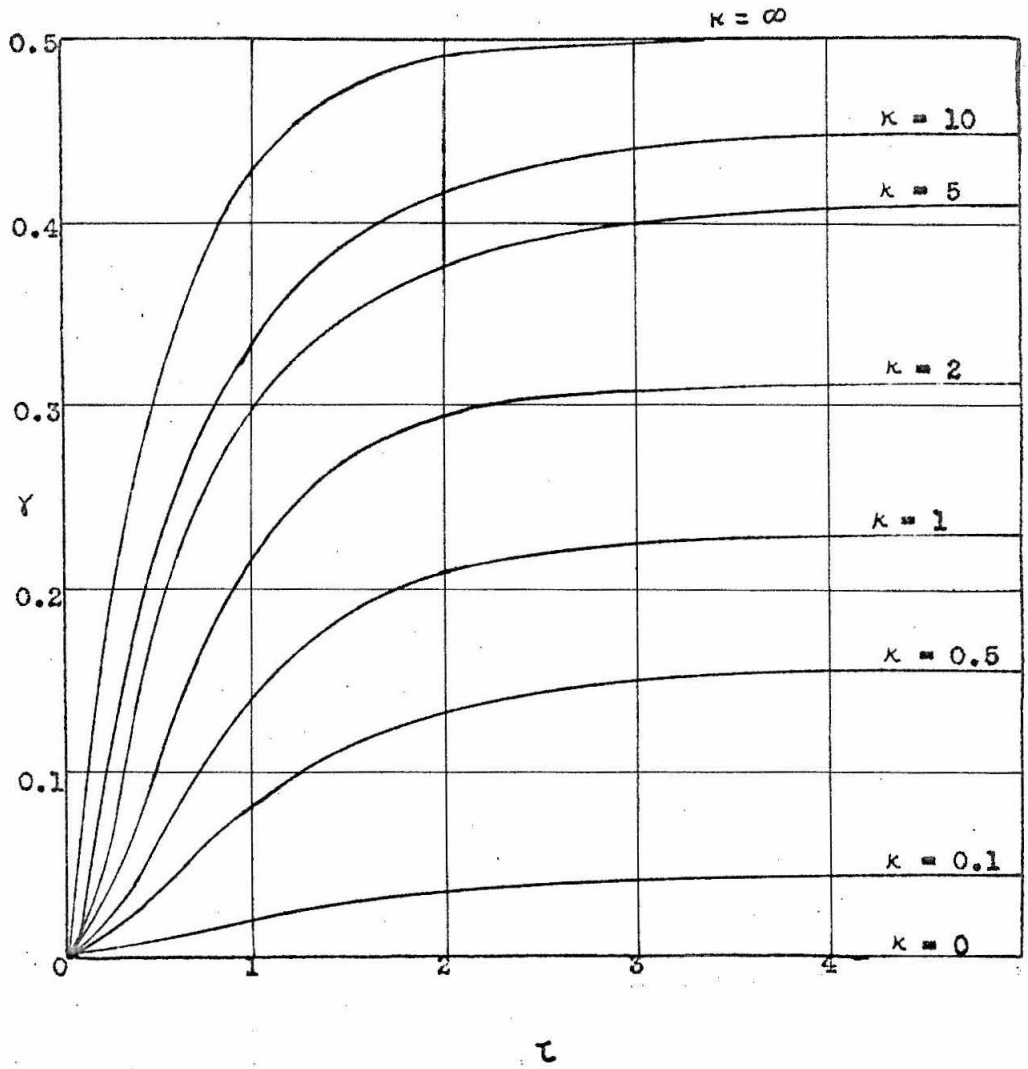

Figure 3

γ vs. τ

Table 1

τ as a function of κ and α

κ	α =0.7 30 % reaction	α =0.6 40 % reaction	α =0.5 50 % reaction	α =0.4 60 % reaction	α =0.3 70 % reaction	α =0.2 80 % reaction
0.1	0.350	0.497	0.673	0.886	1.160	1.526
0.5	0.343	0.465	0.617	0.800	1.034	1.350
1.0	0.315	0.434	0.571	0.732	0.940	1.220
2.0	0.292	0.400	0.518	0.660	0.845	1.082
5.0	0.252	0.343	0.445	0.565	0.720	0.910

Table 2

Time ratios as functions of κ

(t_{70} is the time for 70 per cent reaction, i.e., $\alpha = 0.3$)

κ	t_{30}/t_{50}	t_{30}/t_{40}	t_{80}/t_{50}	t_{80}/t_{60}	t_{70}/t_{30}	t_{70}/t_{40}	t_{70}/t_{50}
0.1	4.36	3.07	2.27	1.721	3.32	2.33	1.699
0.5	3.94	2.91	2.19	1.689	3.02	2.23	1.675
1.0	3.87	2.81	2.14	1.667	2.99	2.17	1.646
2.0	3.71	2.71	2.09	1.641	2.87	2.11	1.630
5.0	3.61	2.65	2.04	1.610	2.85	2.09	1.617

PROPOSITION III

Equations for the critical diameter and the effective diameter of spherical insulation are derived in this proposition. The results show that the selection of good insulating materials is more important for a spherical surface than for a plane or a cylindrical surface.

When thermal energy is transferred across a plane wall, any additional insulation will reduce the heat loss if the heat transfer coefficient between the wall and the surrounding air remains constant. This is not generally true for a curved surface. It has been shown[1, 2, 3] that for a cylindrical surface there exists a critical thickness of insulation. An insulating layer thinner than this critical value not only results in no insulation but increases the thermal flux. In this proposition we shall extend the treatment to the spherical case, which is of practical importance as it may arise when considering the problems of insulating a spherical container or a spherical reactor.

Consider a hollow sphere with an inside diameter D_1 and an outside diameter D_2. On the outer surface of the sphere is a layer of insulation whose diameter is D_{ins}. Let h_1 be the heat transfer coefficient between the inner surface of the sphere and the fluid in the sphere, and h_2 that between the insulation and the surrounding air. For steady-state heat conduction, the total

thermal resistance can be written as

$$R = \frac{1}{\pi}\left[\frac{1}{h_1 D_1^2} + \frac{1}{2k_s}\left(\frac{1}{D_1} - \frac{1}{D_2}\right) + \frac{1}{2k_i}\left(\frac{1}{D_2} - \frac{1}{D_{ins}}\right) + \frac{1}{h_2 D_{ins}^2}\right] \quad (1)$$

where k_s and k_i are the thermal conductivities of the sphere and the insulation, respectively. For simplicity, assume that the thermal conductivities and heat transfer coefficients are constant and, in particular, assume h_2 independent of the diameter.

Differentiating Equation 1 with respect to D_{ins}, we obtain

$$\frac{\partial R}{\partial D_{ins}} = \frac{1}{\pi}\left[\frac{1}{2k_i D_{ins}^2} - \frac{2}{h_2 D_{ins}^3}\right] \quad (2)$$

The derivative vanishes for

$$\frac{1}{2k_i D_{ins}^2} - \frac{2}{h_2 D_{ins}^3} = 0 \quad (3)$$

Hence at a certain critical diameter of insulation

$$D_{cri} = \frac{4k_i}{h_2} \quad (4)$$

the total thermal resistance is a maximum or a minimum. Differentiating again, we have

$$\frac{\partial^2 R}{\partial D_{ins}^2} = \frac{1}{\pi}\left[-\frac{1}{k_i D_{ins}^3} + \frac{6}{h_2 D_{ins}^4}\right] \quad (5)$$

at $D_{ins} = D_{cri}$,

$$\frac{\partial^2 R}{\partial D_{ins}^2} = \frac{1}{128\,\pi}\ \frac{k_i^4}{h_2^3} > 0 \qquad (6)$$

Therefore, at $D_{ins} = D_{cri}$, the thermal resistance of the sphere is minimum and the heat loss from the sphere is maximum. If a poor insulating material (k_i large) is used, the critical diameter may become larger than the outside diameter of the sphere, D_2, and the insulation will increase the heat loss before it reaches a thickness of $\frac{1}{2}(D_{cri} - D_2)$. The above result can be explained physically as follows: the addition of an insulating layer to a sphere increases the outer surface area which is proportional to the square of diameter and increases heat convection to the surroundings. Although the insulation increases the thermal resistance due to conduction, this term is only proportional linearly to the diameter. If the insulating material does not have a low thermal conductivity, the insulating effect may be smaller than the increase of heat loss due to the increase of the outer surface area of the sphere. The better the insulating material the smaller becomes the critical thickness of the insulation. The critical diameter of insulation is independent of the diameter of the sphere, the heat transfer coefficient in the sphere, h_1, and the thermal conductivity of the sphere, k_s. This implies that the critical thickness of insulation is a more important problem for a small sphere than for a large sphere.

The critical diameter of cylindrical insulation is

$$(D_{cri})_{cylinder} = \frac{2k_i}{h_2} \tag{7}$$

For the same insulating material and same heat transfer coefficient, the critical diameter of insulation for a sphere is twice that for a cylinder. The selection of good insulating materials is therefore more important for a sphere than for a cylinder and, of course, than for a flat wall. This can also be understood physically by realizing that for a sphere the surface area is proportional to the square of diameter, but for a cylinder it is proportional linearly to the diameter. The surface area is independent of the thickness of insulation for a plane.

It is also interesting to evaluate the effective thickness of insulation, that is, the thickness of insulation at which the heat loss is equal to the heat loss of an uninsulated sphere. This can be found from

$$\frac{1}{\frac{1}{h_1 D_1^2} + \frac{1}{2k_s}\left(\frac{1}{D_1} - \frac{1}{D_2}\right) + \frac{1}{h_2 D_2^2}} = \frac{1}{\frac{1}{h_1 D_1^2} + \frac{1}{2k_s}\left(\frac{1}{D_1} - \frac{1}{D_2}\right) + \frac{1}{2k_i}\left(\frac{1}{D_2} - \frac{1}{D_{ins}}\right) + \frac{1}{h_2 D_{ins}^2}} \tag{8}$$

Hence, insulation starts to be effective when

$$D_{ins} = \frac{D_{cri} D_2}{2D_2 - D_{cri}} \tag{9}$$

The diameter of the insulation must be greater than the above value in order to gain insulating effects. Equation 9 also contains an important qualitative feature. If the critical diameter of insulation is equal to or larger than 2 times the diameter of the uninsulated sphere, the "insulation," no matter how thick it is, can only increase heat loss to the surroundings. This important fact does not exist in cylindrical insulation as can be seen from the formula which determines the effective diameter of cylindrical insulation:

$$D_{ins} = D_2 e^{\frac{D_{cri}}{D_2}\left(1 - \frac{D_2}{D_{ins}}\right)} \tag{10}$$

This comparison again shows that the selection of good insulating materials is more important for a sphere than for a cylinder.

The results of the above analysis are illustrated in Figure 1, which shows the relationship between the heat loss from a sphere and the thickness of insulation.

It may be pointed out that one can increase the heat flux from a sphere by increasing the thickness of the wall with good conducting materials.

References:

1. Kutateladze, S. S., "Fundamentals of Heat Transfer," translated by Scripta Technica, Inc., Academic Press Inc., N. Y., 1963.

2. Kreith, F., "Principles of Heat Transfer," International Textbook Company, Scranton, 1961.

3. Rohsenow, W. M. and H. Y. Choi, "Heat, Mass and Momentum Transfer," Prentice-Hall, Inc., Englewood Cliffs, N. J., 1961.

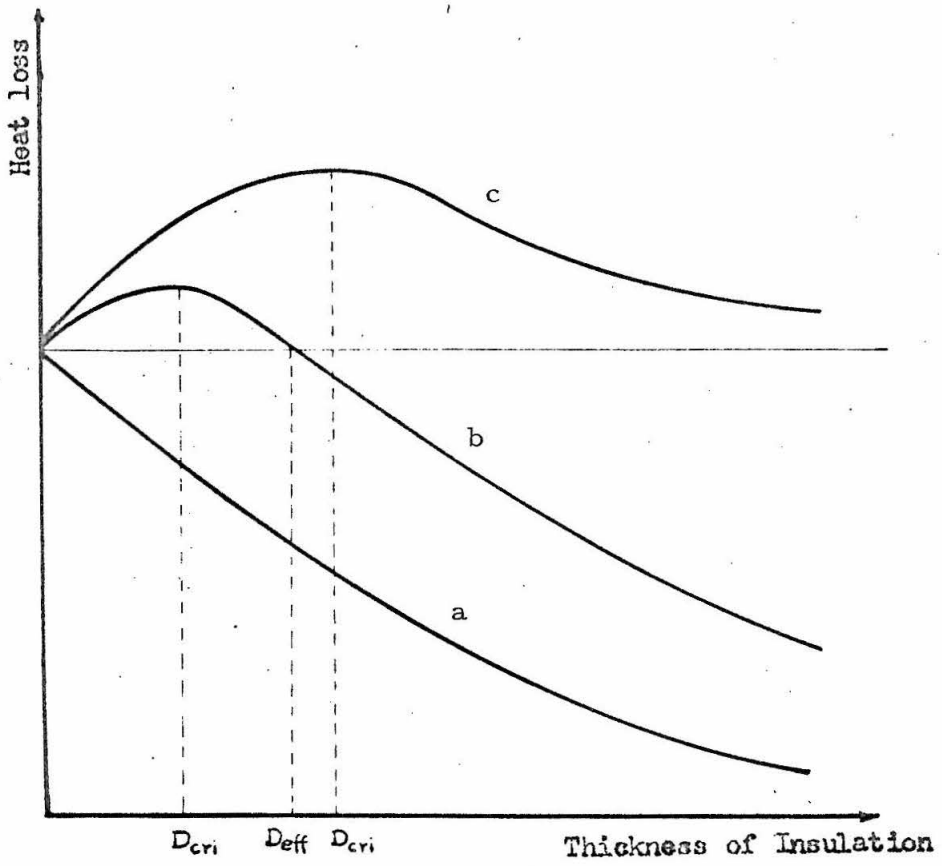

Fig. 1. Heat loss through spherical insulation as a function of its thickness

a. Good insulation $\left(\frac{4k_i}{h_2} < D_2\right)$

b. Poor insulation $\left(\frac{4k_i}{h_2} > D_2\right)$

c. Very poor insulation $\left(\frac{4k_i}{h_2} \geq 2D_2\right)$

PROPOSITION IV

It is proposed that the application of the Mangler transformation to the axisymmetrical, laminar boundary layer flow of a non-Newtonian fluid may introduce serious errors.

In a recent publication Acrivos, Shah and Peterson[1] presented asymptotic solutions for the two-dimensional laminar boundary layer equations for a power-law non-Newtonian fluid. They stated that the solutions also applied to the axisymmetrical case since the axisymmetrical boundary layer equations:

$$u \frac{\partial u}{\partial x} + v \frac{\partial u}{\partial y} = U \frac{dU}{dx} + \frac{K}{\rho} \frac{\partial}{\partial y} \left(\frac{\partial u}{\partial y} \right)^n \qquad (1)$$

and

$$\frac{\partial (ru)}{\partial x} + \frac{\partial (rv)}{\partial y} = 0 \qquad (2)$$

can be reduced to the two-dimensional case by means of the Mangler transformation[2].

The Mangler transformation becomes possible through the assumption that the radial coordinate, whenever it occurs explicitly in the boundary layer equations, may be replaced by the local body radius. In other words, the axisymmetrical boundary layer equations can be written in the Boltze form[3], that is, Equations 1 and 2. This assumption implies that the radius of

the transverse curvature is very large compared with the boundary layer thickness. Without this assumption the laminar boundary layer equations for the axisymmetrical flow of a power-law non-Newtonian fluid are as follows:

$$u\frac{\partial u}{\partial x} + v\frac{\partial v}{\partial y} = U\frac{dU}{dx} + \frac{K}{\rho}\frac{1}{r+y}\frac{\partial}{\partial y}\left[(r+y)\left(\frac{\partial u}{\partial y}\right)^{n}\right] \qquad (3)$$

$$\frac{\partial (r+y)u}{\partial x} + \frac{\partial (r+y)v}{\partial y} = 0 \qquad (4)$$

The Mangler transformation does not apply to Equations 3 and 4.

Since the Boltze formulation neglects the transverse curvature, for the axial flow along a cylinder (r = constant) Equations 1 and 2 automatically reduce to the boundary layer equations for flow along a flat plate. This is not true for the more rigorous formulation, Equations 3 and 4.

For the flow of a gas at high velocities along a body of revolution with a small transverse curvature, the assumptions implied in the Mangler transformation is usually satisfactory. This is the reason for the wide acceptance of the transformation by aerodynamicists. However, the chemical engineer often deals with flows of high-viscosity fluids at relatively low velocities. The assumption that the boundary layer thickness is much smaller than the radius of the transverse curvature may not hold, and the applicability of the Boltze formulation and the Mangler transformation becomes questionable.

Let us consider, for example, a Newtonian liquid with a density of 55 lb/ft^3 and a viscosity of 10 centipoises flowing along a 1-inch-diameter cylinder at a velocity of 5 ft/sec. This problem has been solved by Seban and Bond[4] and Kelly[5]. The solution can be expressed in the following form

$$f_{cyl}/f_{F.P.} = 1 + 2.10(x/r)Re_x^{-1/2} - 1.92(x/r)^2 Re_x^{-1} + \ldots \qquad (5)$$

where f_{cyl} is the local skin-friction coefficient for axisymmetrical flow along a cylinder of radius r, and $f_{F.P.}$ is the local skin-friction coefficient for flow along a flat plate. For the specific problem considered, at a distance x = 1 foot from the leading edge of the cylinder

$$f_{cyl}/f_{F.P.} = 1.22 \qquad (6)$$

This indicates that the application of the solutions of Acrivos, Shah and Peterson to the above case would give an error of 22%. This example leads one to believe that the application of the Boltze formulation and the Mangler transformation to the axisymmetrical flow of a non-Newtonian fluid may result in serious errors.

It is suggested that the influence of the transverse curvature on the skin friction and heat transfer for the axisymmetrical flow of a power-law non-Newtonian fluid along a body of revolution should be studied. For flow along a cylinder, the method used by

Seban and Bond[4] for the Newtonian fluid case, i.e., the expansion of the solution in the form of series in terms of suitable transverse curvature parameters, may also be useful for the non-Newtonian fluid case.

Nomenclature:

f_{cyl} = local skin-friction coefficient for a cylinder

$f_{F.P.}$ = local skin-friction coefficient for a flat plate

K, n = parameters in the power law model

Re_x = Reynolds number, $\rho Ux/\mu$

r(x) = a distance of a point on the surface from the axis of symmetry

U = velocity at the edge of the boundary

u = velocity in x-direction

v = velocity in y-direction

x = distance along the surface from the leading edge

y = distance normal to the surface

ρ = density

μ = viscosity

References:

1. Acrivos, A., M. J. Shah and E. E. Petersen, Chem. Eng. Sci., 20, 101 (1965).

2. Schlichting, H., "Boundary Layer Theory," translated by J. Kestin, McGraw-Hill Book Company, Inc., 1962, p. 190.

3. Ibid, p. 185.

4. Seban, R. A. and R. Bond, J. Aero. Sci., 18, 671 (1951).

5. Kelly, H. R., J. Aero. Sci., 21, 634 (1954).

PROPOSITION V

In order to study experimentally the influence of transverse curvature on heat and mass transfer in turbulent boundary layers, cylinders of different diameters should be tested. It is proposed that boundary layer trips be used to insure turbulent boundary layers over a large range of Reynolds numbers.

Due to the inconsistent results for heat and mass transfer in turbulent boundary layer flows obtained by various investigators, it has been difficult to determine the influence of transverse curvature on heat and mass transfer from bodies of revolution to fluids in axisymmetrical flows by comparing results for cylinders and for flat plates[1]. In order to arrive at a quantitative conclusion, it appears necessary to study heat or mass transfer from cylinders of different diameters under the same experimental conditions. To obtain conclusive results, it is important to have turbulent boundary layers cover a large range of Reynolds numbers.

As is well known, when a fluid is forced to pass an external surface, the boundary layer is always laminar near the leading edge (assuming that the leading edge is smooth enough not to cause boundary layer separation or to trigger turbulence) and becomes turbulent further downstream. To carry out the experiment suggested above, it is necessary to restrict measurements to downstream sections of the cylinders where turbulent boundary

layers have been fully developed. This somewhat narrows the Reynolds number range available for the experiment. Furthermore, transition from the laminar to the turbulent boundary layer may take place at different positions for cylinders of different diameters. This brings additional complication to the experimental data. To avoid the above difficulties, it is proposed that boundary layer trips[2, 3] be used to promote transition at a position near the leading edge to insure that a large range of Reynolds numbers is available for the experiment. Chapman and Kester[2] have successfully employed a 0.02-inch wire trip to obtain turbulent boundary layers on a one-inch cylinder for skin-friction measurements by the direct-force method. Wire trips may be adequate for the experiment described in this proposition.

References:

1. This thesis.
2. Chapman, D. R. and R. H. Kester, NACA TN 3097 (1954).
3. Kuehn, D. M., NASA TR R-117 (1961).